REGULATION OF EXCITATORY NEUROTRANSMISSION, SYNAPTIC PLASTICITY, AND LEARNING BY CYCLIN-DEPENDENT KINASE 5

APPROVED BY SUPERVISORY COMMITTEE

James A. Bibb, Ph.D. (Supervisor)

Donald C. Cooper, Ph.D.

Kimberly Huber, Ph.D. (Chair)

Elliott M. Ross, Ph.D.

DEDICATION

I would like to thank my family, friends, mentors, colleagues, members of my graduate committee, and all others who enriched my graduate school experience.

"Men ought to know that from the brain, and from the brain only, arise our pleasures, joy, laughter and jests, as well as our sorrows, pains, griefs, and tears. . . . all the most acute, most powerful, and most deadly diseases, and those which are most difficult to be understood by the inexperienced, fall upon the brain."

Hippocrates (*circa* 400 B.C.)

REGULATION OF EXCITATORY NEUROTRANSMISSION, SYNAPTIC PLASTICITY, AND LEARNING BY CYCLIN-DEPENDENT KINASE 5

by

AMMAR HAMAMI HAWASLI

DISSERTATION

Presented to the Faculty of the Graduate School of Biomedical Sciences

The University of Texas Southwestern Medical Center at Dallas

In Partial Fulfillment of the Requirements

For the Degree of

DOCTOR OF PHILOSOPHY

The University of Texas Southwestern Medical Center at Dallas

Dallas, Texas

July, 2007

REGULATION OF EXCITATORY NEUROTRANSMISSION, SYNAPTIC PLASTICITY, AND LEARNING BY CYCLIN-DEPENDENT KINASE 5

Ammar H. Hawasli
The University of Texas Southwestern Medical Center at Dallas, 2007

James A. Bibb, Ph.D.

Cyclin-dependent kinase 5 has been implicated many physiological and pathological processes in the central nervous system. To better understand Cyclin-dependent kinase 5's roles in the adult brain, we developed and studied several conditional Cyclin-dependent kinase 5 knockout model systems. Soon after conditional loss of Cyclin-dependent kinase 5, mice displayed improved hippocampal learning and enhanced synaptic plasticity in the hippocampal Schaffer collateral pathway. The genetically enhanced mice displayed increased N-methyl-D-aspartate receptor-mediated currents and elevated levels of the NR2B N-methyl-D-aspartate receptor subunit. The enhancement in synaptic plasticity

was directly attributed to the increased current through NR2B-containing receptors. NR2B levels were elevated in Cyclin-dependent kinase 5 knockout mice due to an impairment in the calpain-mediated degradation of NR2B. Consistently, Cyclin-dependent kinase 5 directly facilitated the degradation of NR2B cytoplasmic-tail *in vitro*. Cyclin-dependent kinase 5, NR2B, and calpain coimmunoprecipitated *in vivo* and directly bound one another *in vitro*. NR2B inhibited Cyclin-dependent kinase 5 activity *in vitro*, indicating a potential feedback mechanism. These findings suggested that Cyclin-dependent kinase 5 interacts directly with NR2B and calpain to facilitate the degradation of NR2B, thereby attenuating synaptic plasticity.

In addition to regulating functional plasticity, Cyclin-dependent kinase 5 also plays roles in structural plasticity and presynaptic function. Cyclin-dependent kinase 5 facilitated the calpain-mediated degradation of spectrin *in vitro*. Spectrin degradation and depolymerized actin levels were decreased in conditional Cyclin-dependent kinase 5 knockout hippocampus. These results implicate Cyclin-dependent kinase 5 dendritic in spine dynamics which is critical for synaptic plasticity. Loss of Cyclin-dependent kinase 5 also led to a presynaptic enhancement in post-tetanic potentiation and a deficit in paired-pulse facilitation, which are consistent with an increase in probability of synaptic vesicle release, due to increased numbers of vesicles in the readily releasable pool or altered sensitivity to presynaptic calcium.

Finally, chronic Cyclin-dependent kinase 5 loss produced increases in behavioral and neuronal excitability followed by electrographic abnormalities *in vivo* and reduced brain weight. These findings suggest that the enhancement in excitatory neurotransmission which initially led to improvements in learning and plasticity preceded excessive excitability and subsequent neuropathology. Consequently, Cyclin-dependent kinase 5 regulates excitatory neurotransmission, synaptic plasticity.

TABLE OF CONTENTS

PRIOR PUBLICATIONS

Hawasli AH and Bibb JA. Alternative roles for Cdk5 in learning and synaptic plasticity. *Biotechnology Journa*l. July, 2007; 2.

Hawasli AH, Benavides DR, Nguyen C, Kansy JW, Hayashi K, Chambon P, Greengard P, Powell CM, Cooper DC, Bibb JA. Cyclin-dependent kinase 5 governs learning and synaptic plasticity via control of NMDAR degradation. *Nature Neuroscience*. **10**, 880-886 (2007)

Hawasli AH, Saifee O, Liu C, Nonet ML, Crowder CM. Resistance to volatile anesthetics by mutations enhancing excitatory neurotransmitter release in Caenorhabditis elegans. *Genetics*. 2004 Oct;168(2):831-43.

LIST OF FIGURES

LIST OF ABBREVIATIONS

AAV, adeno-associated virus

ACSF, artificial cerebrospinal fluid

AMPA, α-amino-3-hydroxy-5-methyl-4-isoxazolepropionic acid

ANOVA, analysis of variance

AP5, 2-amino-5-phosphonopentanoic acid

APP, amyloid-precurser protein

ATP, adenosine triphosphate

BSA, bovine serum albumin

cal, calpeptin

CaMKII, Ca^{2+}/calmodulin-dependent protein kinase II

Cdk, cyclin-dependent kinase

CKI, casein kinase I

cont, control

D32, DARPP-32

DAPI, 4'-6-diamidino-2-phenylindole

DARPP-32, dopamine- and cAMP-regulated phosphoprotein, M_r 32,000

DMEM, Dulbecco's Modified Eagle's Medium

DMSO, dimethyl sulfoxide

DNQX, dinitroquinoxaline-2,3-dione

DTT, dithiothreitol

ECS, Electroconvulsive shock

EDTA, ethylenediamine tetraacetic acid

EEG, electronencephalographic

eGFP, enhanced GFP

EGTA, ethylene glycol-bis(2-aminoethyl ether)-N,N,N',N'-tetraacetic acid

EMG, electromyographic

EPSC, excitatory postsynaptic current

EPSP, excitatory postsynaptic potential

fEPSP, field excitatory postsynaptic potential

FISH, fluorescent *in situ* hybridizations

GSK3, glycogen synthase kinase 3

GFAP, glial fibrillary acidic protein

GFP, green fluorescence protein

H1, Histone subunit 1

HEPES, 4-(2-hydroxyethyl)-1-piperazineethanesulfonic acid

HFS, high frequency stimulus

IACUC, Institutional Animal Care and Use Committees

I-1, protein phosphatase inhibitor-1

ifen, ifenprodil

inhibitor-1, protein phosphatase inhibitor-1

i.p., intra-peritoneal

IPTG, isopropyl-β-D-thiogalactopyranoside

KREB's buffer, Kreb's-Henseleit Buffer

KO, knockout

LTD, long-term depression

LTP, long-term potentiation

MALDI-TOF MS, matrix-assisted laser desorption/ionisation-time of flight mass spectrometry

MAPK, mitogen-activated protein kinase

MK, MK801

Nim, nimodipine

NMDA, N-methyl-D-aspartate

PBS, phosphate-buffered saline

PKA, cAMP-dependent protein kinase, protein kinase A

PKC, protein kinase C

PPF, paired-pulse facilitation

PPD, paired-pulse depression

P_r, probability of vesicle release

PTP, post-tetanic potentiation

PSD-95, post-synaptic density 95

rAAV, recombinant adeno-associated virus

RIPA, RadioImmuno Precipitation Assay

rosc, roscovitine

RT, room temperature

s.c., subcutaneous

SC/CA1, the Schaffer Collateral pathway of the hippocampus

SDS-PAGE, sodium dodecyl sulfate polyacrylamide gel electrophoresis

STEP, Striatal enriched protein tyrosine phosphatase

TBS, theta burst stimulus

TBS-T, Tris-buffered saline-Tween

UT, University of Texas

WT, wild-type

CHAPTER ONE

REVIEW OF CYCLIN-DEPENDENT KINASE 5'S ROLES IN LEARNING AND SYNAPTIC PLASTICITY

Introduction

Although the molecular mechanisms underlying learning and synaptic plasticity are unclear, protein phosphorylation and dephosphorylation have been directly implicated. A plethora of protein kinases, including src, fyn, CaMKII, PKC, PKA, CKI, and MAPK, are known to mediate or modulate long-lasting plastic changes in the synapse as a result of information processing [1,2]. Such kinases control functional or structural changes in synaptic strength. Cyclin-dependent kinase 5 (Cdk5) and its activating cofactors have also been implicated. Studies using pharmacological inhibitors, cofactor knockout mice, and animals overexpressing a Cdk5 cofactor demonstrate that Cdk5 and its cofactors can mediate structural plasticity through phosphorylation of synaptic targets [3-8]. Recent data from conditional Cdk5 knockout mice suggest that Cdk5 also plays a role in regulating functional synaptic plasticity through protein—protein interactions[9] (*see chapter 2*). The information to date suggests a dual role for Cdk5 in synaptic plasticity as a kinase and as a binding partner (Table 1.1).

Cdk5 is a proline-directed serine/throenine kinase with high activity in the central nervous system. Unlike other cyclin-dependent kinases, Cdk5 does not rely on traditional cyclins but rather on its own activating cofactors, p35 or p39. Cyclin A contains 2 "cyclin box folds." In contrast, Cdk5 cofactors only carry a single cyclin box fold[10]. The presence of a serine rather than a threonine on the Cdk5 activation loop may also be important for the selective activation of Cdk5 by its cofactors[11]. Cdk5, p35, and p39 expression is ubiquitous throughout the

adult central nervous system. The distributions of Cdk5 cofactors but not Cdk5 are specific to neurons. Cdk5 and its cofactors are expressed at high levels in the hippocampus, cortex, striatum, piriform cortex, and tinia tecta. They are expressed at low to moderate levels in the olfactory bulb, anterior olfactory nuclei, amygdala, septum, thalamus, and hypothalamus[12]. Although p35 has been studied using traditional p35 *null* mice, the relative contributions of p35 versus p39 are still a mystery. Cdk5 cofactors can be cleaved by the Ca^{2+}-activated protease, calpain. p35 can be cleaved into p25 and p10 while p39 can be cleaved into p29 and p10. Both p25 and p29 activate Cdk5 *in vitro* and *in vivo*. Furthermore, the cleaved cofactors are more resistant to proteosomal degradation than their uncleaved counterparts. Thus, generation of p25 is thought to produce an increase in Cdk5 kinase activity[5]. Non-physiological Ca^{2+} influx as a result of neurotoxicity and ischemia are known to produce p25[13,14]. According to the current dogma, it is thought that Cdk5/p35 and Cdk/p39 play roles in physiological processes, while Cdk5/p25 and Cdk5/p29 contribute to the pathophysiology of many neurological diseases. Although we are unable to detect p25 or p29 in basal brain lysates, it is still unclear if the generation of p25 plays any role in the healthy brain.

Cdk5 is critical for cortical lamination during development as it regulates neuronal migration, differentiation, and connectivity [15]. These functions became apparent during the studies of traditional Cdk5 and p35/p39 double cofactor knockout mice. Both mouse lines exhibited severe disruptions in cortical lamination as neurons failed to migrate to the appropriate layers. The appearance of an inverted cortex is accompanied by aberrations in the cytoarchitecture of other structures including the hippocampus, brainstem, and cerebellum [16-18]. p35 knockout mice displayed similar but milder abnormalities in neuronal migration-dependent cortical lamination [19,20]. In complement with these findings, Cdk5

phosphorylates several adhesion and cytoskeletal proteins critical for neuronal migration [21].

Several lines of evidence suggest that Cdk5 regulates both neurotransmitter release and endocytosis in the adult synapse. Cdk5 has been suggested to both increase [22,23] and decrease [24] neurotransmitter release via phosphorylation of presynaptic substrates. Cdk5 has also been implicated in exocytosis and endocytosis via phosphorylation of numerous substrates including synapsin, amphiphysin I, dynamin, and others [25-27] and contributes to the pathogenesis of several neurodegenerative diseases such as Alzheimer's disease and psychiatric illnesses such as addiction [28-30].

Pharmacological assessment of Cdk5's role in learning and plasticity

Cdk5 was originally implicated in learning and memory in two studies by Fischer *et al*. [6,7]. The first reports showed that in Cdk5 gene expression and protein levels increased following acute immobilization. Treatment with butyrolactone I, a Cdk5 inhibitor, prevented stress-induced contextual fear conditioning. Furthermore, traditional contextual fear conditioning led to septohippocampal elevations in Cdk5 levels and inhibition of Cdk5 caused an impairment in contextual memory. Cdk5 inhibition appeared to only affect learning within a short window after training, suggesting that Cdk5 is primarily involved in the earlier aspects of learning [6,7]. Notwithstanding the nonspecificity intrinsic to pharmacological inhibitors, these studies revealed that Cdk5 is activated and plays an important role in hippocampus-dependent learning.

It is thought that synaptic plasticity is encoded as long term plastic changes in the synaptic compartments of neurons and is a critical component of learning and memory [2]. Therefore, it has been useful to study Cdk5's role in synaptic plasticity using *in vitro* neurophysiological approaches. The Cdk5 inhibitor, roscovitine, was suggested to reduce NMDA receptor-mediated currents

and blunt long term potentiation (LTP) in acute brain slices by attenuating Cdk5 phosphorylation of NR2A [14]. However, treatment of brain slices with the reported levels of roscovitine for such a brief period does not cause apparent reductions in most Cdk5 sites (personal observations). Furthermore, other attempts with both roscovitine and butyrolactone have failed to reproduce the reported impairment in LTP [31]. Interestingly, inhibition of Cdk5 with both roscovitine and butyrolactone reverses LTP impairments caused by synthetic amyloid β-peptide in the hippocampus [31].

Unfortunately, pharmacological Cdk5 inhibitors have a plethora of non-specific effects. The most widely used compound, roscovitine, directly affects Ca^{2+} and K^{+} channel function and neurotransmitter release independent of Cdk5 [32-34]. To complicate matters, butyrolactone, flavopiridol, olomoucine, and other inhibitors have dissimilar effects on receptors and signaling cascades. Nonetheless, the use of Cdk5 inhibitors has provided more evidence that Cdk5 is a key molecule in the signaling mechanisms underlying synaptic plasticity. It would be useful to continue using such inhibitors to assess the acute role of Cdk5 in plasticity and find the common effects of all Cdk5-selective inhibitors on long- and short-term synaptic plasticity. More specific Cdk5 inhibitors, which allow for systemic administration, are likely to serve as valuable tools and have therapeutic applications for neurodegenerative disorders, cognitive impairments, and neuropsychiatric illnesses.

Role of activating cofactor p35 in learning and plasticity

Several studies on learning have been performed with transgenic Cdk5 mouse models[3]. Due to the importance of Cdk5 in the development of the central nervous system, traditional Cdk5 knockout mice and p35/p39 cofactor double knockout mice do not survive after birth[17,18]. Single activating cofactor p35 *null* mutant mice, which survive past birth but display cortical lamination defects and

seizures[19], show deficits in spatial learning and memory as assessed in a water maze[8]. p35 homozygous and heterozygous knockout mice also display impairments in contextual fear conditioned memory[5]. These findings correlate with morphological data showing reduced number of spines and misalignment of cell soma in CA1 pyramidal neurons of p35 *null* mice [5,8]. Although p35 knockout is accompanied by potentially confounding developmental abnormalities and a compensatory elevation in p39 levels[8], these studies once again provide important evidence that Cdk5 is likely to be a critical component for synaptic changes which occur during learning.

Genetic loss of p35 also leads to a variety of interesting synaptic plasticity phenotypes in the Schaffer collateral pathway of the hippocampus. Although loss of p35 does not affect LTP when induced with a high frequency tetanus[8], p35 knockout mice exhibit a lower threshold for theta-burst rhythm-induced LTP [35]. Furthermore, NMDA receptor-mediated long-term depression (LTD) and depotentiation are impaired in p35 *null* mice. The alterations in Schaffer collateral LTP and LTD in p35 knockout mice suggest that there may be perturbations in the Ca^{2+}-dependent signaling pathways common to both forms of synaptic plasticity. However, functional and morphological aberrations in p35 knockout mice may contribute to the learning and plasticity phenotypes. For example, p35 knockout mice display increased excitability in the dentate gyrus of the hippocampus as a result of structural abnormities [36,37]. Although no gross irregularities in lamination are seen in the Schaffer collateral pathway and CA1 cell layer of the p35 *null* hippocampus [8], the abnormalities seen in the CA3 and dentate gyrus layers raise concern. Perhaps most interesting is how p35 *null* mice display a decreased threshold for LTP induction in the face of reduced spine numbers [5,35]. This raises the possibility of functional enhancements in plasticity.

Divergent roles of p25 in learning and plasticity

Study of animals overexpressing p25, the calpain-mediated cleavage product of p35, has served two purposes. Cdk5/p25 was shown to hyperphosphorylate tau, which aggregates as tangles in the neurons of Alzheimer's disease patients [38]. Data linking Cdk5 to Alzheimer's disease suggests that Cdk5/p25 may be detrimental to learning and memory [39]. Thus overexpression of p25 could lead to hyperphosphoyrlation of tau and serve as a mouse model for neurodegenerative diseases [5,40]. At the same time, since pharmacological inhibition of Cdk5 and genetic loss of p35 impair learning, any activation of Cdk5 might be predicted to be beneficial. Thus, transgenic p25 overexpression could either display learning enhancements due to hyper-activation of the kinase or deficiencies as a result of its aberrant Cdk5 activity. Interestingly, both scenarios appear to be correct. Transient and low-level expression of p25 improved plasticity and performance in learning tasks, while long-term overexpression led to memory and plasticity impairments [4,5,40,41].

Studies were performed with a transgenic mouse line which modestly overexpressed p25 in the hippocampus and neocortex. Initially, it was discovered that these mice displayed improvements in water maze reversal learning and cue-conditioned aversive memory [4]. Such enhancements appear sensitive to genetic strain background and predominate in females [41]. This is interesting as Cdk5 activity and expression in the hippocampus differs between mouse strains [7]. The truncated Cdk5 cofactor, p25, also appeared to have sex-specific effects, as mild expression of p25 preferentially impaired contextual learning in male mice [42]. All of these findings indicated that overexpression of p25 was likely to have contrasting roles with regard to its effects on learning and memory. However, it was not clear how these roles overlapped with Cdk5-related neurodegenerative processes.

Some clarification has come from studies using a different transgenic p25 overexpressing mouse line that allowed improved temporal control and higher levels of p25 overexpression [5]. Using this system, transient overexpression of p25 for 2 weeks was found to improve hippocampus-dependent fear conditioned contextual memory and spatial learning in the water maze task. These behavioral improvements correlated with increases in the number of hippocampal synapses and dendritic spines. However, longer periods of overexpression (*i.e.,* 6 weeks) impaired contextual- and cue-elicited fear conditioned memory and performance in the water maze task. Consistently, these learning impairments correlated with neurodegeneration and a decrease in the synapses number. Interestingly, long-term overexpression of p25 (*i.e.*. for 6 weeks) also led to a concomitant increase in dendritic spine number, possibly representing proliferation of nonfunctional synapses or connectivity, and compensation in remaining functional neurons. For a third model of p25 overexpression, p25 was transiently overexpressed for 2 weeks, followed by 4 weeks of p25 repression. Interestingly, this led to long lasting improvements in learning and increases in synapse number. Long-term structural changes observed after 2 weeks of expression and 4 weeks of repression likely contributed to improved learning [5].

Overexpression of p25 has also been found to have opposing effects on synaptic plasticity [5]. Transient high expression of p25 for 2 weeks caused a large increase in the overall magnitude of LTP. Transient overexpression followed by repression of p25 led to a similar, albeit smaller, enhancement in LTP. In contrast, long-term expression of p25 produced an impairment in LTP [5,41]. Both the behavioral and electrophysiological phenotypes correlate with structural changes as detected via immunohistochemistry, electron microscopy, and golgi staining techniques. These changes were also accompanied by increases in the phosphorylation of PAK-1, NMDA receptors, and PSD-95. The cytoarchitectural data support a conclusion that long-term structural changes due to transient

expression of p25 improves synaptic plasticity, while longer-term p25 of expression leads to structural and functional deficits in plasticity. Although much emphasis has been placed on structural plasticity, there is some evidence that overexpression of p25 may affect functional plasticity, as well. Transient but not long-term overexpression of p25 led to an increase in NMDA receptor-mediated current [5]. Given the importance of NMDA receptors to LTP in the Schaffer Collateral, the increase in NMDA receptor-mediated current may contribute to the LTP enhancement. Perhaps, the increase in NMDA receptor-mediated current may be attributed to increased phosphorylation of NR2A [14]. However, this aspect remain unclear, as long-term overexpression (*i.e.,* 6 weeks) of p25 leads to increases in NR2A phosphorylation without differences in NMDA receptor-mediated current.

Given the fundamental relationship between glutamate receptor regulation and structural synaptic plasticity, further study of the NMDA receptor-mediated current in p25 overexpressing mice is warranted. For example, any differences observed in synaptic plasticity between transient overexpression (*i.e.,* 2 weeks) and transient overexpression followed by repression (*i.e.,* 2 weeks on, 2 weeks off) [5] may be due to changes in NMDA receptor-mediated current.

Aberrations in presynaptic function may affect synaptic efficacy and confound the interpretation of synaptic plasticity experiments. Gross measurements of presynaptic function revealed that transient but not long-term overexpression of p25 led to an apparent deficit in the presynaptic vesicle reserve pool [5]. Although a reduction might be thought to ultimately weaken synaptic strength, it may occur in the context of more prevalent enhancements in the postsynaptic machinery. Interestingly, long term overexpression of p25 led to a potential aberration in probability of presynaptic vesicle release [5]. Although unclear, these findings underscore Cdk5's role in the presynaptic compartment, which may affect synaptic transmission and synaptic plasticity.

Although, long-term overexpression of p25 clearly leads to neurodegeneration and associated dysfunction in plasticity and learning [5,40], the exact nature of p25's opposing role in learning and plasticity remains unsolved. While p25 generation has been linked closely to neurotoxicity and neurodegeneration [13,30,39], appreciable levels of p25 have not been detected in normal brain. Nonetheless, these data together with other studies raises the possibility that small amounts of p25 may be generated during excitatory neurotransmission and contribute to synaptic remodeling. This suggests there may be a continuum between the biochemical processes underlying memory and those contributing to neurodegeneration. This model would predict that physiologically relevant synaptic activation may lead to low and transient p25 generation. Meanwhile, excitotoxic insult via NMDA receptors [35] may generate excessive and longer lasting amounts of p25 and ultimately lead to neurodegeneration.

The highly active Cdk5/p25 has been suggested to phosphorylate "aberrant" Cdk5 substrates, such as the NR2A NMDA receptor subunit and tau. Consistently, overexpression of p25 has been reported to increase phosphorylation of NR2A [5]. A panoply of additional aberrant substrates involved in cell death and cell cycling have also been suggested in the literature. Thus, it is not difficult to conjecture on how long term p25 generation may lead to neurodegeneration via multiple pathways. However, why does transient p25 expression lead to enhancements in plasticity? Perhaps Cdk5/p35 functions in the adult hippocampal synapse to attenuate synaptic plasticity. Consistent with this hypothesis, Cdk5 was shown to reduce the PSD-95 multimerization with NMDA receptors [43]. Synaptic activation may lead to a transient and synapse-specific cleavage of p35 to p25 and translocation of Cdk5 towards the cytoplasm. This may remove Cdk5 from its normal substrate pool and prevent Cdk5's attenuation of plasticity. At the same time, it may recruit factors which further contribute to synaptic remodeling. Meanwhile, excitotoxic insult may lead to excessive generation of p25,

phosphorylation of "aberrant substrates," and conversion to the neurodegenerative state. Interestingly, synaptic pruning throughout adulthood and especially after 65 years of age has been suggested to contribute to cognitive decline [44]. Overexpression of p25 and hyperphosphorylation of "aberrant Cdk5 substrates" may accelerate the normal processes which lead to cognitive decline and tip the balance towards pathological neurodegeneration.

Control of learning and functional plasticity via protein-protein interactions

The studies of Cdk5 in learning have, thus far, had depended on pharmacological reagents or cofactor manipulation. Below (*in chapter 2)* we describe recently conducted studies on learning and plasticity performed in conditional Cdk5 knockout mice[9]. These studies reveal a novel mechanism through which Cdk5 modulates functional plasticity via protein—protein interactions.

Table 1.1: Roles of Cdk5 and activating cofactors in hippocampal learning & synaptic plasticity

Finding	Model System	Reference
Roscovitine blocks LTP induction and NMDAR-mediated currents	adult rats	Li *et al. PNAS* 2001
Cdk5 is required for associative learning	BALB/c mice	Fischer *et al. J Neuroscience* 2002
Role of Cdk5 in learning is strain dependent and related to the septo-hippocampal circuitry	BALB/c and C57BL/6J mice	Fischer *et al. J Neuroscience* 2003
Improved reversal learning and altered fear conditioning following p25 overexpression	p25 overexpressing mice	Angelo *et al. EJN* 2003
Roscovitine and butyrolactone do not affect LTP induction but prevent the inhibition of LTP by amyloid β-peptide	adult rats	Wang *et al. J Neuroscience* 2004
p35 null mice exhibit lower threshold for LTP induction	p35 KO mice	Wei *et al., J Neurochemistry* 2005
p35 null mice display impairments in LTD and spatial learning	p35 KO mice	Ohshima *et al., J. Neurochemistry* 2005
Transient expression of p25 enhances hippocampal LTP and learning and increases the number of dendritic spines and synapse number	p25 overexpressing mice	Fischer *et al, Neuron* 2005
Prolonged expression of p25 impaired hippocampal LTP and learning and leads to neuronal loss and decreased synapse numbers	p25 overexpressing mice	
Sexual dimorphisms modulate the effects of p25 overexpression on plasticity and memory	p25 overexpressing mice	Angelo *et al. EJN* 2005
Overexpression of p25 impairs contextual learning but not latent inhibition	p25 overexpressing mice	Mizuno *et al. Neuroreport* 2006
Inhibition of histone deacetylases causes recovery of learning and memory following prolonged p25 overexpression	p25 overexpressing mice	Fischer *et al. Nature* 2007
Conditional Cdk5 KO mice display enhancements in learning and synaptic plasticity	conditional Cdk5 KO mice	Hawasli *et al. Nat. Neuroscience* 2007 (see chapter 2)
Cdk5 modulates plasticity by facilitating NMDAR degradation		

CHAPTER TWO

CYCLIN-DEPENDENT KINASE 5 GOVERNS LEARNING AND SYNAPTIC PLASTICITY VIA CONTROL OF NMDAR DEGRADATION

Summary

Learning is accompanied by modulation of post-synaptic signal transduction pathways in neurons. While the neuronal protein kinase Cyclin-dependent kinase 5 (Cdk5) has been implicated in cognitive disorders, its role in learning has been obscured by the perinatal lethality of constitutive knockout mice. Here we report that conditional knockout (KO) of Cdk5 in the adult mouse brain improved performance in spatial learning tasks and enhanced hippocampal long term potentiation (LTP) and *N*-methyl-D-aspartate ionotropic receptor (NMDAR)-mediated excitatory post-synaptic currents. Enhanced synaptic plasticity in Cdk5 KO mice was attributed to reduced NR2B degradation which caused elevations in total, surface, and synaptic NR2B subunit levels and current through NR2B-containing NMDARs. Cdk5 facilitated the degradation of NR2B by directly interacting with NR2B and its protease, calpain. These findings reveal a novel mechanism through which Cdk5 facilitates calpain-mediated proteolysis of NR2B and may control synaptic plasticity and learning.

Introduction

The cellular and molecular mechanisms underlying declarative learning and memory constitute a predominant area in basic neurobiological research and are of considerable clinical relevance. A generally accepted hypothesis is that memories are formed within specific circuits of the brain through changes in the strength of neuronal synapses[2]. One form of synaptic plasticity, long-term

potentiation (LTP), appears to be a critical component of information processing and memory storage in the hippocampus[2,45]. Information storage at the behavioral and cellular levels depends upon neurotransmitter receptor complexes and downstream intracellular signaling cascades. A better understanding of these biochemical pathways is a crucial step in delineating the processes controlling learning and synaptic plasticity.

The proline-directed serine/threonine protein kinase Cdk5, together with its neuronal-specific activating cofactors p35 and p39, has been implicated in a plethora of normal and pathological processes in the mammalian nervous system[5,6,8,16,18,35,38,46-48]. However, assessment of Cdk5 function in learning and synaptic plasticity has been limited by congenital abnormalities in constitutive knockout mice[8] and by pharmacological non-specificity[33].

To circumvent these confounds, we examined the effects of conditional Cdk5 knockout (KO) on contextual and spatial learning and synaptic plasticity. Loss of Cdk5 in the adult brain improved performance in hippocampal behavioral learning tasks, enhanced synaptic plasticity, and elevated currents through NMDARs. Biochemical and neurophysiological analyses revealed that the enhanced plasticity in Cdk5 KO mice was due to changes in NR2B subunit degradation. These findings reveal a novel pathway through which Cdk5 may regulate ionotropic glutamate receptor composition via protein-protein interactions.

Experimental Procedures

Materials and reagents

All chemicals were from Sigma, except where indicated. Protease

inhibitors, dithiothreitol (DTT), isopropyl-β-D-thiogalactopyranoside (IPTG), and adenosine triphosphate (ATP) were from Roche. [γ-^{32}P]-ATP was from Perkin Elmer Life Sciences. Cdk5 and p25-His_6 were co-expressed in insect Sf9 cultures using baculovirus vectors and affinity-purified by Kanehiro Hayashi (UT Southwestern Medical Center) [49] or purchased from Panvera/Pfizer. Oligonucleotides were ordered from Integrated DNA Technologies.

Knockout Generation, histology, and molecular biology

The *floxed* line was generated by Paul Greengard (Rockefeller University) as previously described[50]. *Floxed* Cdk5 and Cre-ER^T mice (provided by Pierre Chambon, Institut de Génétique et de Biologie Moléculaire et Cellulaire)[51] were crossed and F3 male offspring were treated with 4-hydroxytamoxifen (15 days, 66.67 mg per kg, i.p.). Hydroxytamoxifen (100 mg; Sigma) was suspended in 1.0 mL of absolute ethanol and sonicated (Branson 1510 sonicator) for 30 min at room temperature (RT). After adding sterile sunflower oil (14 mL), the suspension was sonicated for an additional 30 min at RT. The hydroxytamoxifen solution was always prepared in an opaque glass container and injected immediately after preparing syringes as hydroxytamoxifen is extremely light-sensitive. Remaining hydroxytamoxifen was stored in the dark at 4 ^oC and sonicated for 30 min prior to use for the next set of injections. Generally, the hydroxytamoxifen was prepared freshly every other day of injection.

All experiments were performed with 10–12 week old males, 2–4 weeks post-hydroxytamoxifen treatment. PCR genotyping with primers encompassing *loxP* sites or within the Cre-ER^T transgene were used to distinguish genotypes. Primers for Cdk5 allele genotyping had the following nucleotide sequences: 5'-GCAGGCCTTCGTTCCTCCC-3' and 5'-CCTGACACGCTTCAGAGCC-3'. Primers for the Cre-ER^T transgene had the following sequences: 5'-

CAACCGAGCTGAAGCATTCTGCC-3' and 5'-CATCAACGTTTTC TTTTCGGATC-3'. Quantitative real-time PCR was performed as described[52] on whole hippocampus cDNA using the Cdk5 primers, 5'-GGCTAAAAACCGGGAAACTC-3' and 5'-CCATTGCAGCTGTCGAAATA-3', NR2B primers, 5'-TCTGCCTTCTTAG AGCCATT CAG-3' and 5'-AGACAGCTACAGCAGAGAC-3', NR2A primers, 5'-CCTCGAACCCTTCAGCGCCT-3' and 5'-AATGGCAGAGACAATGAGCAG-'3, and NR1 primers, 5'-GCAGGTGGAGTTGAGCACCATGTAC-3' and 5'-AGCTTGTTGTCCCGCACA-3'. Radiolabeled *in situ* hybridizations were performed as described[52,53]. Cdk5 from glia and presynaptic terminals from non-hippocampal regions may have contributed to Cdk5 signal measured using rtPCR, immunoblot, and activity analyses. For more accurate and higher resolution analysis, fluorescent *in situ* hybridizations were performed using digoxigenin-labelled mRNA probes and analyzed with confocal microscopy, essentially as decribed[52]. ^{35}S-UTP (Perkin Elmer)- and digoxigenin-UTP (Roche)-labelled mRNA probes were synthesized from Cdk5 and Cre cDNA with T3 or T7 promoter-dependent reverse transcriptase (Ambion). The template for the Cdk5 *in situ* hybridization probe was created from mouse brain cDNA using the primers: 5'-GCGCGGTACCACCTACGGAACTGTGTT-3' and 5'-GTCGCCGCGGCT TCACAATCTCAGGG-3'. Clones for *in vitro* transcription were prepared by Janice Kansy (UT Southwestern Medical Center). Slide-mounted sixteen micron cryosections were fixed, dehydrated, labelled overnight with the probe, and washed. Radiolabeled slides were placed into a cassette and exposed to X-ray film for 1-4 weeks before developing (KODAK). Fluorescent-labelled *in situ* hybridizations were incubated with secondary horse radish peroxidase-rabbit anti-digoxigenin, washed, and signal was amplified with tyramide signal Cy3/Cy5 amplification (Perkin Elmer). Fluorescent-labelled slices were mounted with DPX, allowed to dry, and visualized on epifluorescent and confocal microscopes

(Olympus). p35 and p39 KO mice were provided by LH Tsai (Massachusetts Institute of Technology) and prepared by Kanehiro Hayashi (UT Southwestern Medical Center).

Immunoprecipitations and surface labeling

Immunoprecipitations, immunoprecipitation-kinase assays, and surface-labelling experiments were performed using standard methodologies[5,47,53,54]. For immunoprecipitations, hippocampi were lysed using a dounce homogenizer and radioimmunoprecipitation assay (RIPA) buffer: 65.2 mM Tris-HCl, 150 mM NaCl, 1 % Triton X-100, 0.1 % SDS, 2 mM EDTA, 0.5 % deoxycholate, 50 mM NaH_2PO_4, 10 mM $Na_4P_2O_7$, 5 mM NaF, 1 mM Na_3VO_4, 0.1 mM phenylmethylsulphonyl fluoride, and mammalian protease inhibitor cocktail tablet (Roche or Sigma). Clarified lysates were incubated with primary antibodies then resin-conjugated protein A or protein G at 4˚C, prior to washes and SDS-PAGE/immunoblot analysis. Alternatively, immunoprecipitated Cdk5 was seeded into a kinase reaction using recombinant histone-1 as a substrate (see kinase reactions *in vitro* description below). For surface labelling experiments, acute hippocampal slices were incubated with Sulfo-NHS-biotin (Pierce) in ACSF (see neurophysiology below for recipe). Following lysis in RIPA buffer and a brief centrifugation, biotinylated proteins were immunoprecipitated using immobilized NeutrAvidin Protein (Pierce). A fractions of each lysate was kept aside for comparison to total protein amounts. Immunoprecipitates were washed and analyzed by SDS-PAGE immunoblot analyses.

Immunoblot analysis of tissue homogenates

Hippocampal slices and gross dissections of brain regions were homogenized by sonication in boiling hot lysis buffer (1% SDS and 50 mM NaF), then immediately boiled for an additional 10 min. An equal amount of total protein (100 μg of brain homogenate) from each sample as determined by the bicinchoninic acid (BCA) protein assay (Pierce) was subjected to 12-15% SDS-PAGE and transferred to nitrocellulose membrane overnight. Membranes were blocked in 5% milk + TBS-Tween (TBS-T) for one hour, then incubated with primary antibodies overnight at 4°C. After a brief rinse with deionized water, membranes were washed 3 x 10 min with TBS-T and incubated with horseradish peroxidase-conjugated goat anti-rabbit secondary antibody (Chemicon, 1:8000) for one hour at room temperature. Following more deionized water rinses and 5 x 10 min washes with TBS-T, membranes were developed with an enhanced chemiluminescence immunodetection system (Amersham Biosciences). All antibody incubations were in 5% milk. All phosphoprotein levels were quantified relative to total protein. Otherwise, immunoblot quantitation is shown relative to tubulin loading controls. Antibodies for immunoblot assays were used at the following dilutions: Calpain (1:200, Santa Cruz), NR2A (1:250, Santa Cruz), pTyr1472 NR2B (1:1000, Phosphosolutions), GluR1 (1:750; Chemicon), pS 1303 NR2B (1:500, Upstate), Cdk5 (1:200, J-3, Santa Cruz), alpha-tubulin (1:5000, Chemicon), PSD-95 (1:500,000, Upstate), ERK (1:500, Santa Cruz), CamKII (1:10,000, Santa Cruz), pS1480 NR2B (1:200, from R. Huganir), NR2B (1:1000, Phosphosolutions), NR1 (1:1,250, BD Biosciences), Cre (1:10,000, Santa Cruz). Antibodies not listed here were provided by laboratory colleagues. For immunoprecipitations, antibodies were used in excess and the amount of antibody used per weight of tissue varied highly from lot to lot. Therefore, antibody amount was optimized for each lot of antibody.

Synaptosomal preparations

Synaptosomes were prepared by Kanehiro Hayashi (UT Southwestern Medical Center). Hippocampi or cortex/striatum from 3 KO or WT mice were dissected and homogenized with buffer A containing 5 mM Tris-HCl (pH 7.4), 1 mM $MgCl_2$, 0.5 mM $CaCl_2$, 1 mM NaF, 0.1 mM PMSF, and protease cocktail inhibitor. Homogenized sample was centrifuged at 1,400 x g for 10 min to obtain P1 and S1 fraction. The P1 fraction was resuspended with buffer A and centrifuged at 700 x g for 10 min to obtain S1' fraction. S1 and S1' fraction was mixed and centrifuged at 13,800 x g for 10 min to obtain P2 fraction (pellet). P2 fraction was resuspended in buffer B containing 6 mM Tris-HCl (pH 8.0), 1 mM NaF, 0.1 mM PMSF, 0.32 mM sucrose containing protease cocktail inhibitor and layered on the top of a discontinuous sucrose gradient consisting of 0.85, 1.0 M and 1.25 M sucrose. The gradient was centrifuged at 82,500 x g for 2 h. Synaptosome fraction was collected and centrifuged at 38,200 x g for 20 min. The pellet was lysed with lysis buffer containing 1 % SDS and 50 mM NaF, and subjected to SDS–PAGE and immunoblot analysis.

Generation of PSD-95 mutant clones

Recombinant wild-type and mutant PSD-95 proteins were derived from a pGEX-2T-PSD-95 vector provided by Marcie Colledge, Ph.D. Single and double mutations were generated using site directed mutagenesis (Stratagene). S19A mutant was generated with primers with the following nucleotide sequences: 5'-CCAAGA TGAAGA CGCGCC CCCTCT GGA-3' and 5'-TCCAGA GGGGGC GCGTCT TCATCT TGG-3'. S25A mutants were generated using primers with the following nucleotide sequences: 5'-CCCCCT CTGGAA CACGCA CCGGCC CACCTC C-3' and 5'-GGAGGT GGGCCG GTGCGT GTTCCA GAGGGG G-3'. Mutagenesis was performed under the following conditions: 95 ºC for 30 sec,

95 ºC for 30 sec, 55 ºC for 60 sec, 68 ºC for 14 min 12 sec, repeat steps 2-4 16 times. Following a digest with Dpn1 restriction enzyme (Stratagene), mutant clones were transfected into chemically-competent *E.coli*, sequenced (McDermott Sequencing Center, UT Southwestern Medical Center), and prepared for protein purification.

Purification of recombinant NR2B and PSD-95

The recombinant full length C-terminus of NR2B-GST (plasmid kindly provided by K. Ulrich Bayer, University of Colorado), GST, protein phosphatase inhibitor–1, PSD-95, and PSD-95 mutants were purified using standard protein purification techniques. Chemically competent BL21 (DE3) *E. coli* were transformed with expression vectors. Cultures were grown at 37°C in LB media until the OD_{600} reached 0.5-0.8, at which time 0.1 mg/ml IPTG was added. Induction proceeded overnight hours at room temperature after which cells were harvested and washed with phosphate-buffered saline (PBS). Pellets from 10,000 x g spins were stored at –80°C for subsequent lysis by French press in PBS and protease inhibitors. Cleared lysates were incubated with a glutathione sepharose resin (Amersham) for 1-2 hours at 4°C, then washed 3 x 10 min in PBS. Bound protein was batch-eluted with elution buffer containing 10 mM reduced glutathione in 50 mM Tris-HCl, pH 8.0. Samples were dialyzed overnight in 10 mM 4-(2-hydroxyethyl)-1-piperazineethanesulfonic acid (HEPES), 1 mM DTT, 5% glycerol, pH 7.4, with two changes of buffer. Proteins were stored at –80°C following analysis for purity by 12.5% sodium dodecyl sulfate polyacrylamide gel electrophoresis (SDS-PAGE) and Coomassie Brilliant Blue staining. A fresh aliquot of protein was used for each experiment, as recombinant C-terminus NR2B is *extremely* sensitive to freeze-thaw degradation. The primary wild-type NR2B band ran ~90 kDa; lower bands, likely correspond to degradation products

or incomplete translation as the GST was fused to the N-terminus. PSD-95-GST purified well and ran at ~98 kDa.

In vitro protein phosphorylation reactions

Protein phosphorylation reactions were generally conducted at 30°C in a final volume of at least 10 µl containing 10 µM substrate, 100 µM ATP, and 0.2-0.4 mCi/ml [γ-^{32}P]-ATP as described[47]. Cdk5 reactions were conducted in 30 mM 3-(N-morpholino)-propanesulfonic acid (MOPS), pH 7.2, and 5 mM $MgCl_2$. A mixture of ATP and [γ-^{32}P]-ATP was used to initiate the reactions. Reactions were stopped by the addition of an equal volume of 5x protein sample buffer (400 mM Tris, pH 6.8, 5% SDS, 35% glycerol, 128 mM DTT, and bromophenol blue). Time-course reactions were performed by removing aliquots from a master reaction at defined times. Dilutions of leftover reaction mixture (5 µl of 1:100 and/or 1:500) spotted onto filter paper served as standards (counts/pmol phosphate) for stoichiometric calculations. Following separation of phosphorylated substrate from unbound [γ-^{32}P]-ATP by 15% SDS-PAGE, the dried gel and standards were analyzed by Phospho Imager technology, and bands were quantitated to determine the amount of phosphorylated product in each reaction. The stoichiometries of reactions lacking [γ-^{32}P]-ATP were inferred from reactions containing [γ-^{32}P]-ATP that were conducted in parallel.

In vitro binding assays

For binding assays, purified NR2B-GST or GST was rebound to glutathione sepaharose resin. Cdk5 was reconjugated to Ni^{2+} agarose. Protein/resin and controls were washed, incubated in Ca^{2+}–free buffer with potential binding partners (NR2B, Cdk5 and/or calpain-1) for 1 hour at 4 ˚C, washed three times, and then analyzed by SDS-PAGE and immunoblotting.

Peptide Microarray

Peptide microarray binding assay were performed by LC Sciences (Houston, TX). Eight amino acid cassettes spanning calpain-1 and the cyotplasmic tail of NR2B were generated and immobilized onto a micro array in triplicate. The array was blocked with 1X PBS, 1% BSA, 0.5% non-fat milk, 0.05% Tween-20, pH 7.0 at 4 ˚C overnight. Array was then washed with 1 mL of PBS, 1% BSA, pH 7.0 and scanned using the LC Sciences proprietary PMT700 device to assess for background signal. Microarray was then incubated with 1.357 mg/mL Cdk5/p25 in binding buffer (100 mM sodium phosphate, 150 mM NaCl, 1% BSA, pH 7) at 4 ˚C for 1 hour, washed, and incubated with Cdk5 mouse monoclonal IgG antibody (10 ng/mL, Santa Cruz, J-3) in binding buffer for 30 min. The array was washed, incubated with a goat anti-mouse secondary IgG Cy5 conjugate antibody for 30 min, washed again, and then scanned using the PMT700 system. Background binding gave a signal intensity of < 250 (arbitrary units). Intensities were plotted and compared with one another. Candidate peptide sequences showed consistent binding (3 out of 3), a gradient of low to high signal intensities, and peak signal intensities >10,000.

In vitro NR2B degradation assays

In vitro calpain-mediated NR2B degradation assays were essentially performed as described[55]. Recombinant full length C-terminus of NR2B (0.5 μM) was incubated at 4 ˚C for 90 min in the presence or absence of Cdk5/p25 (0.1 μg/μL, Panvera) to allow for binding. Time course of NR2B degradation was conducted at 37˚C after the addition of Ca^{2+}-activated calpain I (Sigma, 1:1,000). Cdk5 and calpain activities were blocked by removing adenosine triphosphate/Mg^{2+} and Ca^{2+}, respectively.

Slice Pharmacology

400 μm transverse hippocampal slices were prepared in ice cold KREB's buffer and then allowed to recover in 30 °C oxygenated KREB's buffer for 30 min similarly as described[56]. Slices were then incubated in 50 μM NMDA for 30 or 60 min or KREB's buffer for 60 min. Additional slices were incubated for 60 min in 50 μM NMDA and 20 μM calpeptin, a calpain inhibitor, to confirm calpain-dependence of cNR2B generation.

Behavior

Mice were housed 4–5 per cage in a colony maintained at 23 °C with a 12 h light/dark cycle (lights on from 7:00 A.M. to 7:00 P.M.) and *ad libitum* food and water. All procedures were approved by the UT Southwestern Institutional Animal Care and Use Committees (IACUC). Behavior was performed with the experimenter blind to genotype. Contextual and cue fear conditioning were performed using one or two 1–second 0.8 mA foot shocks, respectively, as described[57]. Animals were placed into a box, and scored for freezing before, during, and after tone/shock pairing. Twenty-four hours later, the animals were re-exposed to the same box and scored for freezing behavior. For extinction trials, freezing to the conditioned context was assessed for 5 min, 24, 48, 72, and 96 h after training and normalized to 24 h post-training value. Nociceptive responses were determined by measuring the stimulus threshold to elicit flinching, jumping, and vocalizing as described[57]. Hotplate latency to hind-paw lick, jumping, or vocalization was assessed after animals were placed on 52 ˚C hotplate. Locomotor activity and elevated plus anxiety maze was performed by David Benavides (UT Southwestern Medical Center) similarly as described[57]. For the open field anxiety test, each animal was placed in the center of a plexiglass box under standard room-lighting conditions. Locomotor activity was quantitated using number of

photoreceptor beam breaks and open field anxiety was measured as time spent in the center of the box using a standard computer tracking system. Water maze task was performed essentially as described[57]. Animals were placed into a pool of opaque water, which was surrounded by 4 visual cues, and allowed to find a submerged hidden platform for 4 trials per day over several days. After indicated number of training days, the platform was removed and spatial learning was tested by testing preference for the target quadrant. For reversal water maze test, the platform was relocated to the opposite quadrant and animals were trained to relearn a the new location. Reversal training was followed by a reversal probe trial in which the platform was once again removed from the pool. For cue-reversal test, animals were tested for spatial preference after 2 of 4 cues had been removed. Data was collected and quantified with a standard video tracking system (Ethovision, USA) and analyzed for statistical significance by 2-way analysis of variance with *post hoc t*-tests or one-way analysis of variance.

Neurophysiology

Transverse hippocampal slices were prepared in cutting saline (200 mM sucrose, 3 mM KCl, 1.4 mM NaH_2PO_4, 26 mM $NaHCO_3$, 2 mM $MgCl_2$, 2 mM $CaCl_2$, 10 mM glucose) and maintained in an interface chamber containing artificial cerebrospinal fluid[58]. Extracellular SC/CA1 voltage measurements in field recordings (fEPSPs) were synaptically evoked at 0.033 Hz and performed at 27 °C. 2 x TBS and 3 x TBS were defined as 10 and 15 bursts, respectively (4 pulses per burst at 100 Hz, 5 Hz burst frequency). 50 and 100 Hz tetani were delivered for 1 sec. Basal input/output measurements, paired-pulse facilitation, and LTP experiments were performed in the absence of any drugs while $fEPSP_{NMDA}$ and fEPSP NMDA:AMPA measurements were performed in the presence of 2 μM SR95531, 1 μM atropine, 50 μM $NiCl_2$, 10 μM nimodipine, and 50 nM tetrodotoxin (TTX). NMDAR-mediated fEPSPs were recorded in the

presence of 20 μM 6,7-dinitroquinoxaline-2,3-dione (DNQX, Tocris) and blocked with 50 μM DL-2-amino-5-phosphonopentanoic acid (DL-AP5). fEPSP data acquisition and analysis were performed using the multielectrode MED64 hardware and software packages, essentially as described[59]. Additional analyses were performed using custom macros running under Igor Pro and Microsoft Excel. Whole-cell voltage-clamp SC/CA1 EPSCs were recorded by Chan Nguyen (UT Southwestern Medical Center), using instruments similar to those described[58], in order to more selectively isolate NMDAR-mediated currents and eliminate threshold non-linearities. Whole-cell recording electrodes (2–3MΩ) were filled with 7.3 pH intracellular cell solution (mM): 110 D-Gluconic acid, 110 CsOH, 20 CsCl, 10 Disodium phospho-creatine, 0.3 NaGTP, 2 MgATP, 10 HEPES, 0.5 EGTA, 5 Lidocaine N-ethyl bromide. EPSCs were evoked at 0.05 Hz at 32˚C, and stimulus intensity was chosen to elicit 125–150 pA EPSCs at –70 mV holding potential. Prior to each sweep, a –5 mV step pulse was injected to assess and control for series resistance. τ for EPSCs was calculated with a single-exponential fit. Whole-cell recordings were performed in the presence of 2 μM SR95531, 1 μM atropine, 50 μM $NiCl_2$, and 10 μM nimodipine. NMDAR-mediated EPSCs were isolated at +40 or +60 mV in the presence of 20 μM DNQX and blocked with 50 μM AP5. NMDA:AMPA EPSC ratio was calculated under +40mV/20 μM DNQX and –70 mV conditions. An alternative whole-cell SC/CA1 EPSC NMDA:AMPA ratio was calculated in the absence of DNQX: the NMDA component was measured as area of the +40mV EPSC from 45 ms to 350 ms in 2 μM SR95531, 1 μM atropine, 50 μM $NiCl_2$, and 10 μM nimodipine. Ifenprodil-sensitive NMDAR-mediated currents were recorded at +60 mV holding potential in the presence of 20 μM DNQX. Quantitation for $I_{\text{ifen-sensitive}}$ was calculated as area between I_{NMDA} and $I_{\text{ifen-resistant}}$, normalized to I_{NMDA}. Whole cell data acquisition and analysis were performed using custom macros running under Igor Pro, Microsoft Excel, and GraphPad Prism.

Data analysis

Image J (NIH) was used to quantitate immunoblots. Results are stated as percentage decrease or fold increase of the mean ± standard error. Individual bands of representative blots were always taken from the same exposure of the same membrane, and all represented total bands were derived from the same sample on the same membrane. Differences between data groups were evaluated for significance using analysis of variance (ANOVA). When applicable, interactions between genotype and day/trial/time/etc. were analyzed statistically using a two-way analysis of variance with *post hoc t*-tests. Statistical significance was set to $p < 0.05$.

The data analysis and subsequent interpretation were entirely dependent on the use of statistics to determine whether a particular finding was real or occurred by chance. Analysis of variance and *t*-tests were employed to determine statistical significance. A statistical significant of 0.05 indicated that there was a 5% probability the a "difference" occurred by chance. Therefore, in order to assess whether a given finding was real, it was essential to repeat each experiment multiple times. When the differences were small enough to warrant suspicion, it was especially critical to observe the same finding several times over the course of several experiments. Thus, the statistically different findings emphasized in this chapter and throughout the dissertation are real and not a consequence of random chance.

Results

Conditional loss of Cdk5 in the adult mouse brain

We generated an inducible conditional Cdk5 knockdown model to study the role of Cdk5 in learning and synaptic plasticity. This Cre/*loxP* system allowed temporal control of Cdk5 gene deletion in adult brain. Using homologous

recombination, exons encoding vital Cdk5 catalytic domain components were flanked with *loxP* elements (*floxed*; **Fig. 2.1**). Homozygous *floxed* Cdk5 mice were crossed with animals bearing an inducible Cre-ER^T recombinase transgene under control of the prion protein promoter[51].

Conditional Cdk5 knockdown in homozygous *floxed* mice carrying the Cre transgene (KO) was achieved by administration of hydroxytamoxifen, an estrogen receptor antagonist that induces nuclear translocation of the Cre-ER^T recombinase[51]. This technique allowed for temporal control of knockout induction. *Floxed* alleles, the Cre transgene, and drug treatment had no individual effects on Cdk5 levels (**Supplementary Fig. 2.1a**). Hydroxytamoxifen-dosed homozygous *floxed* mice lacking the Cre-ER^T transgene also exhibited no loss in Cdk5 and served as controls (WT; **Supplementary Fig. 2.1a**). Furthermore, Cdk5 KO did not alter the apparent basic hippocampal cytoarchitecture (**Supplementary Fig. 2.1b**). Optimization of the hydroxytamoxifen dosing regimen ensured consistent Cdk5 knockdown in the mouse forebrain (**Fig. 2.2**). There was a dose-dependent decrease in Cdk5 expression following treatment with hydroxytamoxifen. Moreover, administration of hydroxytamoxifen led to similar Cdk5 knockdown 2 and 6 weeks following treatment as assessed by *in situ* hybridization analyses. This indicates that treatment with hydroxytamoxifen resulted in long-term knockdown of Cdk5 message. Regional knockdown of Cdk5 in mouse forebrain correlated with Cre mRNA detected by *in situ hybridization* (**Fig. 2.2**, bottom-right). The empirically-optimized drug treatment (66.7 mg/kg, 15 day) reduced mRNA levels in whole hippocampus, striatum, cortex, cerebellum, and hippocampal CA1, CA3, and dentate gyrus layers by 45.7 ± 8.8%, 59.3 ± 8.3%, 75.9 ± 7.4%, 73.8 ± 6.8%, 71.4 ± 3.0%, 55.7 ± 3.2% and 49.0 ± 2.6% compared to WT, respectively (**Fig. 2.3a**). Real-time polymerase chain reaction (rtPCR) also revealed a 43.6 ± 6.8% reduction in Cdk5 mRNA from

Cdk5 KO whole hippocampus (**Fig. 2.3b**). Decreases in hippocampal Cdk5 protein level (59.2 ± 4.9%, **Fig. 2.3c**) and activity (44.1 ± 0.2%, **Fig. 2.3d)** were detected by quantitative immunoblots and immunoprecipitation-kinase assays, respectively.

Cdk5 from glia and presynaptic terminals from non-hippocampal regions may have contributed to measurements of Cdk5 using whole hippocampus, mRNA, immunoblot, and activity analyses. Therefore, we focused on the hippocampal pyramidal cell body layers, which are essentially devoid of glial cells (personal communication, Amelia Eisch, UT Southwestern Medical Center). Pseudocolor quantitation of Cdk5 mRNA confirmed robust knockdown of Cdk5 message in all three hippocampal cell body layers (**Fig. 2.4a**). For more accurate and higher resolution analysis, fluorescent *in situ* hybridizations were performed using digoxigenin-labelled mRNA probes and analyzed with confocal microscopy. High-resolution confocal analyses of fluorescent *in situ* hybridizations (FISH) were conducted to assess Cdk5 KO in CA1 neurons. FISH revealed that 90.9 ± 7.7% of cells in the *stratum pyramidale* of Cdk5 KO lacked any Cdk5 mRNA (**Fig. 2.4b**). An equivalent proportion of CA1 cells in Cdk5 KO mice expressed the Cre-ER^{T} mRNA (**Fig. 2.4b**). Consequently, temporally-controlled, conditional loss of Cdk5 was achieved, allowing for the study of hippocampal learning and synaptic plasticity.

Improved performance in hippocampal learning tasks.

The role of Cdk5 in associative learning and memory was evaluated via contextual and cued fear conditioning behavioral tests. Animals were placed in a novel context, analyzed for baseline behavior, and exposed to cue/foot shock pairings. Twenty-four hours post-training, memory to context was assessed by examining freezing behavior. Cdk5 KO mice exhibited significantly increased

contextual memory (61.4 ± 4.1% for KO vs. 42.1 ± 3.8% for WT; **Fig. 2.5a**). Fear-conditioned memory prior to Cdk5 knockout was also equivalent between genotypes (**Supplementary Fig. 2.2a**). Moreover, no significant confounding differences were observed in baseline freezing (**Fig. 2.2a**), nociception (**Supplementary Fig. 2.2b**), general locomotion (**Supplementary Fig. 2.2c**), or anxiety (**Supplementary Fig. 2.2d—f**). The increased freezing upon re-exposure to context indicates enhanced hippocampus-dependent memory.

The role of Cdk5 in the amygdala is not defined. Cdk5 and it cofactors are moderately expressed in the amygdala[12]. *In situ* hybridization analyses of the amygdala suggests that there *may* be (1) mild expression of Cre in the PRP-Cre transgenic line and (2) a mild knockdown of Cdk5 in conditional Cdk5 KO mice. However, cue-conditioned memory, which is dependent on the amygdala, was not different between WT and KO mice (**Fig. 2.5a**). Quantitation and more careful analyses of mRNA and protein in the amygdala will be required. Although these studies indicate that forebrain knockdown of Cdk5 produced no difference in amygdala-dependent learning, focused studies on Cdk5's role in the amygdala are necessary.

Rate and extent of contextual fear-extinction was examined by re-exposing the animals to the conditioned context over several trials. Cdk5 KO mice exhibited greater contextual extinction over several re-exposures than controls (**Fig. 2.5b** and **2.6**). Two-way ANOVA revealed a significant interaction between genotype and context re-exposure and *post hoc* analysis found that Cdk5 KO mice froze significantly less during the 4th re-exposure than WT (96-h after training, 29.8 ± 4.4% freezing for KO vs. 71.1 ± 12.6% for WT, **Fig. 2.6**). Thus, conditional Cdk5 KO resulted in increased hippocampus- and NMDAR-dependent[60] cognitive flexibility.

To assess the effect of conditional Cdk5 KO on spatial learning and memory, the hippocampus- and NMDAR-dependent water maze task was used[61,62]. Animals were trained to find a submerged platform using distant visual cues after which the platform was removed to test spatial memory. Hippocampus-dependent[4,62,63] cognitive flexibility was then assessed by retraining the mice to find a platform in the opposite quadrant (reversal). While both genotypes showed equally successful learning during initial training sessions (**Fig. 2.7a**), KO mice exhibited shortened escape latencies during the reversal task (**Fig. 2.7b**). The enhancement of reversal learning was apparent as early as the second trial of day 1 and first trial of day 2, indicating single-trial and long-term spatial learning enhancements (**Fig. 2.7b**). Reversal differences were not due to disparities in velocity (**Fig. 2.8**). Better reversal-learning was accompanied by superior spatial memory, as assessed by a platform-removal probe trial. While both genotypes showed significant preferences for the target quadrant after 11 training days (**Fig. 2.7a**), only KO mice showed a preference for the new target region following reversal training (**Fig. 2.7b**). Consequently, conditional Cdk5 KO resulted in improved performance in the hippocampus-dependent[62] reversal spatial learning task which correlates with the enhancement in contextual extinction described above.

Although Cdk5 KO mice displayed improved performance in the reversal learning task, additional data suggests that perhaps the KO mice learn differently from controls. After initial training, spatial preference was tested when 2 of 4 cues were removed. WT mice displayed a spatial preference for target region after removing these cues. In contrast, the KO mice displayed no preference (**Fig. 2.9**). This variation of the water maze task and pattern recognition mechanisms are poorly understood. However, this data suggests that Cdk5 KO mice may use more

cues than controls for spatial memory. It is entirely unclear, however, whether this difference is related to the enhancement in reversal learning.

Enhanced synaptic plasticity and NMDAR-mediated currents.

Since alterations in the strength of synaptic connection between hippocampal neurons are believed to underlie contextual and spatial memories[2,61], synaptic plasticity in the hippocampal Schaffer collateral pathway (SC/CA1) pathway was analyzed. No differences between WT and KO groups were observed in α-amino-3-hydroxy-5-methyl-4-isoxazole-propionic acid receptor (AMPAR)-mediated synaptic transmission or 25—800 ms paired-pulse facilitation (**Fig. 2.10**), as measured by extracellularly-recorded field excitatory post-synaptic potentials (fEPSPs). A weak theta-burst stimulus (2 x TBS) had no effect on WT (2.0 ± 6.9% change from baseline) but induced robust LTP in KO slices (34.0 ± 4.0%; **Fig. 2.11a,b**). Similar results were obtained following a weak 50 Hz tetanus (0.1 ± 2.3 % for WT vs. 31.1 ± 5.9 % for KO; **Fig. 2.11b**). A stronger theta-burst stimulation (3 x TBS) induced LTP of similar magnitude in WT and KO slices (34.2 ± 6.3% vs. 49.7 ± 1.0%, respectively; **Fig. 2.11a**), and elevated post-tetanic potentiation in KO slices relative to WT (123.4 ± 8.9% vs. 52.4 ± 14.7%, respectively; **Fig. 2.11a**). Strong 100 Hz tetanus also produced equivalent LTP in WT and KO slices (48.3 ± 5.4% vs. 49.1 ± 4.9%, respectively; **Fig. 2.11b**). These results indicated that Cdk5 knockout reduced the induction threshold for LTP in the SC/CA1 pathway. The reduction in the threshold for synaptic plasticity *in vitro* correlates with enhancements in learning and memory.

NMDAR-mediated currents are essential for LTP[2]. To investigate the LTP enhancement mechanism, we assessed the relative contribution of synaptically-evoked NMDAR-mediated current. The stimulus intensity versus fiber-volley magnitude relationship was equivalent between groups, indicating a lack of

differential axonal stimulation (data not shown). In addition, there were no disparities in AMPAR-mediated synaptic transmission (**Fig. 2.10a**) or whole-cell currents (3601 ± 400 vs. 3800 ± 313 EPSC area for WT and KO; p = 0.71, Student's *t*-test). Voltage measurements in field recordings from Cdk5 KO slices revealed increased NMDAR-mediated synaptic transmission (**Fig. 2.12a**, left) and a 9.0 ± 2.4-fold larger NMDA:AMPA fEPSP ratio (**Fig. 2.12a**, right) relative to WT. Whole-cell voltage-clamp synaptically-evoked NMDAR-mediated excitatory post-synaptic currents ($EPSC_{NMDA}$) in CA1 pyramidal neurons revealed no difference in NMDAR reversal potential but a 1.4 ± 0.2-fold larger NMDA:AMPA EPSC ratio (**Fig. 2.12b,c**). The disparities between these measures can be attributed to differences in recording techniques and cellular properties that were being measured. Nonetheless, both data demonstrate that loss of Cdk5 resulted in larger NMDAR-mediated fEPSPs and currents. Since LTP in the SC/CA1 pathway is dependent on NMDARs, the increase in NMDAR-mediated current correlates with and likely contributes to the enhancement in synaptic plasticity observed in Cdk5 KO mice.

Increases in ifenprodil-sensitive current and NR2B in conditional Cdk5 KO mice.

NMDAR-mediated current in the adult hippocampal SC/CA1 pathway is predominantly mediated by receptor complexes consisting of NR1 and NR2A and/or NR2B subunits[64]. Relative subunit contributions to the increased $EPSC_{NMDA}$ were determined by measuring sensitivity to a NR2B-selective inhibitor, ifenprodil[65,66]. Ifenprodil-sensitive $EPSC_{NMDA}$ areas were 3.2 ± 0.5-fold greater in Cdk5 KO slices compared to WT (**Fig. 2.13a**). Consistent with this observation, the ifenprodil-sensitive current relative to total NMDAR-mediated current was smaller in KO versus WT ($P < 0.05$, Student's *t*-test). Moreover, the decay constant for the $EPSC_{NMDA}$ was longer in KO (74.2 ± 7.2 ms) than WT (51.5 ± 4.7 ms, **Fig. 2.13a**). The elevated $EPSC_{NMDA}$ decay constant is consistent

with increased numbers of NR2B-containing receptors. Interestingly, immunoblot analysis of Cdk5 KO hippocampal homogenates revealed a 1.33 ± 0.07-fold increase in total NR2B levels, while NR2A, NR1, and GluR1 levels were unaltered (0.86 ± 0.06, 0.96 ± 0.11, and 0.99 ± 0.18 vs. WT, respectively; **Fig. 2.13b**). Furthermore, cell surface receptor-labelling experiments revealed a 1.9 ± 0.2-fold increase in NR2B surface-to-total ratio in KO slices (**Fig. 2.13c**).

Synaptic plasticity is dependent on several kinase-mediated intracellular signaling cascades. Therefore, we assessed the phosphorylation states of several kinase targets relevant to synaptic plasticity. Immunoblot analyses of hippocampal lysates revealed no significant differences between WT and KO in phosphorylation states of phospho-1480 NR2B, phospho-845 GluR1, phospho-1303 NR2B, phospho-286 CamKII, phospho-185 ERK-1, phospho-187 ERK-2 (**Fig. 2.14a**). Furthermore, no differences were observed in the total levels of CamKII, ERK-1, and ERK-2 (**Fig. 2.14b**). In contrast, the phosphorylation state of Tyr 1472 NR2B was consistently and significantly reduced in Cdk5 KO mice when compared to WT (**Fig. 2.14a**). Previous reports have indicated that dephosphorylation of Tyr1472 tags NMDARs for internalization[67,68]. The elevation in NR2B levels after Cdk5 KO mice may have indirectly led to a compensatory reduction in phospho-Tyr 1472 (see chapter 3 for more discussion).

The increases in NR2B levels and current through NR2B-containing receptors correlated with a hippocampus-specific 2.0-fold increase in synaptosomal NR2B (**Fig. 2.15**), indicating that the increase in surface NR2B was manifested at synapses. Consequently, Cdk5 KO may have altered the subunit composition of NMDARs due to increased synaptic and surface levels of NR2B. Moreover, the elevations in surface and synaptic NR2B levels correlated with an increases in total and ifenprodil-sensitive NMDAR-mediated currents.

There was also a non-hippocampus-selective increase in synaptic PSD-95 levels (**Fig. 2.16**). PSD-95 was elevated in the both the hippocampus and striatum; meanwhile, NR2B was selectively elevated in the hippocampus. This suggests that the hippocampal elevation in NR2B may not be dependent on that changes in PSD-95. Fascinatingly, Cdk5 was suggested to regulate PSD-95 multimerization via phosphorylation of residues 19, 25, and 35[43]. MALDI-TOF analysis of preparatively phosphorylated recombinant PSD-95 confirmed Cdk5 phosphorylated PSD-95 between amino acid residues 18 and 42 (Fragment isolated: DTPPLEHSPAHLPNQANSPPVIVNT; Haydn Ball, UT Southwestern Medical Center). Site-directed mutants T19A and S25A of PSD-95 were generated and, saturated phosphorylation reactions indicated that S25A but not T19A reduced phosphorylation of PSD-95 by nearly 40% (**Supplementary Fig. 2.3**). Additional MALDI-TOF analyses and experiments with site-directed PSD-95 mutants have revealed additional Cdk5 sites on PSD-95 (personal communication, Oludotun Adeyo, UT Southwestern Medical Center). Therefore, phosphorylation of these novel sites and interactions between phosphorylation sites likely account for the remaining ^{32}P-ATP incorporation in the S25A PSD-95 mutant. The importance of these phosphorylation sites are yet undetermined. Furthermore, it is unclear whether any of the phenotypes observed in Cdk5 KO mice are due to aberration in a Cdk5—PSD-95 pathway.

Increased ifenprodil-sensitive NMDAR-mediated current accounts for enhanced synaptic plasticity in Cdk5 knockout mice.

The previous data showed correlations between learning enhancements, the enhancement in plasticity, increase in NMDAR-mediated currents, and elevated NR2B levels. To confirm causality, the contribution of increased NR2B-containing NMDAR-mediated current to the enhancement of plasticity in conditional Cdk5 KO mice was evaluated. As previously reported[69], the NR2B-

selective inhibitor, ifenprodil, had no effect on LTP induction in WT slices following a sufficient tetanus (48.8 ± 3.5% change from baseline, n = 3). This data confirmed that NR2B-containing receptors are not obligatory for SC/CA1 LTP induction in normal adult mice. The LTP enhancement in Cdk5 KO mice was entirely reversed by ifenprodil (2.3 ± 3.5%) or a general NMDAR antagonist (AP5, 0.5 ± 0.9%; **Fig. 2.17**). Therefore, the increase in synaptic plasticity resulting from Cdk5 KO may be directly attributed to increased current through NR2B-containing NMDARs.

Analysis of p39 and p35 knockout mice

To gain more insight on the cofactor specificity of Cdk5's roles in synaptic plasticity, hippocampal NR2B levels and memory were tested in Cdk5 cofactor knockout mice (kindly provided by L.H. Tsai, Massachusetts Institute of Technology). Immunoblot analyses of hippocampal lysates from 2 — 3 week old p39 *null* mice revealed a 78.3 ± 3.0 % decrease in NR2B levels (**Fig. 2.18a**). Immunoblot analysis from 2 — 3 week old p35 *null* mice revealed a similar but statistically insignificant 58.0 ± 9.8 % decrease in hippocampal NR2B levels (**Fig. 2.18a**). Interestingly, NR1 levels were also reduced in hippocampi from 2 — 3 week old p39 and p35 *null* mice (data not shown). Six to 8 week old p39 knockout mice showed a 1.78 ± 0.13-fold increase in hippocampal NR2B. In contrast, p35 *null* adults displayed no increase in NR2B levels (**Fig. 2.18b,c**). These results suggest that Cdk5 and its cofactors, p35 and p39, may both play critical roles in regulating the levels of NMDAR subunits during development and early life. In contrast, p39 but not p35 appears to play an important role in the regulation of NR2B levels in an older adult brain. The increase in NR2B is consistent with the phenotype seen in the conditional Cdk5 KO mouse.

p35 null mice are known to have deficiencies in learning, perhaps due to cytoarchitectural abnormalities[8]. Since NR2B levels were elevated in the hippocampus from adult p39 null mice, we assessed whether p39 null mice displayed superior contextual memory as assessed via fear conditioned learning. Fear conditioning experiments revealed no differences between p39 KO and WT animals in context- or cue-elicited memory (**Fig. 2.18d**). Thus, initial studies have revealed no differences in basic fear conditioned memory in p39 KO mice. It remains unclear whether p39 plays any roles in plasticity. First of all, it will be essential to analyze surface and synaptic levels of NR2B in p39 KO mice. Furthermore, because NMDAR subunit levels are altered in p35 and p39 knockout mice, additional plasticity and learning studies are warranted before any conclusions can be drawn. Finally, the decreased levels of NMDAR subunits during development likely have significant importance on the maturation of synaptic connections. However, it is not possible to make any conclusions regarding the elevated NR2B levels in the adult p39 KO mice. Additional analyses must be undertaken with caution. Although the increased NR2B levels in p39 KO mice correlates with previous data from Cdk5 KO mice, it is possible that this represents an unrelated, artifactual, or physiologically insignificant finding.

Cdk5 knockout reduced calpain-mediated NR2B degradation.

The increase in NR2B levels in Cdk5 KO mice could be due to increased gene expression or reduced protein degradation. Analysis of Cdk5 KO hippocampal tissue by rtPCR showed no increase in NR2B mRNA (**Fig. 2.19**), suggesting a post-transcriptional mechanism. NMDA is known to induce degradation of NR2B by calpain, a Ca^{2+}-dependent protease[55,70,71]. Calpain cleaves NR2B to a 115 kDa form which is then further degraded[55,70,71]. We examined the generation of the cleaved form of NR2B in Cdk5 KO and WT mice following NMDAR activation. Significantly less calpain-mediated NR2B

cleavage was detected following NMDAR activation in hippocampal KO slices than controls (3.6 ± 12.8% and 22.5 ± 8.2% of WT after 30- and 60-min, respectively; **Fig. 2.20a**). Furthermore, Cdk5/p25 dramatically enhanced calpain-mediated cleavage of the NR2B C-terminus *in vitro* (**Fig. 2.20b**). These *ex vivo* and *in vitro* findings suggest that Cdk5 normally facilitates calpain-mediated cleavage of NR2B. Furthermore, reduced cleavage of NR2B in Cdk5 KO mice likely caused the increase elevations in functional NR2B-containing NMDARs.

Protein-protein interactions between Cdk5, NR2B, and calpain

Cdk5 could affect calpain-mediated cleavage of NR2B either via phosphorylation or direct binding. However, Cdk5 phosphorylated neither calpain (not shown) nor NR2B *in vitro* (**Fig. 2.21**), and activated calpain in the absence of Mg^{2+} and ATP (**Fig. 2.20b**). Thus cleavage-enhancement was independent of kinase activity. On the other hand, NR2B, Cdk5, p35, and calpain coimmunoprecipitated with one another and the postsynaptic density marker, PSD-95, in WT hippocampal lysates (**Fig. 2.22a**). Additionally, Cdk5 KO reduced the coimmunoprecipitation of NR2B with Cdk5 to 23.1 ± 2.6% of WT controls (**Fig. 2.23a**). Although equal amounts of the Cdk5 cofactor p35 immunoprecipitated from WT and KO lysates, levels of NR2B associated with p35 were reduced to 48.4 ± 4.8% compared to WT (**Fig. 2.23b**). These data indicate that NR2B, Cdk5, p35, and calpain occur in a post-synaptic complex and Cdk5 mediates the interactions between NR2B and p35. NR2B–PSD–95 interaction ratios were unaffected by Cdk5 KO (**Fig. 2.23c**), suggesting no major changes in PSD-95's regulation of NR2B levels. Finally, *in vitro* pull-down assays demonstrated that resin-conjugated NR2B bound Cdk5 and calpain, and resin-conjugated Cdk5 bound NR2B and calpain (**Fig. 2.22b**). The data from *in vitro* cleavage assays demonstrate that Cdk5 directly facilitated the degradation of NR2B. The interaction data suggest that Cdk5 binds calpain and NR2B. Through

such protein-protein interactions, Cdk5 likely facilitates the calpain-mediated cleavage of NR2B. The data further suggests that the elevated NR2B levels in the Cdk5 KO hippocampus resulted from the loss of these critical interactions.

To further characterize Cdk5's interactions with NR2B and calpain, we performed a peptide microarray binding assay with Cdk5/p25 and peptides spanning both NR2B and calpain. Overlapping eight amino acid peptide cassettes the of the NR2B cytoplasmic tail and calpain-1 were synthesized and immobilized onto a microarray. A binding assay with Cdk5/p25 was performed *in vitro* and binding was assessed via a *far western* for Cdk5. The peptide microarray binding assays identified 4 candidate NR2B peptides and 5 candidate calpain peptides which bound with Cdk5/p25 (**Fig. 2.24**). These candidate peptides will serve as a starting point for further characterization of the protein—protein interactions between Cdk5/p25, NR2B, and calpain.

Discussion

The effects of conditional Cdk5 KO revealed a novel role for Cdk5 in regulating glutamate receptor degradation. Previous reports separately implicate both Cdk5[5,6,8,48] and CA1 hippocampal NMDARs[2,54,60,61,64,66,69,72,73] in spatial learning and synaptic plasticity. The present study demonstrates that conditional loss of Cdk5 caused an increase in NR2B-containing NMDAR levels and related currents. Interestingly, transgenic overexpression of the NR2B subunit[60] resulted in similar learning and plasticity enhancements to those of Cdk5 KO mice. Our data also show NR2B degradation is facilitated by interactions between Cdk5, calpain, and NR2B. These findings are consistent with previous reports showing that calpain is a major component of the NMDAR complex[74], and that calpain-mediated cleavage of NR2B decreases the number of functional NMDARs[70,71]. Cdk5 may function structurally to increase interactions between NR2B and

calpain, and facilitate NR2B degradation in response to synaptic activity. Calpain also cleaves Cdk5's activating cofactors[13] and numerous Cdk5 substrates[75]. In addition, PSD-95 has been suggested to regulate NMDAR degradation by calpain[76]. Cdk5 has also been reported to modulate PSD-95 levels[43] and may thus contribute to the modulation of NMDARs via multiple pathways.

Ultimately, the increase in NR2B containing NMDARs may lengthen the integration time window for NMDAR coincidence detection[60] and decrease the threshold to induce the long term synaptic changes. Consistent with previous reports[77,78], the increase in NMDAR-mediated current and reduction in plasticity threshold may facilitate information processing and learning. While these findings advance our understanding of Cdk5's role in learning and plasticity, it is important to note that in order to further understand the molecular mechanism of memory, the relationship between plasticity and learning suggested here will require clarification. Furthermore, while we have focused on the role of Cdk5 in regulating functional plasticity via NMDARs, Cdk5 knockout likely affects learning via additional pathways. Nonetheless, these observations reveal a novel molecular mechanism through which Cdk5 directly interacts with the NR2B NMDAR subunit and calpain to facilitate NR2B degradation. Through such interactions, Cdk5 may influence NMDAR constituency, synaptic plasticity, and learning.

Cdk5's regulation of calpain-mediated cleavage of NR2B offers a novel and phosphorylation-independent role for Cdk5 in plasticity. Although proteins often are often multifunctional in nature, studies of Cdk5, like those of other protein kinases, have primarily focused on the phosphorylation of substrates. The data from the conditional Cdk5 knockout mice and *in vitro* assays, however, reveal that Cdk5 facilitates calpain activity towards NR2B via protein—protein

interactions. We hypothesize that Cdk5/p35 interacts with the NR2B NMDA receptor subunit. Following NMDA receptor activation and Ca^{2+} influx, calpain interacts with Cdk5 and NR2B, leading to proteolysis of the NR2B C-terminus (**Fig. 2.6**). Cdk5 may serve as a structural link between NR2B and its protease or bind with calpain to increase its proteolytic activity towards substrates. Cdk5's role in NR2B degradation and the facilitation of calpain activity is an exciting new regulatory pathway with broader implications. For example, calpain is known to play roles in neurodegenerative disorders, human immunodeficiency virus replication, erythrocyte sickling, and other diseases [79]. Thus, further studies of the relationships between Cdk5, calpain, and NR2B have significant clinical relevance and may facilitate development of useful therapeutics.

Conditional Cdk5 knockout mice display phenotypes mirroring several aspects of both p35 knockout and p25 overexpressing mice. Both p35 knockout mice and conditional Cdk5 knockout mice display reduced thresholds to induce long term potentiation in the Schaffer collateral pathway of the hippocampus. The behavioral and elctrophysiological similarities observed between conditional Cdk5 knockout and transient (*i.e.,* for 2 weeks) p25 overexpressing mice suggest that Cdk5 may function in a cofactor-specific manner to attenuate processes underlying learning and plasticity. Interestingly, conditional loss of Cdk5 and transient overexpression of p25 both appear to lead to increases in NMDA receptor-mediated currents. Since loss of Cdk5 mimics the beneficial effects of transient but not long-term p25 overexpression, perhaps transient overexpression of p25 enhances plasticity by removing Cdk5 from its normal pools. This is consistent with the hypothesis that Cdk5 appears to serve as a pro-growth and anti-synaptic connection factor during development. Since, Cdk5 kinase activity is entirely dependent on activating cofactors, it is critical to determine the precise roles of p35, p39, p25, and p29 in plasticity.

Conclusion

The studies to date provide overwhelming evidence that implicates Cdk5 in learning and plasticity. Genetic manipulations reveal that Cdk5 and its cofactors play multiple roles in regulating both structural and functional plasticity. Since Cdk5 depends on its activating cofactors, it will be necessary to further understand the function of each Cdk5 cofactor in various aspects of learning and plasticity. Cdk5 localization is dependent on its interaction with p35, which is predominantly located in membranes, and p25, which is localized to the cytosol. It is possible that signaling events within the cell leads to translocation of Cdk5 and its cofactors. Such movements may shift Cdk5 towards alternative substrate pools and binding partners to modulate plasticity. Additional information about the dynamic localization of Cdk5 and its cofactors in response to learning or plasticity will be important. Interestingly, activation of calpain leads to its translocation to the membrane surface [79]. It will be informative to determine whether Cdk5 interacts with calpain while it is in the cytosol or associated with the membrane.

Although the functional and anatomical segregation of Cdk5/p35 and Cdk5/p25 play critical roles in learning and plasticity, the recent data implicate Cdk5 in functional plasticity via protein—protein interactions. Cdk5's interaction with the NMDA receptor subunit and calpain to facilitate receptor degradation represents a novel pathway independent of Cdk5 kinase activity. The Cdk5—NR2b—Calpain interactions echo the interactions between CaMKII and its synaptic binding partners. As discussed elsewhere, CaMKII modulates synaptic plasticity by binding to several postsynaptic density proteins including PSD95, α-actinin, densin-180, and NMDA receptor subunits [1,80,81]. Structural studies of the massive holo-CaMKII complex implicate it as a major structural component of the postsynaptic density [82]. Both Cdk5 and CaMKII appear to have dual roles in regulating synaptic plasticity: both act via phosphorylation of synaptic substrates

and via direct protein-protein interactions. It will be useful to identify additional synaptic Cdk5 binding partners and examine how such protein interactions affect phosphorylation of synaptic substrates, Cdk5 kinase activity, and synaptic plasticity.

Acknowledgments

I would like to thank David R. Benavides, Chan Nguyen, Janice W. Kansy, and Kanehiro Hayashi (UT Southwestern Medical Center) for assistance with experiments, Pierre Chambon (Institut de Génétique et de Biologie Moléculaire et Cellulaire) and Paul Greengard (The Rockefeller University) for providing mouse lines and Craig M. Powell, Donald C. Cooper, and James A. Bibb (UT Southwestern Medical Center) who helped design experiment and provided supervision and mentorship.

I thank B. Potts, S. Gold, J. Pick, and M. Waung for assistance with experiments, D. Metzger for characterization of Cre-ER^T line, C. Steffen for assistance with animal husbandry, and K. Bayer for the NR2B clone. This work was made possible by the US National Institutes of Drug Abuse National Research Service Award training grant, US National Institutes of Health individual National Research Service Awards, US National Alliance for Research on Schizophrenia and Depression Young Investigator awards, grant funding from the US National Institutes of Drug Abuse and Mental Health and the Ella McFadden Charitable Trust Fund at the Southwestern Medical Foundation.

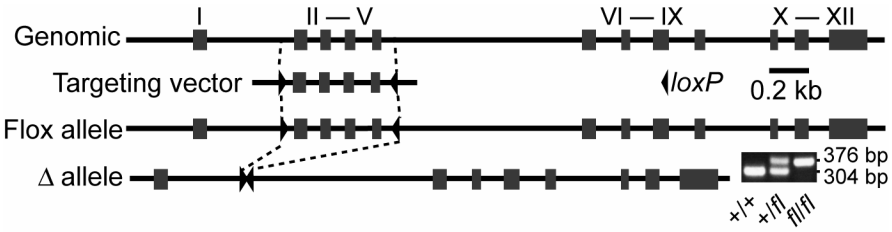

Figure 2.1. Conditional Cdk5 knockout strategy. Cdk5 gene targeting strategy. 36 base pair *loxP* sequences were inserted around exons II and V (*floxed*). Inset: PCR genotyping of WT (+) and floxed (*fl*) alleles shows a 72 base pair (bp) difference between WT and floxed alleles.

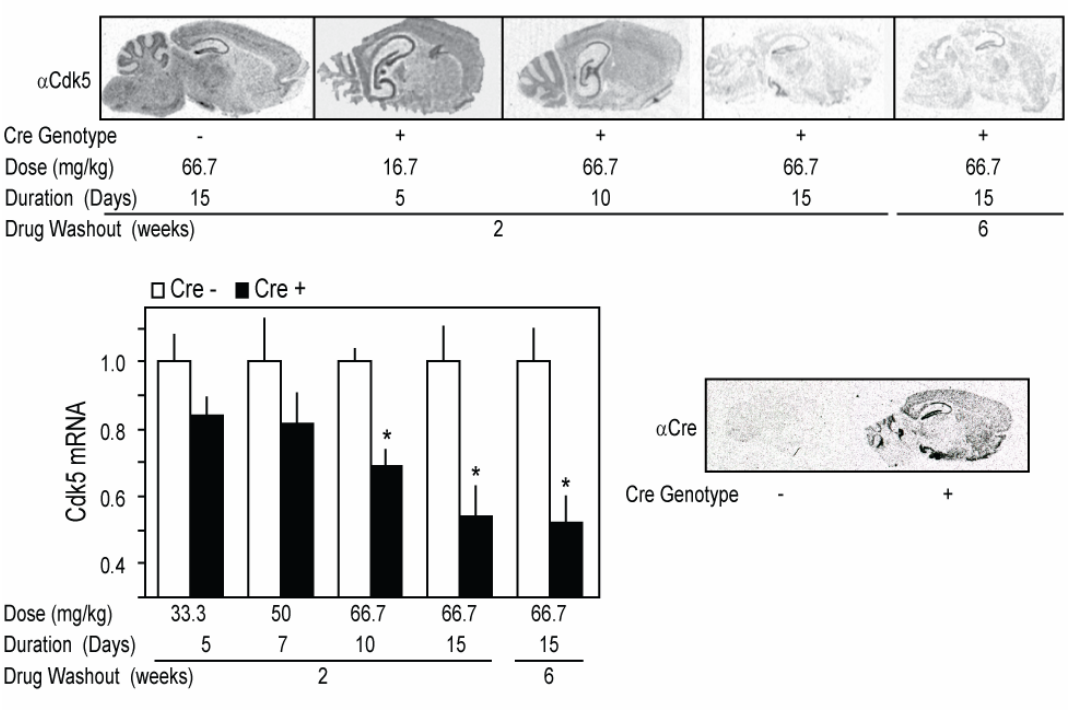

Figure 2.2. Optimization of conditional Cdk5 knockout. Hydroxytamoxifen dose-response analysis for Cdk5 KO and Cre expression. Representative *in situ* hybridizations for Cdk5 mRNA following indicated drug regimens (top) are shown with quantitation of hippocampal Cdk5 mRNA (bottom left, n=6-8) and a representative *in situ* hybridizations for Cre mRNA (bottom right). Data represent means±s.e.m, *P < 0.05 vs. WT; Student's *t*-test.

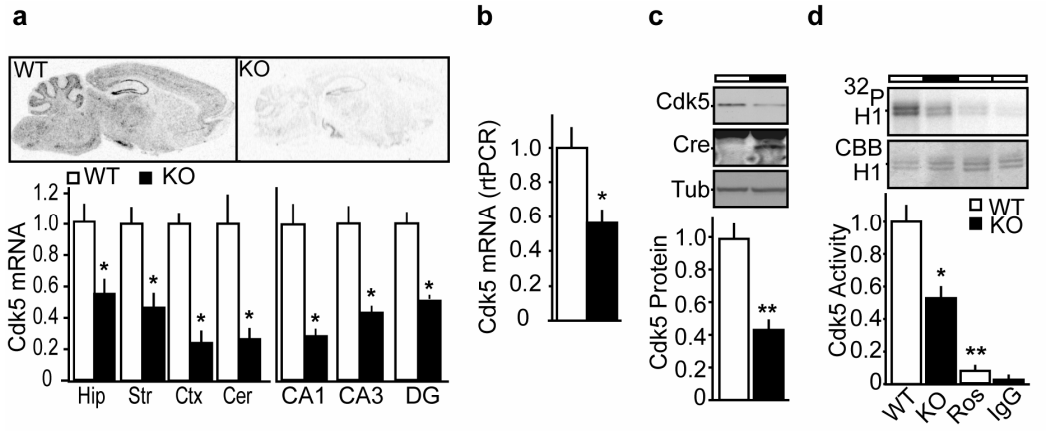

Figure 2.3. Conditional loss of Cdk5 in adult mouse brain. (a) Representative ^{35}S-UTP labeled *in situ* hybridization radiographs with mRNA quantitation for hippocampus (Hip), striatum (Str), cortex (Ctx), cerebellum (Cer), and hippocampal layers (n = 6–8). (b) Quantitative real-time polymerase chain reaction (rtPCR) analysis of hippocampal Cdk5 mRNA levels. Cdk5 mRNA was quantitated relative to glyceraldehyde-3-phosphate dehydrogenase mRNA levels, which were unaffected by Cdk5 KO; n = 9. (c) Quantitative immunoblots of Cdk5, Cre and α-tubulin (Tub) in hippocampal homogenates (n = 20). (d) Cdk5 kinase activity immunoprecipitated from hippocampus. Radiolabeled (32P-H1) and Coomassie-stained (CBB) H1 histone from WT and KO mice are compared to roscovitine (Ros) and IgG controls (n = 6). Data represent means ± s.e.m.; *P < 0.05, **P < 0.01, vs. WT; Student's *t*-test. Open and filled bars represent WT and KO, respectively.

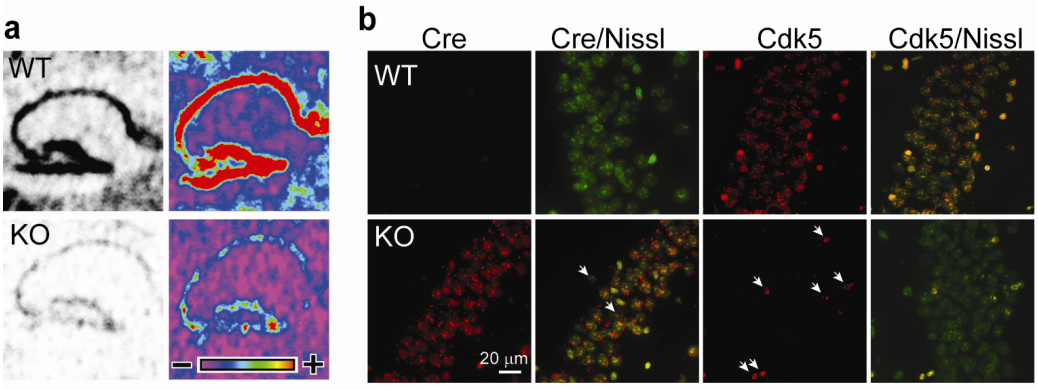

Figure 2.4. Conditional loss of Cdk5 in adult mouse hippocampus. (a) Representative ^{35}S-UTP labeled *in situ* hybridization for hippocampal Cdk5 mRNA with pseudocolor quantitation (+ indicates high signal; – indicates low signal) (b) Cdk5 and Cre mRNA fluorescent *in situ* hybridizations with Nissl counterstains in WT and KO CA1 pyramidal neurons. Markers indicate neurons with no Cre mRNA or Cdk5 loss.

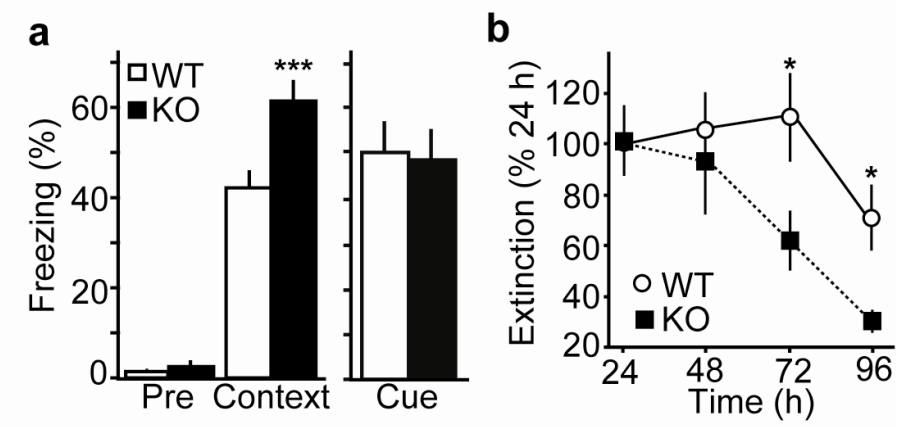

Figure 2.5. Improved performance of conditional Cdk5 KO mice in contextual fear conditioning and extinction behavioral tasks. (a) Context- and cue-elicited memory 24-h post-training. Freezing time before conditioning (Pre) and following context (n = 20) or cue (n = 11–12) re-exposure are shown with extinction (b, n = 10) learning to contextual environment. Data represent means ± s.e.m; ***P < 0.01 vs. WT; Student's *t*-test. P < 0.005 for interaction between genotype and re-expsoure, 2-way ANOVA. *P < 0.05, *post hoc*, vs. WT; Student's *t*-test.

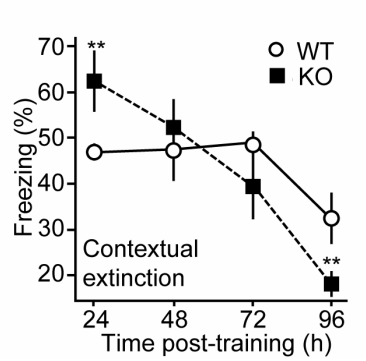

Figure 2.6. Contextual extinction in Cdk5 KO mice. Percentage of time spent freezing during re-exposures to conditioned context after training. Animals were scored for freezing behavior after the indicated following training. Data represent means ± s.e.m. n = 10—12; $P < 0.01$ for interaction between genotype and re-exposure, 2-way ANOVA. **$P < 0.05$ different from WT; *post hoc* Student's *t*-test.

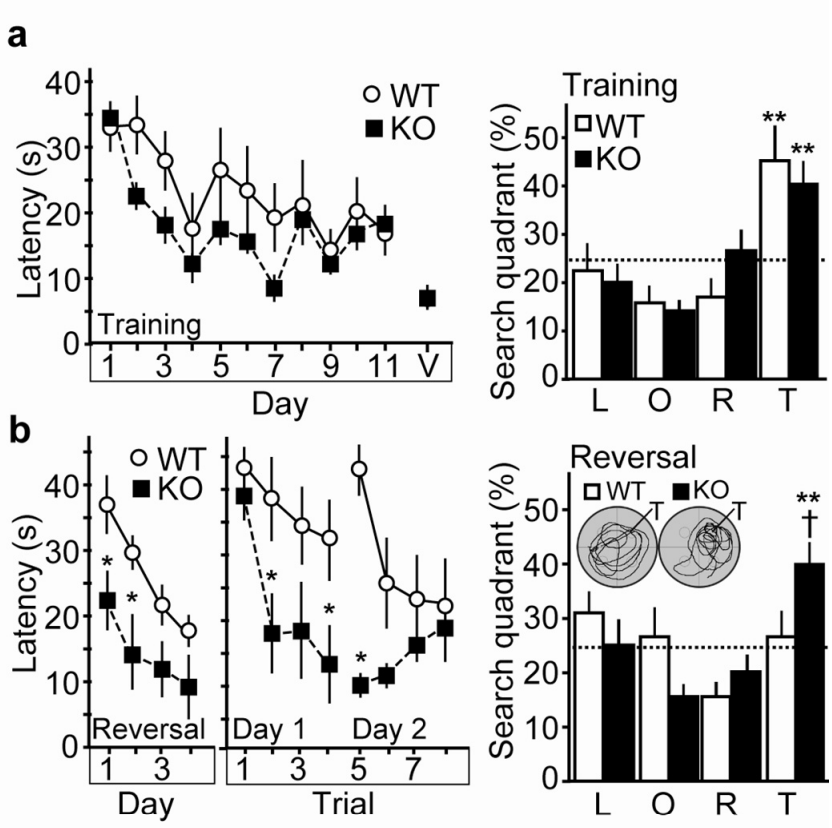

Figure 2.7 Superior performance of conditional Cdk5 KO mice in water maze reversal learning and memory tasks. (a) Escape latencies of training (4 trials per day) are shown with visual acuity assessment (V; left). Spatial preferences after initial training are shown as percent time spent in target quadrant (T; right). (b) Escape latencies of reversal training (4 trials per day) are shown with individual trials 1–8 on reversal days 1–2 (left). Spatial preferences and representative paths after reversal training are shown as percent time spent in target quadrant (T; right). L, O, & R indicate left, opposite, and right quadrants, respectively; n = 10–11. Data represent means±s.e.m; $P < 0.01$ for interaction between genotype and reversal training day/trial, 2-way ANOVA. *$P < 0.05$, *post hoc*, ***$P < 0.01$ vs. WT; **$P < 0.05$, vs. other quadrants; $^{\dagger}P < 0.05$, vs. WT in T; Student's *t*-test.

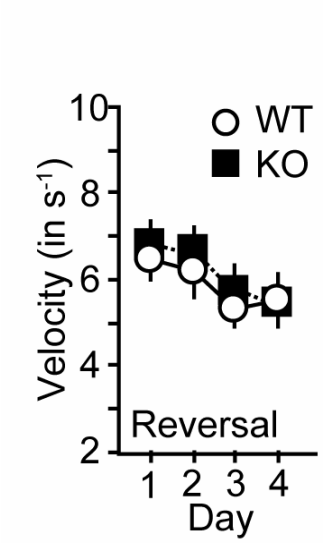

Figure 2.8. Swim velocity during water maze reversal training. Swim velocities were determined during water maze tasks. 4 trials per animal per day. n = 10—12 animals. Data represent means ± s.e.m.

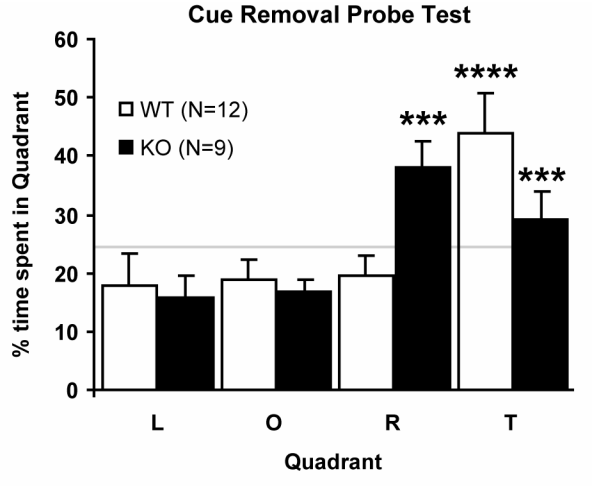

Figure 2.9. Cdk5 KO mice depend on more cues for spatial memory. Spatial preferences after 2 of 4 cues have been removed are shown as percent of time spent in the target quadrant (T). L, O, & R, indicate left, opposite, and right quadrants respectively; n = 10-11. Data represents mean ± s.e.m.; ***P < 0.05 vs. KO (L and O); ****P < 0.05, vs. WT (L, O, R) and KO (L, O, T); Student's *t*-test.

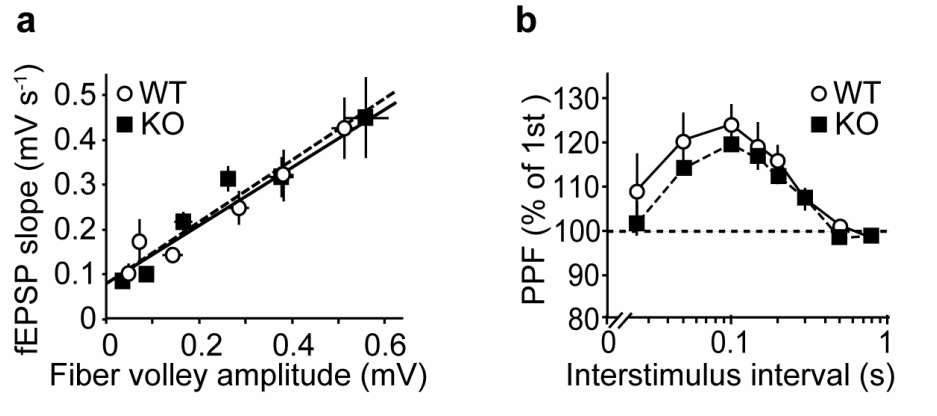

Figure 2.10. Normal basal synaptic transmission and 25—800 ms paired pulse facilitation in the hippocampal SC/CA1 pathway of conditional Cdk5 KO mice. (a) Basal input/output curve. fEPSP slopes were measured following synaptic stimulations that elicited the indicated presynaptic fiber volley magnitudes. Similar results were obtained with fEPSP amplitude measurements. (b) Paired-pulse facilitation (PPF; 25–800 ms) were measured following synaptic stimulation. n = 7–9 slices, 5 animals per genotype. Data represent means ± s.e.m.

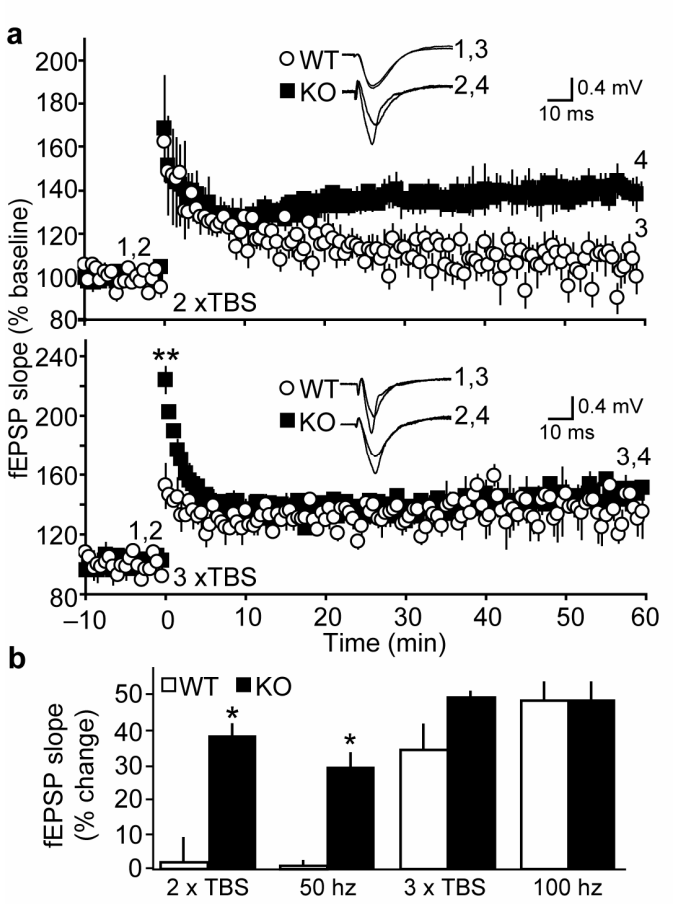

Figure 2.11. Enhanced synaptic plasticity in the hippocampal SC/CA1 pathway of conditional Cdk5 KO mice. (a) LTP after 2 x TBS and 3 x TBS plotted as percent of baseline (–10–0 min). Representative traces at baseline (1, 2) and 60-min (3, 4) are shown. (b) LTP 57–60-min after 2xTBS, 50 Hz, 3xTBS, and 100 Hz represented as percent change from baseline (n = 7–8 slices, 4–5 animals per group). Data represent means ± s.e.m.; *P < 0.05, *post* hoc; Student's *t*-test.

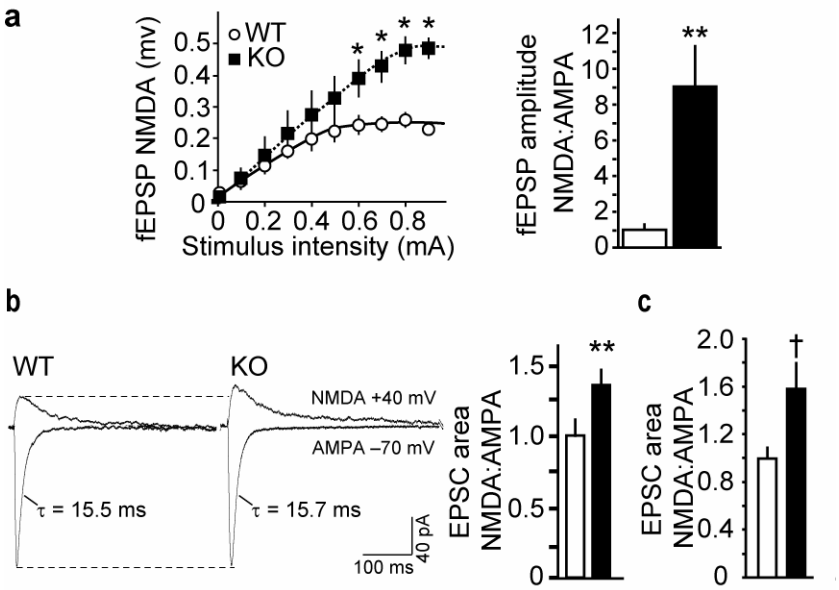

Figure 2.12. Increased NMDAR-mediated currents in the hippocampal SC/CA1 pathway of conditional Cdk5 KO mice. (a) NMDAR-mediated fEPSP (fEPSP NMDA) input/output relationship and NMDA:AMPA ratio. AMPA- and NMDA-mediated fEPSPs were measured in 2 and 0 mM Mg^{2+} and 0 and 20 μM DNQX, respectively (n = 6 slices, 3 animals per genotype). (b) Whole-cell NMDA:AMPA EPSC area ratio with representative traces. AMPA- and NMDA-mediated EPSCs were measured at –70 mV and +40 mV/20 μM DNQX, respectively (n = 7–10 cells, 5–7 animals per genotype). τ (decay constant) is shown for AMPA-mediated EPSCs. (c) Alternative measurement for EPSC NMDA:AMPA ratio. AMPAR- and NMDAR-mediated EPSCs were measured at -70 mV (0 ms – 44 ms) and +40 mV (45 ms – 350 ms), respectively (n = 7—10 cells, 5—7 animals per genotype). Data represent means ± s.e.m.; *P < 0.05, *post* hoc; **P < 0.05, †P < 0.05 vs. WT; Student's *t*-test. Open and filled bars represent WT and KO, respectively.

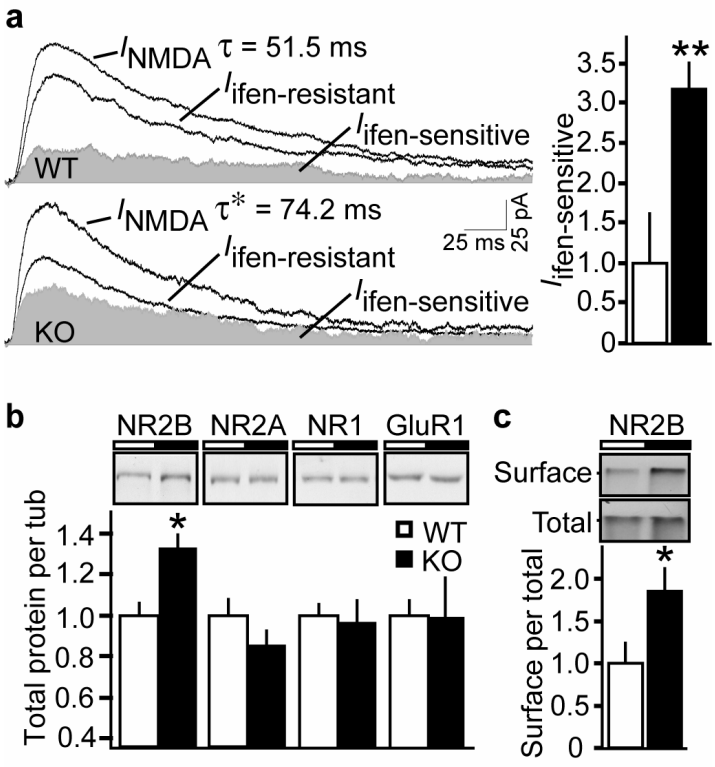

Figure 2.13. Increased ifenprodil-sensitive NMDAR-mediated current and NR2B levels in Cdk5 KO mice. (a) Effect of ifenprodil (ifen) on NMDAR-mediated EPSCs. Representative traces of NMDAR-mediated EPSCs before (I_{NMDA}) and after ($I_{ifen\text{-}resistant}$) 10 μM ifenprodil are shown with quantitation for $I_{ifen\text{-}sensitive}$ and τ for I_{NMDA}; n = 6–8 cells, 6–7 animals per genotype. (b) Representative immunoblots for indicated hippocampal glutamate receptor subunits and quantitation relative to tubulin (tub) loading control; n = 9–12. (c) Hippocampal NR2B surface:total ratio. Labeled surface receptors were immunoprecipitated, immunoblotted for NR2B, and compared with total lysates. Quantitation for surface to total are shown. Absolute surface levels were also elevated; n = 6 slices, 3 animals per genotype. Data represent means ± s.e.m.; *P < 0.05, **P < 0.01, vs. WT; Student's *t*-test. Open and filled bars represent WT and KO, respectively.

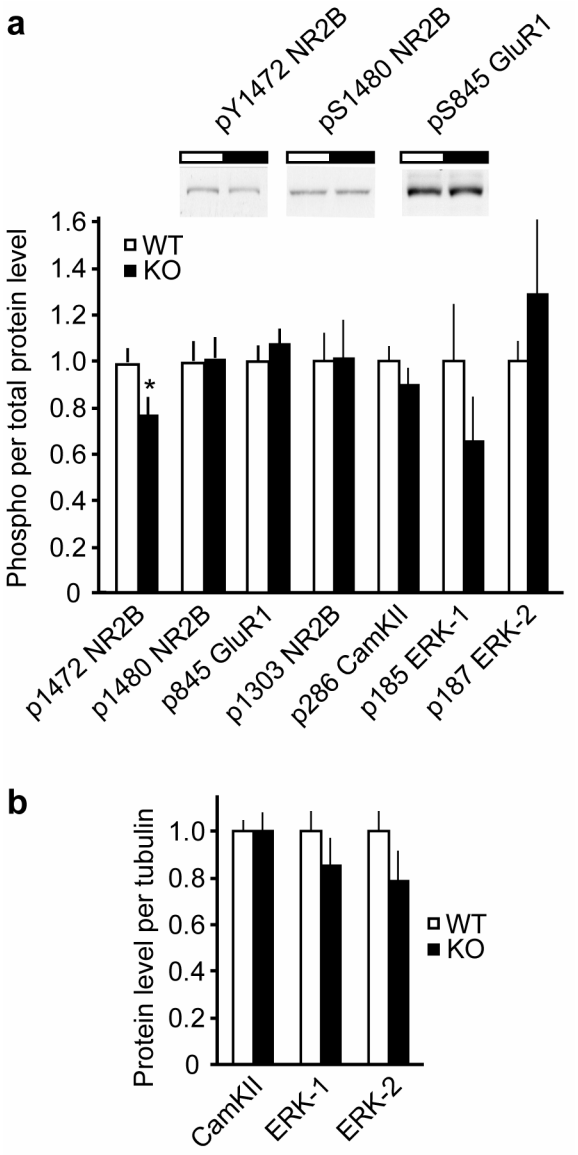

Figure 2.14. Analyses of levels of phosphorylation sites and proteins relevant to synaptic plasticity. (a) Representative immunoblots and quantitation are shown for indicated phosphorylation sites in hippocampal lysates. Phosphoprotein levels are normalized to total protein levels. (b) Quantitation of immunoblots for indicated proteins. Total protein levels are normalized to tubulin. n = 3-6; data represent means ± s.e.m.; *P < 0.05 different from WT; Student's *t*-test. Open and filled bars indicate WT an KO, respectively.

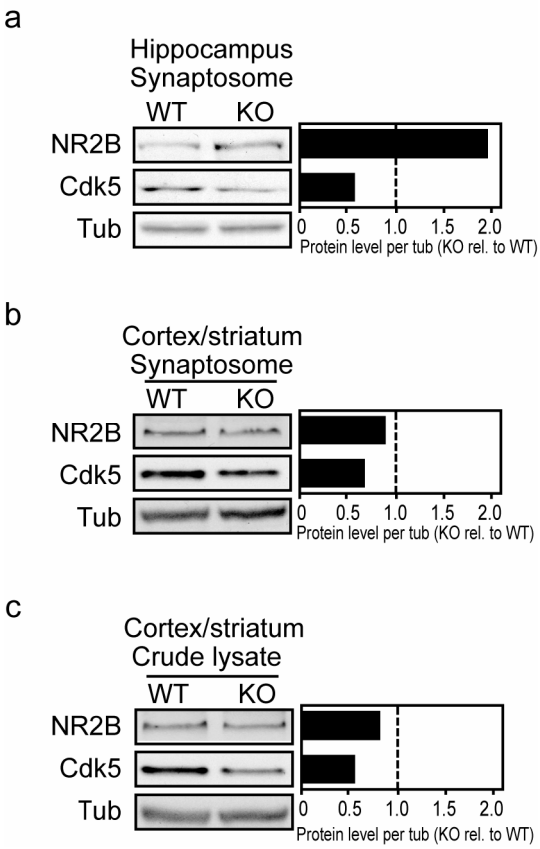

Figure 2.15. Hippocampus-specific increase in synaptic NR2B levels in Cdk5 KO mice. Immunoblots of NR2B, Cdk5, and tubulin (tub) in hippocampal synaptosomes (**a**), cortical/striatal synaptosomes (**b**), or cortical/striatal crude lysates (**c**) are shown with quantitation relative to tubulin loading control. Tissues from 3 animals per genotype were pooled for purification of synaptosomes. Data is representative of 2-3 separate experiments

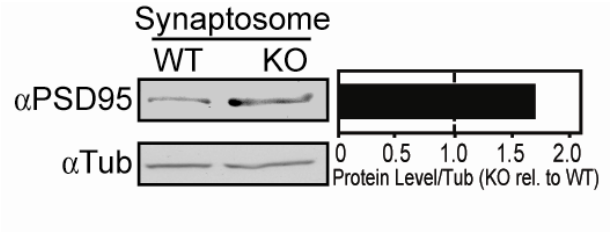

Figure 2.16. Analysis of synaptic PSD-95 level in Cdk5 KO hippocampus. Immunoblots of PSD-95 and tubulin in hippocampal synaptosomes with quantitation shown with quantitation relative to tubulin loading control. Tissues from 3 animals per genotype were pooled for purification of synaptosomes. Data is representative of 3 separate experiments.

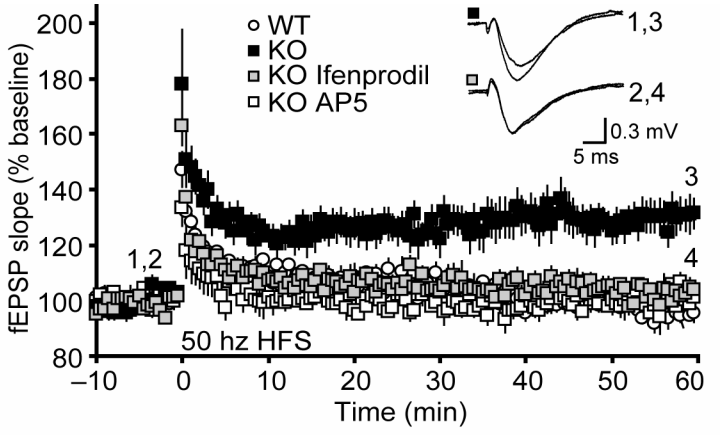

Figure 2.17. Increased ifenprodil-sensitive NMDAR-mediated current accounts for enhanced synaptic plasticity in Cdk5 KO mice. Effects of ifenprodil (20 μM) and AP5 (50 μM) on LTP enhancement, with representative baseline (1,2) and 60 min (3,4) traces (n = 6). Ifenprodil had no effect on threshold LTP induction in WT slices and reversed synaptic plasticity enhancement in Cdk5 KO slices. Data represent means ± s.e.m.

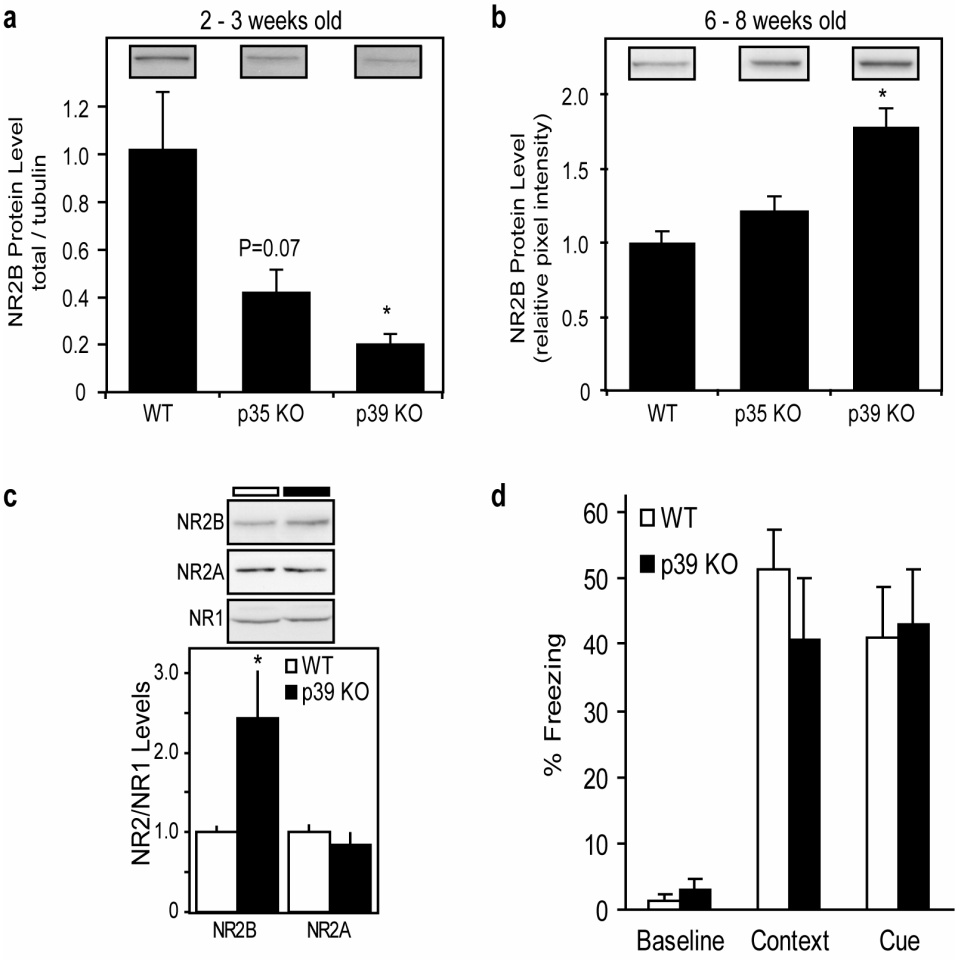

Figure 2.18. Analysis of Cdk5 cofactor knockout mice. (a) Representative immunoblots and quantitative analysis of NR2B in hippocampal lysates from 2—3 week old p35 and p39 KO mice. NR2B levels are normalized to tubulin. (b) Representative immunoblots and quantitative analysis of NR2B in hippocampal lysates from 6—8 week old p35 and p39 KO mice. NR2B levels displayed as pixel intensity; n= 5 — 8 for a and b and *P < 0.05 vs. WT; Student's t-test. (c) Representative immunoblots and quantitation of NMDAR subunits in hippocampal lysates from 6—8 week old p39 KO mice. NR2 subunits levels are quantitated relative to NR1 levels. Knockout of p39 had no effect on NR1 levels in hippocampal lysates form 6—8 week old mice. n= 5 — 8, *P < 0.01 vs. WT; Mann-Whitney U Test. (d) Fear-conditioning in p39 KO mice following training with one 0.8 mA foot shock pairing. Data represents means ± s.e.m.

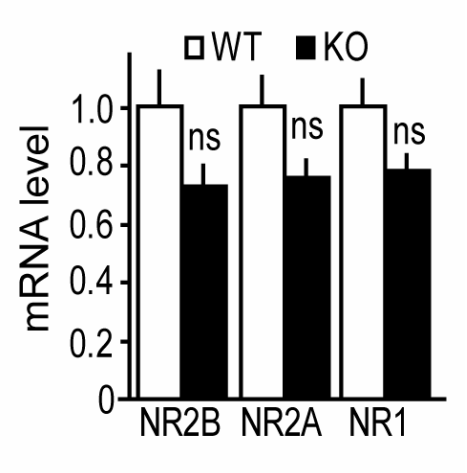

Figure 2.19. mRNA levels of NMDAR subunits in the Cdk5 KO hippocampus. mRNA levels of NR2B, NR2A, and NR1 in hippocampus as quantitated by real-time PCR; n = 9, *ns* = P > 0.1 vs. WT, Student's *t*-test. Data represent means ± s.e.m.

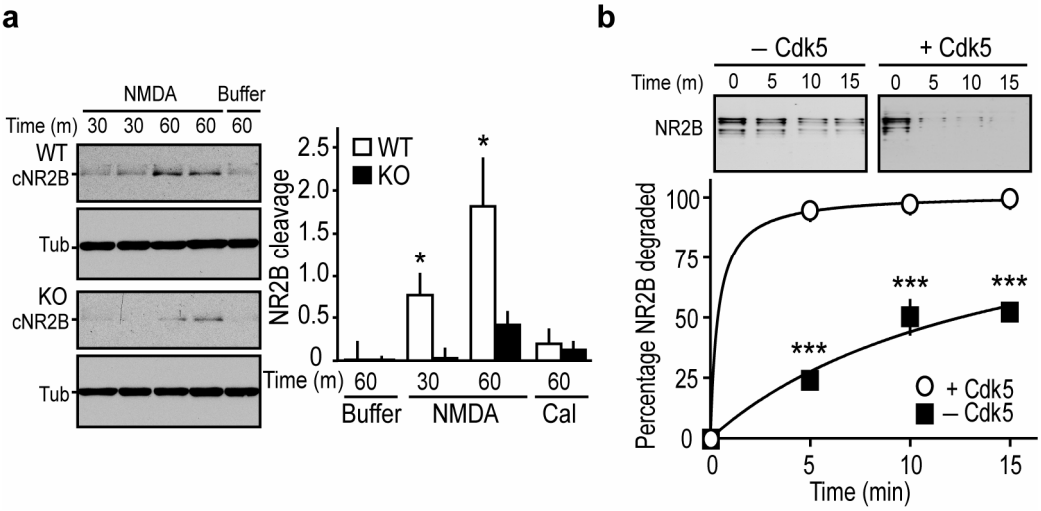

Figure 2.20. Cdk5 facilitates the calpain-mediated cleavage of NR2B *in vivo* and *in vitro*. (a) Calpain-mediated NR2B cleavage in hippocampal slices post-NMDA treatment. Cleaved NR2B (cNR2B) was detected following 30- or 60-min treatment with buffer, 50 μM NMDA, or 50 μM NMDA/20 μM calpeptin (Cal) Tubulin (Tub) served as a loading control; n = 4–6. (b) Calpain-mediated degradation of NR2B *in vitro* in the presence or absence of Cdk5/p25 (n = 3). Data represent means ± s.e.m.; *P < 0.05, ***P < 0.05 (*post hoc*) vs. WT; Student's *t*-test.

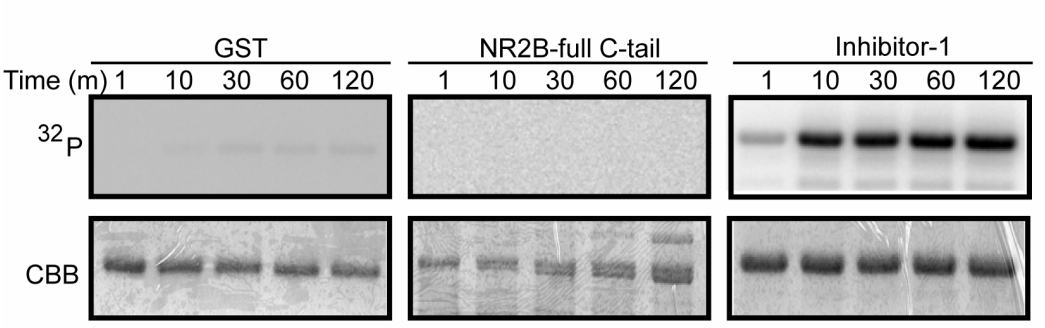

Figure 2.21. Analysis of NR2B cytoplasmic tail as a candidate Cdk5 phosphorylation substrate *in vitro*. *In vitro* Cdk5 phosphorylation time course reactions using purified GST (negative control), NR2B cytoplasmic tail, and protein phosphatase inhibitor-1 (positive control) as substrates. Radiolabeled (top) and Coomassie-stained (bottom) proteins are shown for time course reactions conducted for the indicated periods of time. No ^{32}P-ATP incorporation was detected for GST or NR2B.

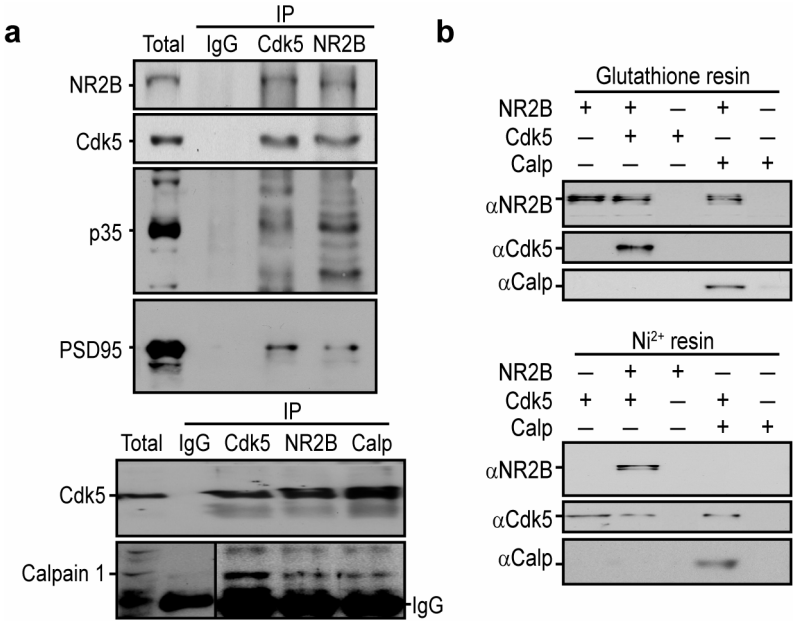

Figure 2.22. Cdk5, NR2B, and calpain interact *in vivo* and directly bind one another *in vitro.* (a) Coimmunoprecipitation of NR2B, Cdk5, and calpain-1 from WT hippocampus. Lysates or immunoprecipitates derived using the antibodies indicated (IP) were immunoblotted for proteins denoted (left). Representative of 8 experiments. 10% of lysates used for immunoprecipitations was loaded into total lanes. (b) Cytoplasmic NR2B, Cdk5, and calpain binding assays. Immobilized NR2B C-terminus (top) or Cdk5/p25 (bottom) were incubated with Cdk5/p25, NR2B, and/or non-activated calpain. Immunoblots show selective binding of Cdk5, NR2B, and calpain. Representative of 12 experiments.

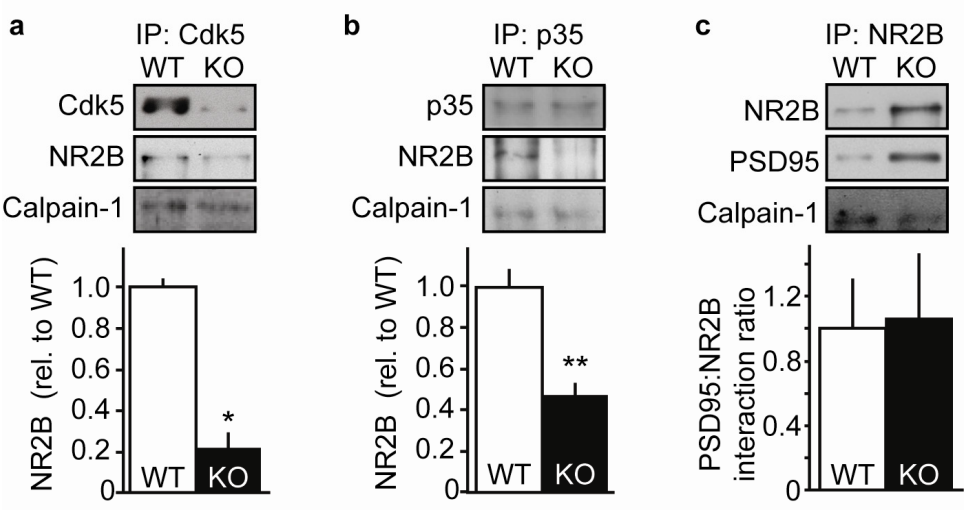

Figure 2.23. Coimmunoprecipitation analysis in Cdk5 KO hippocampus.
(**a** and **b**) Immunoblots of Cdk5, p35, NR2B, and calpain-1 following Cdk5 or p35 immunoprecipitation (IP) with quantitation of NR2B pull down. (**c**) Immunoblots of NR2B, PSD95, and calpain-1 following NR2B immunoprecipitation (IP) with quantitation of relative PSD95:NR2B coimmunoprecipitation ratio. Excess antibody was used for all immunoprecipitation assays; n = 3—6. Data represent means ± s.e.m. *P < 0.05, **P < 0.005 different from WT; Student's *t*-test.

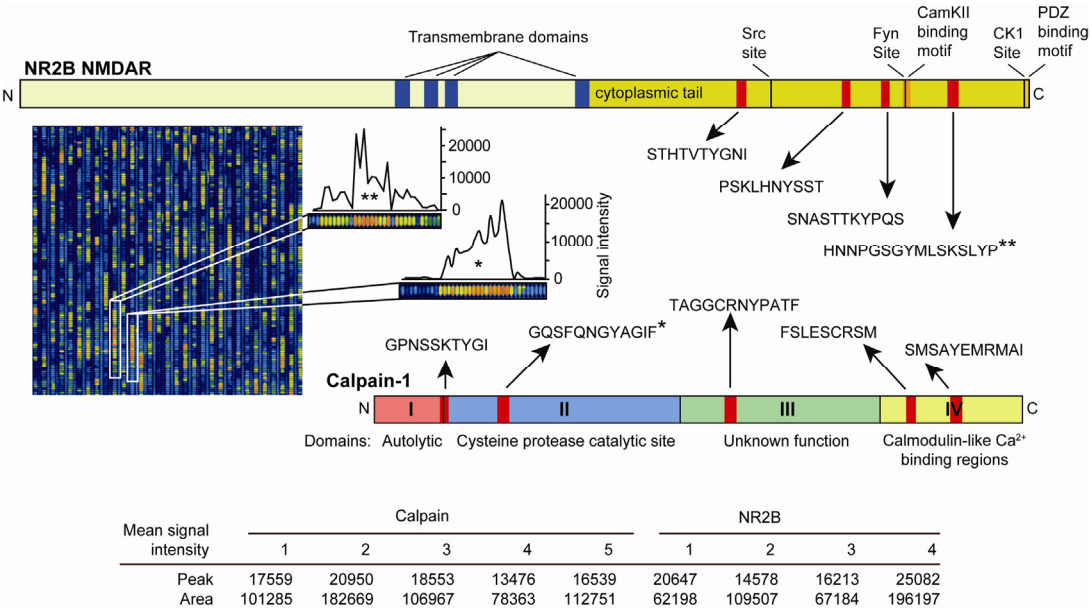

Mean signal intensity	Calpain					NR2B			
	1	2	3	4	5	1	2	3	4
Peak	17559	20950	18553	13476	16539	20647	14578	16213	25082
Area	101285	182669	106967	78363	112751	62198	109507	67184	196197

Figure 2.24. Peptide array analysis of Cdk5/p25 binding domains on NR2B and calpain-1.

In vitro Cdk5/p25 binding assays were performed on a peptide array that contained overlapping amino acid cassettes for NR2B and calpain. Signal intensity for the entire chip and select sequences are shown with quantitation (inset; red = strong; blue = weak). Diagrams of NR2B and calpain-1 are shown with sequences with the highest affinity for Cdk5/p25. Below is quantitation of mean signal intensity peak and area for each candidate peptide in arbitrary units. Binding assays were done in triplicate for each peptide and there was no observable background detection.

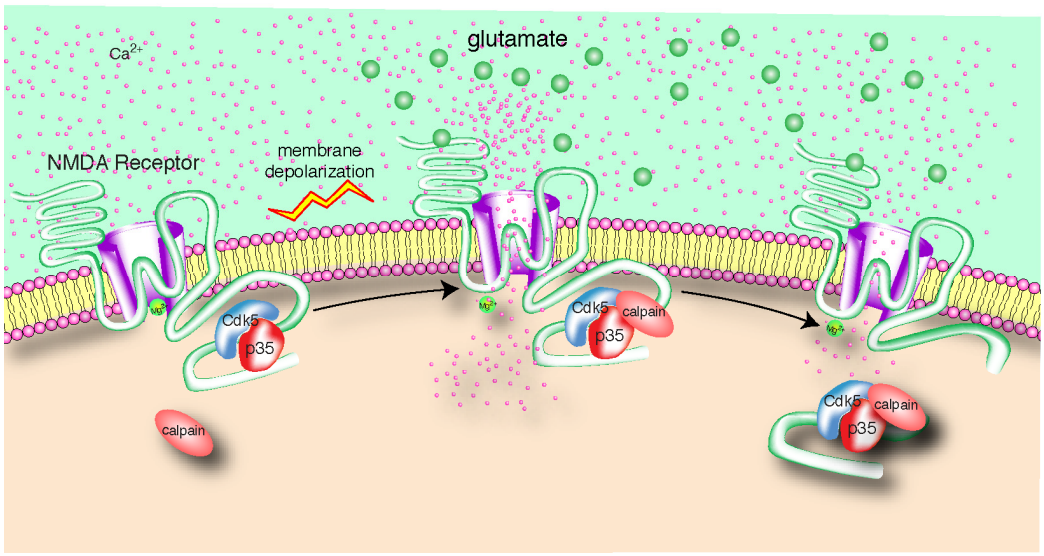

Figure 2.25. Schematic of Cdk5's role in degradation of the NR2B NMDA receptor subunit.
The Cdk5/p35 complex is depicted as bound the NR2B NMDA receptor subunit. Depolarization leads to activation of the NMDA receptor and calpain. Cdk5 binds with calpain and facilitates proteolysis of the NR2B C-terminus. Cleavage of p35 to p25 is not shown.

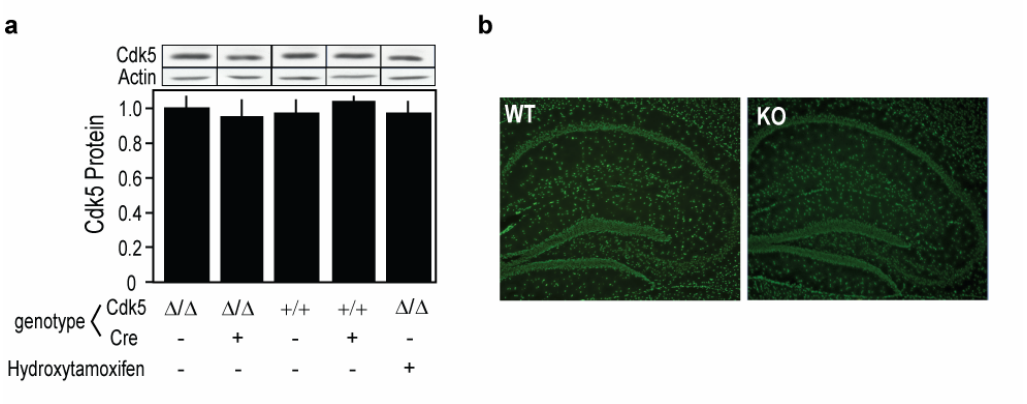

Supplementary Figure 2.1. Controls for hippocampal Cdk5 levels and cytoarchitecture. (**a**) Quantitative immunoblot analysis of hippocampal Cdk5 relative to actin loading control in littermate and drug control mice. Δ/Δ indicates floxed Cdk5 alleles, +/+ indicates WT Cdk5 alleles. The presence of the Cre transgene and hydroxytamoxifen treatment are also indicated. n = 4, P > 0.9, Student's *t*-test. No differences were observed in pixel intensity for actin. (**b**) Representative fluoro-Nissl stains of WT and KO hippocampi 2—4 weeks following Cdk5 KO mice show no gross aberrations in hippocampal cytoarchitecture. Data represent means ± s.e.m.

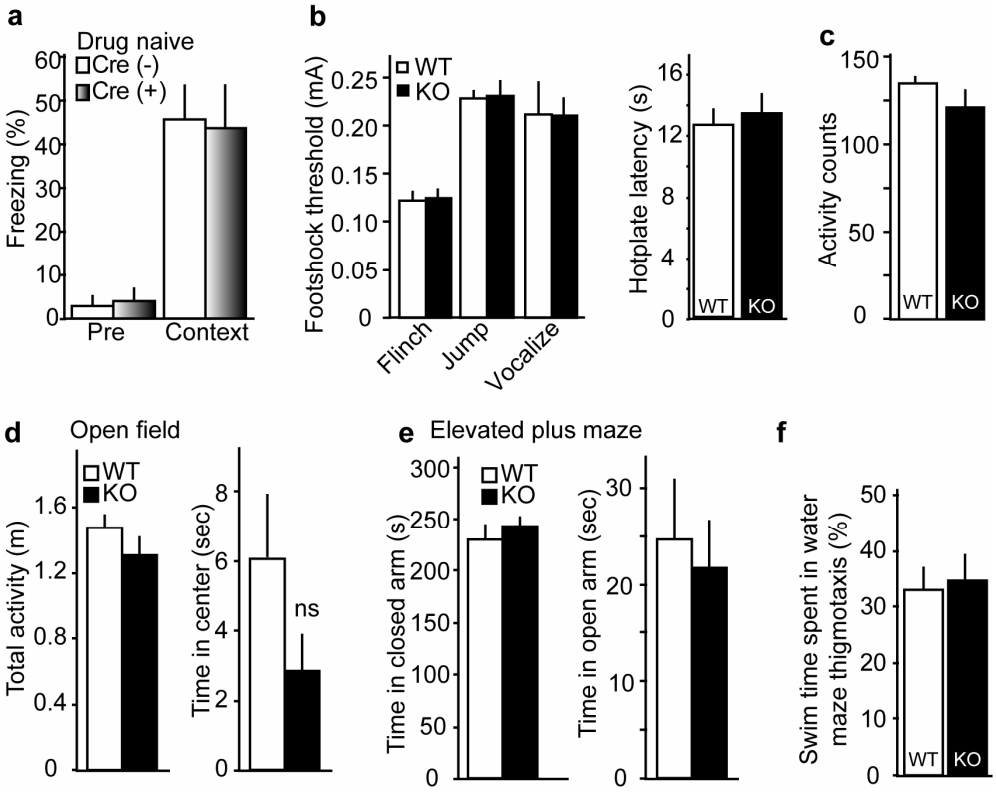

Supplementary Figure 2.2. Controls for pre-knockout memory and effects of Cdk5 knockout on nociception, anxiety, and locomotion. (a) Context- and cue-elicited memory 24-h post-training in animals not dosed with hydroxytamoxifen. Freezing time before conditioning (Pre) and following context re-exposure are shown (n = 6). (b) Foot shock threshold and hotplate hind paw lick/jump latency are shown for Cdk5 WT vs. KO (n = 10—12). (c) Spontaneous locomotor activity recorded over 5 min; mean locomotor counts ± s.e.m., n = 16—17. (d and e) Open field and elevated plus maze anxiety assays. Total activity and amount of time spent in the center of open field, and time in closed/open arms of elevated plus maze are shown (n = 27—31; *ns* = P > 0.1, Student's *t*-test). (f) Percent of time spent in the thigmotaxis of water maze during first day of water maze training. Data represent means ± s.e.m.

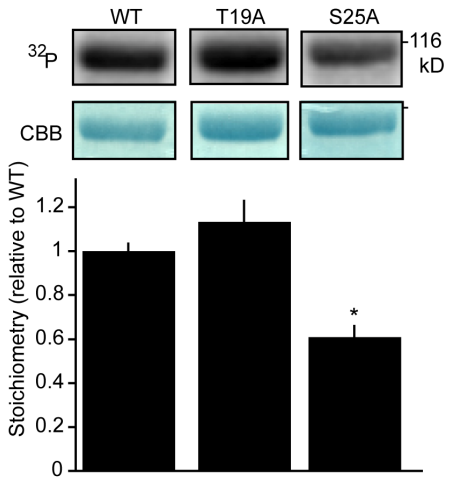

Supplementary Figure 2.3. Cdk5 phosphorylates serine 25 residue on PSD-95 *in vitro*. Cdk5 phosphorylation reactions *in vitro* using purified wild-type PSD-95, T19A PSD-95 mutant, and S25A PSD-95 mutant as substrates. Radiolabeled (top) and Coomassie-stained (bottom) proteins are shown with quantitation for saturated reactions. n = 3, *P < 0.05 Student's t-test. Data represent means ± s.e.m.

CHAPTER THREE

EVALUATION OF ACTIN POLYMERIZATION AND SPECTRIN DEGRADATION IN CONDITIONAL CDK5 KNOCKOUT MICE

Summary

Cdk5 controls learning and plasticity via regulation of functional synaptic plasticity. Data from conditional Cdk5 KO mice suggest that Cdk5 may also play a role in structural plasticity. NMDAR activation following synaptic transmission can lead to calpain activation, spectrin cleavage, actin depolymerization, and morphological changes in dendritic spines [83]. Conditional loss of Cdk5 led to decreases in total and synaptic levels of depolymerized actin in the hippocampus. Consistently, conditional knockout of Cdk5 also led to an impairment in calpain-mediated degradation of spectrin *ex vivo*. Lastly, recombinant Cdk5 directly facilitated the calpain-mediated degradation of spectrin *in vitro*. These studies suggest that Cdk5 regulates the calpain-mediated degradation of spectrin and actin polymerization, thereby implicating Cdk5 in spine dynamics and the modulation of spine shape and size during synaptic remodeling.

Introduction

Learning and memory is thought to depend on short- and long-term plastic changes in synapses. Such changes may consist of functional alterations in ion channel properties, recruitment of silent synapses, changes in synapse number, or alteration in spine morphology[2]. Much attention has focused on the phosphorylation/dephosphorylation events which modulate functional plasticity and the addition of new synapses. However, spine dynamics also plays an

important role. Synaptic depolarization leads to activation of calpain, cleavage of spectrin, depolymerization of actin, and remodeling of the dendritic spine [83,84]. Modulation of this pathway may alter spine size and shape thereby affecting neuronal excitability and synaptic plasticity. Since Cdk5 has been implicated in structural plasticity[5], we examined Cdk5's role in the regulation of spectrin degradation and actin depolymerization *in vitro* and *in vivo*.

Experimental Procedures

Spectrin cleavage in vitro

Spectrin cleavage assay *in vitro* was performed similarly to the NR2B cleavage assay described in chapter 2. Purified spectrin (Sigma) was incubated with calpain for 0, 5, 10, and 15 minutes in the presence of Cdk5 or Cdk5 buffer . Reactions were stopped with protein sample buffer and spectrin levels were analyzed by 8% SDS-PAGE and western immunoblot analyses. Spectrin was detected using rabbit anti-human spectrin antibody (Sigma, 1:400).

Slice pharmacology and immunoblots

NMDA treatment slice pharmacology was performed exactly as described in chapter 2. Synaptosomal preparations, hippocampal tissue from slice pharmacology, and crude lysates were lysed in SDS and analyzed by 12.5% or 15% SDS-PAGE and immunoblot analyses (see chapter 2). To measure actin levels, samples were run on a standard 15% SDS-PAGE which only allowed for depolymerized actin to enter the resolving gel. Brain spectrin was detected in *ex vivo* slice pharmacology experiments using a rabbit polyclonal anti-brain spectrin antibody (240/235E; Chemicon 1:500). Cleaved spectrin ran at 150/145 kDa[85,86]

and was quantified and compared to untreated controls. p25 and p35 Cdk5 cofactors were detected using a rabbit polyclonal antibody (Santa Cruz, 1:200). Striatal enriched protein tyrosine phosphatase (STEP) was detected in hippocampal synaptosomes (see chapter 2) using a mouse monoclonal antibody provided by Paul Lombroso (Yale University; 23E5, 1:1000).

Statistical analysis

All data was represented at mean ± s.e.m. Errors for fold changes were calculated using standard error propagation rules. Differences between data groups were evaluated for significance using analysis of variance with *post hoc t*-tests and statistical significance was set to $p < 0.05$.

Results

Reduced levels of depolymerized actin in the hippocampus and synapses of Cdk5 KO mice

Actin is a critical component of the cytoskeleton of cells and plays roles in the in neuronal dendritic spine dynamics[87,88]. Consequently, changes that alter actin polymerization mechanisms have major effects on spine dynamics, synaptic plasticity, and learning[89]. Standard 15% acrylamide gel electrophoresis requires that actin be depolymerized in order to enter the resolving gel. Polymerized actin and very large protein complexes will remain in the stacking layer of a SDS-PAGE gel. Conditional loss of Cdk5 decreased the level of depolymerized actin in hippocampal lysates (100.0 ± 3.7 % and 78.3 ± 2.9 % for WT and KO, respectively, **Fig. 3.1A**). Since changes in synaptic actin polymerization contribute to spine dynamics, we examined the levels of depolymerized actin in synaptosomal preparations. Conditional loss of Cdk5 led to a 82.7% decrease in

synaptosomal depolymerized actin levels (**Fig. 3.2A**). In contrast, Cdk5 KO did not alter detected levels of alpha-tubulin (not shown), which served as a loading control. Consequently, loss of Cdk5 decreased total and synaptic levels of depolymerized actin.

Cdk5 facilitates calpain-mediated cleavage of spectrin and other substrates ex vivo and in vitro

Dynamic actin filaments are involved in the formation of dendritic spines during development, structural plasticity at mature synapses[89], and many other processes throughout the cell. Spectrin, another cytoskeletal element, stabilizes polymerized actin in the synapse. Calpain-mediated degradation of spectrin leads to destabilization and depolymerization of actin filaments[83,84]. Conditional loss of Cdk5 was previously shown to blunt calpain-mediated cleavage of NR2B *ex vivo* (see chapter 2). Calpain-mediated cleavage of brain spectrin was altered in Cdk5 KO slices (**Fig. 3.1B**). Thirty-minute treatment with NMDA led to equivalent spectrin cleavage in WT and KO slices. However, 60-minute treatment with NMDA led to 1.82 ± 0.08- and 0.87 ± 0.09-fold increases in the cleaved 150/145 kDa form of spectrin in WT and KO slices, respectively. This finding suggests that loss of Cdk5 (1) blunted the calpain-mediated cleavage of spectrin following 60 min treatment with NMDA, or (2) Cdk5 facilitated subsequent steps in spectrin degradation. If the former is true, the data correlate with the decreased levels of depolymerized actin in Cdk5 KO tissue. However, additional experiments will be necessary. Furthermore, it is not clear if this modulation by Cdk5 *in vivo* plays any important role in the healthy or pathological brain.

Similarly to what was observed with NR2B, recombinant Cdk5/p25 dramatically increased the calpain mediated cleavage of spectrin *in vitro* (**Fig. 3.1C**). In an optimized cleavage-assay, addition of Cdk5 led to complete degradation of spectrin after 10 minutes of incubation. In contrast, little-to-no

cleavage was seen with Cdk5 buffer alone. Cdk5/p25 was shown to directly bind with calpain *in vitro* (see chapter 2). It is unclear whether or not Cdk5 binds with or phosphorylates spectrin. Since the *in vitro* cleavage assay contained no ATP or Mg^{2+}, it is likely that Cdk5/p25 facilitated the calpain-mediated degradation of spectrin via direct protein—protein interactions with calpain and/or spectrin.

Interestingly, Cdk5 may also regulate the degradation of additional calpain substrates. Conditional loss of Cdk5 impaired generation of p25 *ex vivo*. Treatment of hippocampal slices with NMDA for 1 hour led to a significant accumulation of p25 in WT but not KO slices (**Fig. 3.2A**). Analysis of untreated whole hippocampal lysates also showed impaired p25 generation following Cdk5 loss. Hippocampal p25 levels were low in young adult WT and KO mice. However, an age-dependent accumulation of p25 was blunted in Cdk5 KO mice (**Fig. 3.2B**). These data correlate with one another and suggest that Cdk5 may facilitate the calpain-mediated generation of p25. The latter data is particularly interesting because it suggests that (1) p25 accumulates in the hippocampus with age and (2) Cdk5 may regulate age-dependent calpain-mediated p25 generation.

STEP is degraded by calpain *in vitro* and *in vivo* (personal communication, Paul Lombroso, Yale University). Interestingly, this calpain-mediated degradation of STEP was facilitated by Cdk5 *in vitro* (personal communication, Oludotun Adeyo, UT Southwestern Medical Center). Consistently, Cdk5 KO led to increased levels of synaptic STEP. Synaptosomal STEP levels were elevated by 1.3- and 1.4-fold the Cdk5 KO corticostriatum and hippocampus (**Fig. 3.3**). STEP was not elevated in total hippocampal or corticostriatal lysates (not shown), suggesting that STEP may be selectively elevated in the synaptic compartments. In unison, the data presented here and in chapter 2 correlate with one another and suggest that Cdk5 may facilitate calpain-mediated cleavage of numerous substrates including NR2B, spectrin, p25, and

STEP *in vivo* and *in vitro*. Consequently, loss of Cdk5 *in vivo* blunts the calpain-mediated degradation of substrates.

Discussion

Cdk5 has been implicated in a large number of physiological processes and pathologies. Consequently, it is not surprising that conditional loss of Cdk5 in the adult brain produces several phenotypes. In chapters 2 and 3, we discuss three of the possible roles for Cdk5 in functional plasticity and spine dynamics.

Although other laboratories have focused on the roles of Cdk5 in structural plasticity (*e.g.* spine numbers), the research presented in chapter 2 focused on Cdk5's role in functional plasticity. During the course of our studies it became apparent that conditional loss of Cdk5 may also have effects on structural plasticity. Initial studies in biocytin-labeled neurons revealed no major differences in spine numbers or density 2-4 weeks following of Cdk5 KO (personal communication; Kanehiro Hayashi, University of Texas Southwestern Medical Center). However, spine dynamics, shape, and size all play major roles in synaptic plasticity and recent data has further implicated Cdk5 in adult spine dynamics[90,91]. Thus, it was not surprising to find that Cdk5 regulated spectrin degradation and actin polymerization. Synaptic depolarization and Ca^{2+} influx can lead to calpain activation, spectrin degradation, and actin depolymerization [83,84]. This process directly modulates synaptic plasticity by altering spine shape and size. We hypothesize that Cdk5 directly facilitates the calpain-mediated degradation of spectrin thereby leading to decreased levels of polymerized actin (**Fig. 3.4**).

Interestingly, Cdk5 also facilitated the calpain-mediated degradation of STEP (personal communication; Oludotun Adeyo, UT Southwestern Medical Center) and Cdk5 KO produces and synaptic elevation in STEP levels. In correlation, Cdk5 KO also led to a decrease in the levels of phospho-Tyr 1472 NR2B, a STEP dephosphorylation site (see chapter 2). We hypothesize that the

elevation in synaptic STEP may contribute to decrease in phospho-Tyr 1472 NR2B. This may represent another interesting feedback mechanism in the neuron. It would be useful to assess the activity of immunoprecipitated STEP from Cdk5 KO tissue and examine the phosphorylation states of additional STEP substrates.

The data suggest that Cdk5 facilitates calpain-mediated cleavage of numerous substrates. This is particularly fascinating and opens the possibility that Cdk5 may facilitate the degradation of other biologically relevant calpain substrates. For example, previous reports have implicated calpain[92] and Cdks [93-96] in the replication of viruses, such as the human immunodeficiency virus. Thus, inhibition of the Cdk5—calpain interaction may serve as a potential anti-viral therapy. Cdk5 and calpain have also been heavily implicated in stroke and excitotoxic injury[14,97,98]. Although most of the previous reports and focused on the calpain-mediated generation of p25, little is understood about the role Cdk5—calpain interactions in stroke and neurodegeneration. Disruption of this interaction may prevent, minimize, and/or ameliorate damage that occurs during stroke and other excitotoxic insults. Clearly, in order to disrupt this interaction, further analysis of the Cdk5—calpain relationship is necessary. In addition to completing a full characterization of the activation and binding *in vitro*, it will be essential to fully determine the binding domains on both Cdk5 and calpain. Furthermore, it will be useful to establish high throughput binding and cleavage assays to screen for drugs which will inhibit or enhance the interaction/facilitation. Lastly, the data suggests that Cdk5 may facilitate the calpain-dependent cleavage of numerous substrates. However, these observations are merely correlative and it will be essential to further characterize where and when Cdk5 affects calpain's activity in the cell.

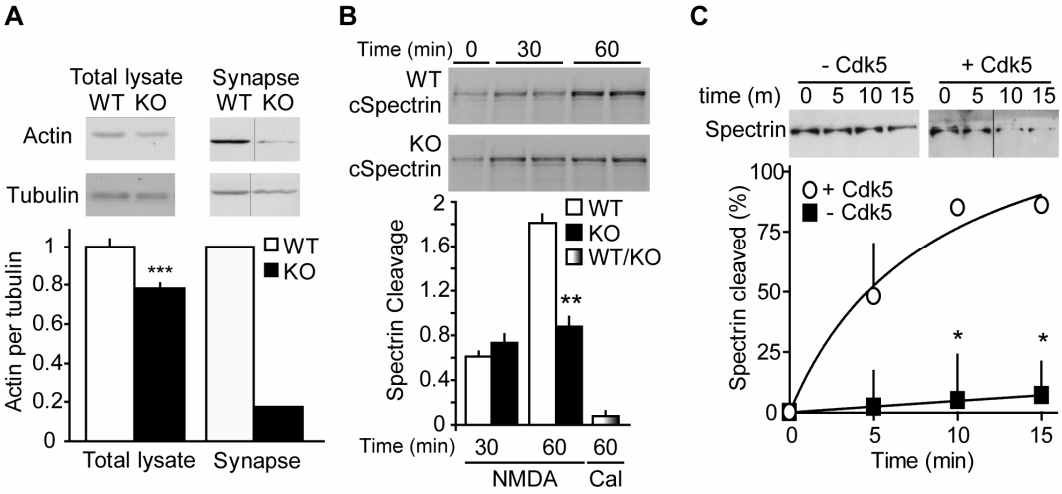

Figure 3.1. Regulation of actin polymerization and spectrin degradation by Cdk5. (**A**) Immunoblot analysis of depolymerized actin in total hippocampal lysates (left) and forebrain synaptosomes (right) in Cdk5 KO and control (WT) mice with quantitation relative to tubulin. For crude lysates, n = 6. For synaptic preparation, tissues from 3 animals per genotype were pooled and data is representative of 3 separate experiments. (**B**) Calpain-mediated brain spectrin cleavage in hippocampal slices after NMDA treatment. Cleaved spectrin (cSpectrin, 150/145 kDa) was detected and quantified following 30- or 60-min treatment with 50 μM NMDA or 50 μM NMDA + 20 μM calpeptin (Cal). Quantitation of cSpectrin levels is normalized to tubulin; n = 3-4. (**C**) Calpain-mediated degradation of spectrin *in vitro* in the presence or absence of Cdk5/p25 (n = 3). *P < 0.05, *post hoc* Student's *t*-test; **P < 0.01, *** P < 0.002 vs. control, Student's *t*-test.

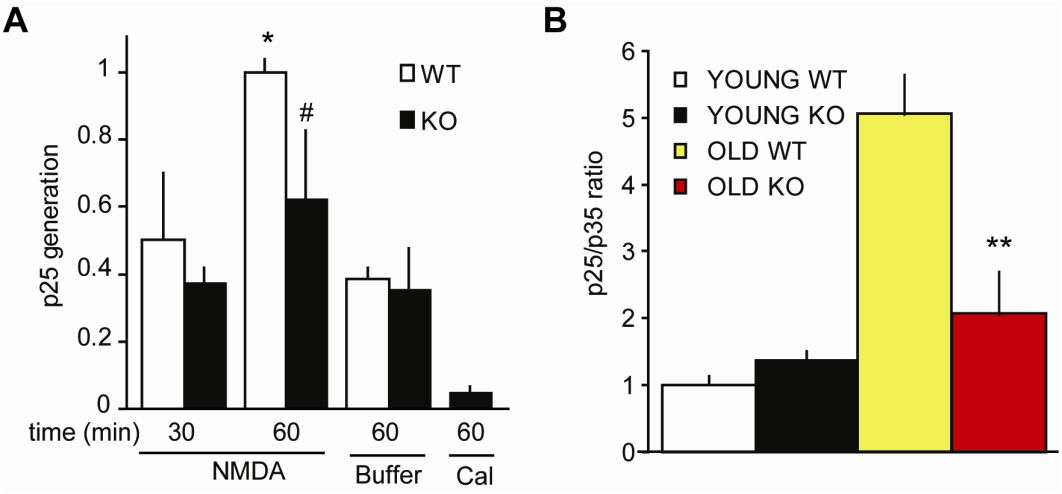

Figure 3.2. Impaired p25 generation in Cdk5 KO mice. (**A**) Calpain-mediated p25 generation in hippocampal slices after NMDA treatment. p25 was detected by immunoblot analysis and quantified following 30- or 60-min treatment with 50 μM NMDA, buffer alone, or 50 μM NMDA/20 μM calpeptin (Cal); n = 6. p25 levels are normalized to tubulin. Asterisk indicates different from 30 min and buffer ($P < 0.05$). # indicates no difference from 30 min and buffer ($P > 0.8$, Student's *t*-test). (**B**) Quantitation of hippocampal p25:p35 ratio in young and aged adult mice. Crude lysates were immunoblotted for p25 and p35. Young adult mice were ~8 weeks old and ~2 weeks post-hydroxytamoxifen treatment. Aged mice were ~12 weeks old and ~6 weeks post-hydroxytamoxifen treatment. Double asterisk indicates $P < 0.05$ versus aged WT, Student's *t*-test; n = 3-4. Data represent means ± s.e.m.

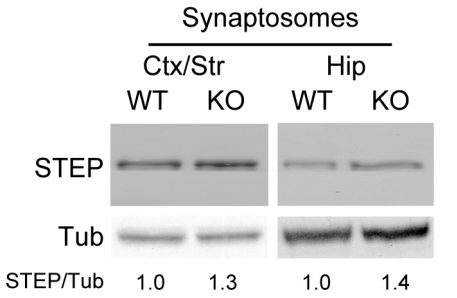

Figure 3.3. Effects of conditional Cdk5 KO on synaptic STEP levels. Immunoblot analysis and quantitation of STEP-61 and tubulin loading controls in hippocampal synaptosomes. For synaptic preparations, tissues from 3 animals per genotype were pooled.

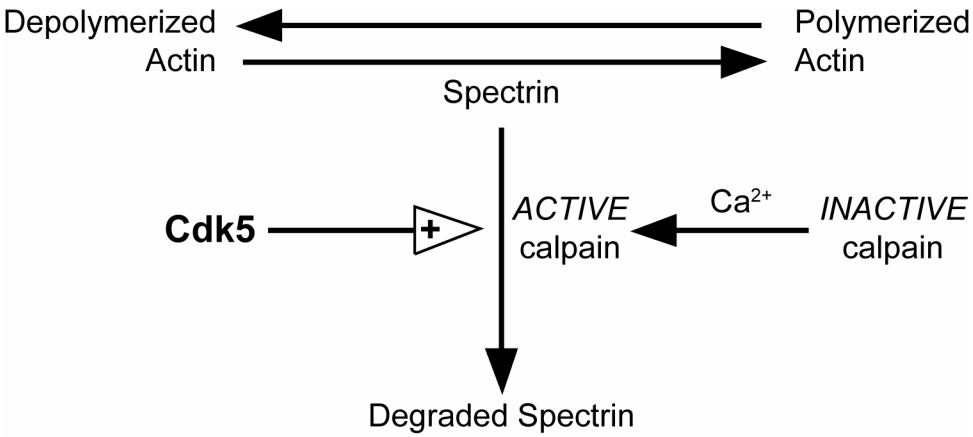

Figure 3.4. Model for the regulation of actin polymerization by Cdk5. The schematic diagrams a hypothesized role of Cdk5 in actin polymerization in which Cdk5 facilitates the calpain-dependent spectrin degradation.

CHAPTER FOUR

CYCLIN-DEPENDENT KINASE 5 REGULATES SEIZURE SUSCEPTIBILITY AND HIPPOCAMPAL NEURONAL EXCITABILITY

Summary

Cyclin-dependent kinase 5 (Cdk5) is a proline-directed serine/threonine kinase essential for nervous system development that has been implicated in learning, synaptic plasticity, neurotransmission, and several neurological disorders. Expression and activity of Cdk5 and its cofactors are elevated in tissues from hippocampal sclerosis and cortical dysplasia epilepsy patients. In addition, Cdk5-activating cofactor p35 knockout mice display seizures and lethality. We assessed the role of Cdk5 in seizure susceptibility and neuronal excitability. Chemically-induced status epilepticus and electroconvulsive shock in wild-type animals led to an increase in levels of the Cdk5-activating cofactor, p25. Chronic conditional knockout of Cdk5 in the adult brain led to an increase in seizure susceptibility and lethality. Extracellular field excitatory post-synaptic potentials (fEPSPs) from the Schaffer collateral CA1 subregion of the hippocampus (SC/CA1) revealed a neuronal repolarization impairment, lower threshold for epileptiform activity, and elevated Mg^{2+}-sensitive currents in conditional Cdk5 knockout mice. Increased seizure susceptibility and neuronal excitability was followed by signs of neurodegenerative sequelae. Recurrent seizures in chronic Cdk5 KO mice were associated with impairments in synaptic transmission. Finally, prolonged loss of Cdk5 for 6 months led to electroencephalographic generalized slow waves and reduced brain weight. These results suggest that

Cdk5 plays an important role in reducing seizure susceptibility and neuronal excitability and may be a useful and novel pharmacological target for anticonvulsant therapy.

Introduction

Five percent of the population report a non-febrile seizure at some time in their lives [99,100]. Current anticonvulsant therapeutics increase inhibitory neurotransmission, suppress high frequency neuronal firing through increasing the refractory period of voltage-gated Na^+ channels, or inhibit voltage-gated T-type Ca^{2+}-channels. Such therapeutic options produce unwanted side effects, are only efficacious in 70% of adults suffering from recurrent seizures [99], and generally alleviate the symptoms rather than curing or modifying the underlying etiology [101]. Aberrations in neuronal excitability can produce abnormal electrical discharges in the brain. Thus, a better understanding of the cellular mechanisms underlying neuronal excitability will aid in the development of novel therapeutics.

Cyclin-dependent kinase 5 (Cdk5), a proline-directed serine/threonine protein kinase, and its neuronal-specific activating cofactors have been implicated in a plethora of physiological and pathological processes in the mammalian nervous system [8,9,16,18,35,38,46-48]. Cdk5 plays critical roles in neuronal migration during developmental cortical lamination[15]: it has been implicated in neurotransmitter release and endocytosis in the adult synapse. Cdk5 has been suggested to both modulate neurotransmitter release[22,23,24] and has specifically been implicated in exocytosis and endocytosis via phosphorylation of numerous substrates including synapsin, amphiphysin I, and dynamin[25-27,102]. In addition, Cdk5 has been heavily implicated in hippocampal learning and synaptic plasticity [3,5,6,9,103,104] and the pathogenesis of several neurodegenerative disorders such as Alzheimer's disease and neuropsychiatric illnesses such as addiction [28-30].

Evidence to date suggests that Cdk5 may play important roles in regulating neuronal excitability and reducing susceptibility towards seizures. Abnormal expression and dysregulation of Cdk5 and its cofactors have been demonstrated in tissues from human cortical dysplasia [105,106] and hippocampal sclerosis [107,108]. Second, knockout of p35 leads to cortical lamination defects, seizures, and lethality [19,36,37]. Mice lacking p35 also display abnormal morphological and functional organization of the hippocampus, dysplastic hippocampi, heterotopic pyramidal cells, and granule cell dispersion and may serve as a model for cortical dysplasia [37,109]. Lastly, conditional loss of Cdk5 and transient overexpression of Cdk5-activating cofactor, p25, led to increases in N-methyl-D-aspartate receptor (NMDAR)-mediated synaptic transmission [5,9]. These studies support the possibility that aberrations in Cdk5 may lead to elevations in neuronal excitability and increase the susceptibility to seizures. Further investigations in this area are necessary.

After investigating the effects of seizure-induction and electroconvulsive shock on Cdk5 cofactor generation, we studied the role of Cdk5 in seizure susceptibility and neuronal excitability using conditional Cdk5 knockout (KO) mice (see chapter 2)[9]. Lastly, we examined the sequelae of increased neuronal excitability an seizure susceptibility in conditional KO mice. Pharmacologically-induced status epilepticus and electroconvulsive shock triggered the generation of p25, a highly active Cdk5 cofactor. Loss of Cdk5 initially resulted in improved learning and synaptic plasticity 2-4 weeks after knockout (Hawasli et al 2007). However, longer-term loss of Cdk5 in conditional knockout mice led to increases in seizure susceptibilities, lethality, repolarization impairments, a lower threshold for *in vitro* epileptiform activity, and an elevation in Mg^{2+}-sensitive currents. Recurrent seizures in Cdk5 KO mice were associated with an impairment in excitatory synaptic transmission. Lastly, prolonged loss of Cdk5 for 6 months led

to electronencephalographic pathologies and reduced brain mass which are suggestive of neurodegeneration.

Experimental Procedures

Animals and reagents

Unless otherwise noted, mice were housed 4 per cage in a colony maintained at 23°C with a 12 h light/dark cycle (lights on from 7:00 A.M. to 7:00 P.M.) and *ad libitum* food and water. All procedures were approved by the UT Southwestern Institutional Animal Care and Use Committees (IACUC). Breeding, genotyping, and knockout induction were performed as previously described (see chapter 2) [9]. Unless otherwise specified, reagents were purchased from Sigma.

Pharmacologically-induced status epilepticus and electroconvulsive shock

Six-week old C57BL/6 (Charles River Labs) wild-type mice were injected with vehicle (saline, *i.p.*), kainate (50 mg/kg, *i.p.*; Tocris), scopolamine (2 mg/kg, *s.c.*)/saline (*i.p.)*, or scopolamine (2 mg/kg, *s.c.*)/pilocarpine (280 mg/kg, *i.p.*). Scopolamine was injected 5 min prior to pilocarpine. Animals were scored for latencies to and frequencies of seizure stages including head nodding, wet dog shakes, forelimb clonus, tonic-clonic seizures, rearing, and, rearing/falling. Hippocampi were dissected 25 min after first robust episode of rearing/falling, flash frozen, and stored at -80˚C.

Electroconvulsive shock (ECS) was administered by Kanehiro Hayashi (University of Texas Southwestern Medical Center) and Stephan J. Gold (Merck Laboratories) to adult male Sprague−Dawley rats (175—200 g) by delivering a current of 50 mA for 0.3 sec via bilateral ear clips essentially as described [110]. Hippocampi were dissected at the specified time-points after stimulation, flash frozen, and stored at -80˚C. Animals which did not receive the shock served as

controls.

Immunoblot analysis

Frozen samples were sonicated in boiling 1% SDS containing 50 mM NaF and boiled for an additional 5 min. Protein concentrations were determined by the BCA protein assay (Pierce) using bovine serum albumin standards. An equal amount of total protein (100 μg) from each sample was subjected to SDS-PAGE followed by electrophoretic transfer to nitrocellulose membranes (Whatman). The membranes were immunoblotted using antibodies for p35/p25 (1:200; C-19 Santa Cruz) and alpha-tubulin (1:5000), followed by incubation with a horseradish peroxidase-conjugated anti-rabbit or anti-mouse secondary antibody (1:8000; Chemicon). Antibody binding was detected by autoradiography using the enhanced chemiluminescence immunoblotting detection system (Amersham Biosciences) and quantified by densitometry using Image J software (NIH). Other immunoblot experiments were performed with antibodies to phospho-Thr205 Tau (1:1000, Sigma), phospho-Thr668 APP, and GFAP (1:2000, DAKO).

Seizures and startle response behaviors

All behavioral experiments were performed with 8—14 week old males, 2—8 weeks following the last dose of hydroxytamoxifen (*i.e.,* 2—8 post-knockout), with the experimenter blind to genotype. Behavioral seizures were scored based on the Racine scale [109,111,112]. Seizure classes one through five were scored as mouth movements, head nodding or wet dog shakes, clonus, rearing, and rearing/falling, respectively. Behavioral seizure parameters such as wild running, tonic-clonic seizures, and tonus were also scored. To assess handling-induced seizures, animals which experienced daily handling were initially observed for signs of spontaneous seizures in home cage for 30 min and then assessed for 30 min after tail lift and scruffing. Handling-induced seizures

generally included head nodding, clonus, or clonus with loss of balance. Chemically induced seizures were studied in mice 8-weeks post-KO. Animals were given scopolamine (2.75 mg/kg, *s.c.*) 5 min prior to pilocarpine (325 mg/kg, *i.p.*). Latency to and frequency of wet-dog shakes, clonus, tonus, rearing and falling and other seizures classes were recorded.

Audiogenic seizures were induced 8-weeks post-KO in a plexiglass shock box with clear front and rear walls (MedAssociates). Mice were scored for baseline behavior for 3 min and scored during exposure to a 90 db, 2,800 Hz pulse tone for 3 min. Frequency of and latency to wild running, tonic-clonic seizures, tonus, other seizure stages, and death were recorded. Startle response behavior was studied 3—6 weeks post-KO using the SR-Lab system (San Diego Instruments) as described [113]. Animals were placed into the SR-Lab system and exposed to white noise at various decibels in a random order. The velocity of movement in response to each tone was detected by a dynamic driver, compiled, and averaged.

Electrophysiological recordings

Transverse hippocampal slices from 8-14 week old males were prepared in cutting saline (200 mM sucrose, 3 mM KCl, 1.4 mM NaH_2PO_4, 26 mM $NaHCO_3$, 2 mM $MgCl_2$, 2 mM $CaCl_2$, 10 mM glucose) and maintained in an interface chamber containing artificial cerebrospinal fluid [58]. Extracellular field excitatory post-synaptic potentials (fEPSPs) in the Schaffer Collateral/CA1 hippocampal pathway (SC/CA1) were synaptically evoked at 0.033 Hz and recorded in the *stratum pyramidale* and *stratum radiatum* layers using a 64-channel array (150 μm interpolar distance, MED-P5155, Alpha MED Sciences). Input-output measurements were performed as described in chapter 2[9] and, unless otherwise stated, fEPSPs were evoked using a stimulation intensity which elicited 50% maximal response. Data acquisition and analysis were performed using the

Multielectrode MED64 hardware and software packages (Panasonic) essentially as described in chapter 2[9]. Stimulus artifacts were removed and additional analyses were performed using custom macros running under Igor Pro, Microsoft Excel, and Graphpad Prism.

fEPSP repolarization: Repolarization experiments were performed 2—6 weeks post-KO. To examine the contributions of $GABA_A$ receptors, *N*-methyl-D-aspartic acid receptors, and voltage-gated Ca^{2+} channels on fEPSP amplitudes, slopes, and half-widths, fEPSPs were measured before and after treatment with 2 μM SR95531, 75 μM AP5, and 0.1 or 0.5 mM NiCl, respectively. Some experiments were performed in the presence of 50 nM TTX to prevent population spikes.

Epileptiform activity and fEPSP measurements in Mg^{2+}-free conditions: Epileptiform activity experiments were performed 4—8 weeks post-KO. fEPSP input/output measurements were made in regular ACSF to determine the stimulation intensities required for 20% of maximal fEPSP amplitudes. Baseline and Mg^{2+}-sensitive fEPSP amplitudes and areas were measured in regular ACSF and Mg^{2+}-free ACSF, respectively. Mg^{2+}-sensitive fEPSP measurements in the *stratum radiatum* were recorded using the 20%-maximal stimulation intensity, which allowed for accurate measurement of fEPSP magnitude in the absence of population spikes and epileptiform activity. Any fEPSP measurements contaminated with population spikes were excluded from calculations. Evoked population spikes and epileptiform activity in the *stratum pyramidale* were also recorded in Mg^{2+}-free buffer. For each slice, fEPSP input/output measurements were performed in triplicate in Mg^{2+}-free buffer and analyzed for the presence of population spikes. Stimulation intensities were binned and data was fit with a sigmoidal curve with $R^2 > 95\%$. Most measurements were performed in the presence of 50 nM TTX, 2 μM SR95531, 50 μM $NiCl_2$, and 10 μM nimodipine.

Electronencephalographic (EEG)-Electromyographic (EMG) recordings.

Male mice (10-26 weeks old) were surgically implanted for long-term EEG/EMG monitoring as previously described [114]. Mice were anesthetized with a mixture containing 25 mg/ml ketamine and 2.5 mg/ml xylazine (administered i.p. at a dose of 0.1 mL/mouse). They were then held in a stereotaxic frame fitted with a mouse adaptor (David Kopf Instruments, Tujunga, CA). The cranium was exposed, cleaned of all connective tissue, and 4 burr holes were drilled, anterior and posterior to bregma, bilaterally (AP 1.1, ML ±1.45 and AP -3.5, ML ±1.45). A prefabricated implant, with 4 EEG and 2 EMG electrodes, was then stereotaxically lowered and cemented to the skull using glass ionomer dental cement (Ketac-Cem Aplicap; ESPE, Norristown, PA). EMG wire electrodes were inserted contralaterally into the nuchal musculature using blunt dissection techniques. After suturing, the mouse was removed from the stereotaxic frame and allowed to recover from anesthesia. This design for the EEG/EMG implant allowed precise insertion of electrodes, targeting the frontal and occipital cortices at a consistent depth, just touching the dura, while minimizing surgical trauma.

Mice were housed individually under a 12 h light-dark cycle at 24 ± 1°C, with standard laboratory chow (Harlan Teklad, Madison, WI) and water being replenished as necessary each day. Mice were not otherwise disturbed. They were habituated to these conditions for a week before EEG/EMG signals were recorded over 24 hour duration. Connections were made from the implanted cranial electrodes to the amplifier (Grass Model 78; Grass Instruments, West Warwick, RI) using a flexible, freely moving, lightweight cable. Amplified and filtered (EEG: 0.3 - 100 Hz; EMG: 30 - 300 Hz) signals were digitized at a sampling rate of 250 Hz, displayed using custom polygraph software, and archived for subsequent off-line analysis. Subsequently, the EEG/EMG record was visually screened for seizure epochs. EEG/EMG recordings and analyses were performed

by Della Koovakkattu, Shiori Ogawa, and Christopher Sinton (University of Texas Southwestern Medical Center).

Statistical analysis

All data was represented at mean ± s.e.m. Errors for fold changes were calculated using standard error propagation rules. Differences between data groups were evaluated for significance using analysis of variance with *post hoc t*-tests and statistical significance was set to $p < 0.05$.

Results

Status epilepticus and electroconvulsive shock leads to the production of Cdk5 activating cofactor in the hippocampus

Both conditional knockout of Cdk5 [9] and transient overexpression of p25 [5] result in increased synaptic plasticity and learning, suggesting common mechanistic features between loss of Cdk5 and diversion of Cdk5 to form a complex with p25. Interestingly, human hippocampal sclerosis is accompanied by p25 generation and elevated Cdk5 activity [107]. To further assess the role of Cdk5 in acute seizures and the homeostasis of neuronal excitability, status epilepticus was induced pharmacologically in wild type mice and p25 levels were assessed in hippocampal lysates. Kainate-induced status epilepticus led to 5.0 ± 2.7- and 3.9 ± 1.3-fold increases in p25 level and p25/p35 ratio, respectively (**Fig. 4.1*A***, left). Similarly, pilocarpine-induced status epilepticus caused 2.8 ± 0.8- and 2.5 ± 0.6-fold increases in p25 level and p25/p35 ratio (**Fig. 4.1*A***, right). Generation of p29 was not assessed. Hence, chemically-induced status epilepticus in wild-type animals led to generation of p25 in hippocampal lysates.

Chemically-induced acute seizures only represents one of many models used to study abnormal electrical discharges in the brain. Generation of p25 was

also analyzed following electroconvulsive shock. Electroconvulsive shock, which causes broad forebrain epileptiform activity, is clinically used to treat mental depression [115] and experimentally used for the generation of seizures [116]. Electroconvulsive shock is also thought to induce synaptic remodelling by altering neuronal biochemistry [117]. Acute electroconvulsive shock resulted in time-dependent accumulation in p25 in hippocampus (**Fig. 4.1*B***). Sixty minutes following electroconvulsive shock, p25 levels increased 2.47 ± 0.08-fold when compared to unshocked controls. The findings suggest that both pharmacologically- and electrically-induced epileptiform activity in the brain results in the hippocampal accumulation of Cdk5 activating cofactor p25. p25 may play physiological roles in healthy neurons to regulate neuronal excitability. Alternatively, generation of p25 due to non-physiological influx of Ca2+ may lead to the phosphorylation of *aberrant* substrates (i.e., substrates whose phosphorylation is associated with neurodegeneration).

Increased seizure susceptibility follows chronic loss of Cdk5

Conditional knockout of Cdk5 was achieved by deriving mice in which *loxP* elements flanked critical exons in both *Cdk5* alleles. Recombination was mediated with a transgenic estrogen receptor-Cre recombinase fusion, under control of the prion promoter [51] (see chapter 2[9]). In characterizing these mice, it was noted that prolonged loss of Cdk5 (for ≥ 8 weeks) was associated with handling induced seizures and lethality when compared with controls. This observation prompted assessment of susceptibilities to handling-, pharmacologically-, and audiogenically-induced seizures. Vehicle-dosed and hydroxytamoxifen-dosed (WT) control mice displayed no spontaneous, handling-induced, or audiogenically-induced seizures. Furthermore, behavioral seizure susceptibilities and latencies were equivalent between the vehicle-dosed and WT groups (not shown). Chronic loss of Cdk5 led to handling-induced head nodding,

wet dog shakes, or clonus behavioural seizures in 80% of mice after 8 weeks of Cdk5 KO (*i.e.,* 8 weeks post-KO; **Table 4.1, Fig. 4.2*A***). While mild handling induced Racine scale 1-3 class seizures, more stressful conditions, such as water immersion, often triggered Racine scale 3-5 seizures or tonus followed by death in different cohorts of chronic KO mice (not shown). Increased seizure susceptibility was associated with several other pathological phenotypes. First, seizure susceptibility correlated highly with lethality: loss of Cdk5 for 8 weeks was associated with 40% mortality (**Table 4.1, Fig. 4.2*B***). Secondly, loss of Cdk5 prevented a typical age-dependent weight gain observed during adulthood (**Fig. 4.3**). Over the course of 6 months, WT mice gained 13.8 ± 2.5 grams. This represented a 48.8% increase in body weight. In contrast, Cdk5 KO mice only gained 3.8 ± 2.0 grams. This represented a 14.7% increase in body weight. Consequently, chronic loss of Cdk5 increased susceptibility to handling-induced seizures, led to lethality, and prevented age-dependent weight-gain.

To quantify behavioral seizure susceptibility in Cdk5 KO mice, seizure latencies were scored after animals were treated with pilocarpine, a muscarinic agonist and convulsant. Cdk5 KO mice displayed increased susceptibilities (**Table 4.1**) and significantly shorter latencies than WT to wet dog shakes (5.4 ± 0.6 vs. 17.3 ± 4.3 min, respectively), clonus (9.0 ± 3.0 vs. 19.3 ± 4.8 min), and rearing and falling (12.53 ± 1.9 vs. 37.0 ± 12.3 min; **Fig. 4.4*A***). These results signify 68.7%, 53.7%, and 66.2% decreases in mean latencies to induce wet dog shakes, clonus, and rearing and falling classes of behavioral seizures. Hence, chronic loss of Cdk5 decreased the threshold for chemically-induced behavioral seizures.

Chronic loss of Cdk5 also increased susceptibility to audiogenically-induced seizures. As illustrated in **Table 4.1** and **Figure 4.4*B***, high frequency audiogenic stimulation had no effect on WT but induced wild running in 37% of KO mice in 32.3 sec. Wild running progressed to tonic-clonic seizures and tonus

followed by death in 18% of KO animals within 56.0 sec. While chemically-induced seizures are generally thought to model seizures of hippocampal or temporal lobe origin, audiogenic seizures may originate in the brainstem [109]. Therefore, brainstem primary acoustic startle circuit was examined by measuring acoustic startle reactivity. Cdk5 KO startle responses were 1.9 ± 0.7-, 1.8 ± 0.7-, 2.2 ± 0.6-, and 2.2 ± 0.6-fold larger than WT after 90, 100, 110, and 120 db pulses, respectively (**Fig. 4.4*C***). In contrast, no differences between WT and KO were observed in short-term habituation or pre-pulse inhibition (**Fig. 4.5**). Consequently, chronic loss of Cdk5 in the adult brain increased the propensity towards acoustically-induced behavioral seizures and elevated the acoustic startle responses.

Loss of Cdk5 leads to increased fEPSP half-width in the SC/CA1 hippocampal pathway

Limbic seizures, which are thought to originate in the hippocampus [118], can be caused by aberrations in neuronal excitability [101,109,119,120]. Statistical analysis of basal synaptic responses in the SC/CA1 *stratum radiatum* layer revealed that Cdk5 KO mice had significantly longer fEPSP half-widths than WT (7.6 ± 0.3 vs. 6.4 ± 0.4 ms, respectively; **Fig. 4.6*A***). This increase in fEPSP duration in the Cdk5 KO SC/CA1 pathway likely represents an impairment in repolarization, possibly as a result of alterations in ion channel function or regulation by interneurons.

Since aberrations in Na^+ channel properties can affect neuronal firing and repolarization characteristics [121-124] and Na^+ channel serve as a therapeutic target for epilepsy, we examined the basal population-spike threshold and the effects of partial Na^+ channel blockade on fEPSP half-width. To analyze basal population spike threshold, input/output measurements were collected in the *strata radiatum* and *pyramidale*. The stimulation thresholds to induce population spikes in both

layers were equivalent between groups. Furthermore, partial blockade of Na^+ channels with 50 nM TTX produced no changes from baseline in fEPSP amplitudes or half-widths in KO and WT groups (not shown). Thus, loss of Cdk5 likely conferred no gross changes in Na^+ channel activation threshold and partial Na^+ channel blockade did not exacerbate or reverse the fEPSP half-width enlargement in Cdk5 KO mice.

Since Cdk5 KO mice display enhancements in NMDA receptor-mediated synaptic transmission [9], we asked whether a NMDA receptor antagonist reversed the increased fEPSP half-width in Cdk5 KO mice. Administration of an NMDA receptor antagonist, DL-AP5, had no significant effect on basal fEPSP amplitudes in either genotype (not shown). The NMDA receptor antagonist also had no major effect on fEPSP half-widths in WT (5.2 ± 0.3 ms to 5.4 ± 0.3 ms) and KO (6.5 ± 0.2 ms to 6.4 ± 0.2 ms) slices. Additionally, treatment with 100 μM and 500 μM NiCl, a low-selectivity Ca^{2+} channel blocker, did not reverse the elevated fEPSP half-width in Cdk5 KOs. These results suggest that the impairment in fEPSP repolarization was not directly due to alterations in NMDA receptors or voltage-gated Ca^{2+} channel function.

Impairments in inhibitory signaling could result in seizures [101,119,125]. Therefore, the effects of $GABA_A$ channel antagonists on fEPSPs were measured. Administration of SR95531 led to equivalent increases in fEPSP amplitudes in WT and KO (18.6 ± 4.8 vs. 25.0 ± 12.2 % increase from baseline, respectively; **Fig. 4.6*B***, left). However, SR95531 decreased the fEPSP half-width in WT but not KO slices (-12.9 ± 6.1 % vs. +5.8 ± 1.5 % change, respectively; **Fig. 4.6*B***, right). These results suggests that GABA-mediated signaling in Cdk5 KO mice may not contribute to, but rather compensates for the increased fEPSP duration. Therefore, blocking GABA-mediated transmission unmasked and exacerbated the repolarization impairment in Cdk5 KO mice.

Chronic loss of Cdk5 leads to epileptiform activity and elevated Mg^{2+}-sensitive currents.

Hippocampal NMDAR activation is a critical step in many seizure models *in vivo* and *in vitro* [101]. Neuronal hyperexcitablity can produce epileptiform-like activity in acute brain slices and can be characterized by an increased propensity for population spikes (*i.e.*, action potentials) and the presence of abnormal population spikes. We examined whether conditional loss of Cdk5 increased susceptibility to *in vitro* epileptiform activity in the SC/CA1 after unmasking NMDARs. Synaptically-evoked fEPSPs in the *stratum pyramidale* were measured in Mg^{2+}-free conditions. Stimulation of the SC/CA1 pathway at 20%-maximal stimulation intensity produced population spikes in 3.7 ± 2.5% and 10.4 ± 5.0% of WT and KO slices, respectively. A stronger 50%-maximal stimulation intensity produced population spikes in 89.6 ± 4.0% of KO slices but only 16.74 ± 7.7% of WT slices (**Fig. 4.7*A***). Population spikes at threshold stimulations occurred individually or in groups. Due to the variability in spike number, quantiation of population spike size was not possible in many slices. Stronger stimulation intensities elicited population spikes in greater numbers and larger magnitudes for both KO and WT slices. These results suggest that loss of Cdk5 reduced the threshold to induce evoked epileptiform activity in hippocampal slices.

Mg^{2+}-sensitive evoked fEPSP measurements were recorded in the *stratum radiatum* of hippocampal slices. The removal of NMDA receptor Mg^{2+}-blockade produced a 1.71-fold larger fEPSP amplitude change in KO than WT (148.9 ± 7.6 vs. 128.6 ± 4.7 % of baseline, respectively; **Fig. 4.7*B***). Furthermore, overall charge transfer during Mg^{2+}-free fEPSPs were larger in KO than WT slices (162.3 ± 4.4 vs. 145.2 ± 5.7 % of fEPSP area baseline, respectively; **Fig. 4.7*C***).

Recurrent handling-induced seizures after chronic loss of Cdk5 are associated with a functional impairment in hippocampal synaptic transmission.

Recurrent seizures due to aberrations in neuronal excitability can lead to functional impairments in synaptic excitation [126-128]. Loss of Cdk5 for 2—4 (see chapter 2)[9] and 4—8 (not shown) weeks had no significant effects on basal synaptic transmission as assessed by input/output analyses. We assessed the functional consequence of recurrent seizures in chronic Cdk5 KO mice (8—10 weeks post-KO) that displayed at least 3 episodes of Racine class 2—5 seizures upon handling. Significantly smaller fEPSP amplitudes (0.93 ± 0.11 vs. 0.60 ± 0.04 mV for WT and KO, respectively, **Fig. 4.8*A***) and impaired synaptic transmission (**Fig. 4.8*B***) were found in Cdk5 KO mice which displayed behavioral seizures. Consequently, recurrent handling-induced seizures after chronic loss of Cdk5 were associated with functional impairments in excitatory synaptic transmission.

Electronencephalographic generalized slow waves following 6 months of Cdk5 loss

Chronic loss of Cdk5 for 6 months led to abnormal electronencephalographic (EEG)-electromyographic (EMG) patterns. Generalized slow waves were observed 22 weeks after conditional Cdk5 knockout (**Fig. 4.9**). Slow wave episodes were not observed in littermate controls nor in animals 2-8 weeks post-KO (not shown). During a 24-hour recording session, the generalized slow wave duration in Cdk5 KO mice ranged from 52.67 to 406.67 min. Mean episode duration and mean episode frequency ranged from 47.16 to 117.7 sec and from 11.43 to 55.38 min, respectively. The phenotype was characterized by an EEG with prolonged episodes of low amplitude irregular slow waves at 3-4 Hz, with occasional intermittent and isolated rhythmical delta waves at higher amplitude. We also noted an occasional isolated spike on the EEG. Periods of

slow wave activity were typically accompanied by sustained atonic periods on the EMG, or periods of low muscle activity. These were interspersed with rhythmic contractions which did not correlate with changes in the EEG signal.

Reduced brain mass 6 months after Cdk5 knockout

Generalized slow waves in EEGs are generally associated with neurodegeneration and gliosis[129,130]. To assess whether loss of Cdk5 for 6 months led to tissue degeneration, brains from age-matched KO, WT, and controls not treated with hydroxytamoxifen were weighed. The prolonged loss of Cdk5 for 6 months led to a decrease in overall brain mass (**Fig. 4.10**). Brains from undosed animals with and without the recombinase transgene weighed 577.25 ± 16.29 mg and 561.26 ± 15.05 mg, respectively. Brains from hydroxytamoxifen-dosed Cdk5 WT and KO animals weighed 565.33 ± 16.40 mg and 493.00 ± 8.55 mg, respectively. Thus, prolonged loss of Cdk5 led to a 12.8 % reduction in brain mass which is suggestive of neurodegeneration.

Interestingly, changes in brain weight and generalized slow waves were not associated with hyperphosphorylation of Tau or amyloid-precurser protein (APP), which are markers of neurodegeneration. Hippocampal phospho- Thr 205 Tau and phospho-Thr 668 APP were reduced in Cdk5 KO animals which had displayed EEG generalized slow waves (data not shown). These findings are consistent with previous reports which identified phospho-Thr 205 Tau and phospho-Thr 668 APP as Cdk5 phosphorylation sites[30,97]. There were also no significant differences in hippocampal glial fibrillary acidic protein (GFAP) levels by immunoblot analysis. Phospho-205 Tau, phospho-668 APP, and GFAP are merely three markers of neurodegeneration. Thus, it would be interesting examine other biochemical markers of neurodegeneration such as amyloid-beta-42 and activated caspase-3.

Discussion

The data presented here show that Cdk5 regulates neuronal excitability and seizure susceptibility. We found that chemically-induced status epilepticus and electroconvulsive shock induced an acute generation of a Cdk5-activating cofactor, p25. Generation of p25 correlated directly with an increase in Cdk5 activity [5,38]. Recent data have demonstrated dual roles for both Cdk5 and its activating cofactor, p25, in learning and plasticity [5,9]. A dichotomy may also exist for Cdk5's roles in seizures and neuronal excitability. Cdk5 may function through several pathways to dampen excitatory transmission and inhibit epileptiform activity. Alternatively, over-excitation could lead to excessive p25 generation, aberrant Cdk5 activity, and neuronal cell death [14]. Thus, Cdk5 may serve to inhibit abnormal epileptiform activity when a neuron is in a physiological state or promote cell death following non-physiological Ca^{2+} influx.

The present study demonstrates that Cdk5 plays a crucial in reducing seizure susceptibility and neuronal excitability role in the adult brain. We previously demonstrated that loss of Cdk5 led to enhanced learning and synaptic plasticity, elevated NR2B levels, and increased NMDAR-mediated currents 2—4 weeks following knockout induction [9]. Over time however, conditional Cdk5 KO mice displayed an increase in seizure susceptibility. Chronic loss of Cdk5 increased the propensity for pharmacologically- and audiogenically-induced behavioral seizures. In addition, conditional Cdk5 KO mice also displayed an increase in behavioral startle reactivity. We also found an association between the seizure phenotype and the lethality in Cdk5 KO mice such that the frequencies and intensities of spontaneous and handling-induced behavioral seizures generally increased over time and resulted in death. After 10 weeks of Cdk5 KO, the majority of Cdk5 KO mice displayed signs of increased excitability and propensity towards handling-induced seizures. Up to 40% of these mice died soon after displaying these phenotypes.

Interestingly, loss of Cdk5 was also associated with a deficit in age-dependent weight gain during adulthood. Although the increase excitability in Cdk5 KO mice may contribute to this phenotype, it is more likely that the weight-related phenotype is due to other mechanisms which are yet to be described. For example Cdk5 has been implicated in leptin-dependent hypothalamic feeding behaviors (personal communication, Ralph DiLeone, Yale Unviersity). Thus, Cdk5 knockout in hypothalamic pathways may produce deficits in feeding behavior which are unrelated to the observations made during the current studies.

Electrophysiological extracellular recordings *in vitro* revealed that conditional loss of Cdk5 led to increased propensity towards epileptiform activity, elevations in Mg^{2+}-sensitive currents, and impaired neuronal repolarization in the hippocampal SC/CA1 pathway. Although loss of Cdk5 increased the neuronal excitability, it appears that this was partially compensated for by GABA receptor-mediated signaling. Interestingly, the NR2B NMDAR subunit directly modulates neuronal excitability, and contributes to seizures [131-134]. Thus, the elevated levels of the NR2B NMDAR subunit[9] and impairment in fEPSP repolarization in conditional Cdk5 KO mice likely contribute to increases in neuronal excitability and seizure susceptibility.

Genetic deletion of Cdk5 activating cofactor p35 also led to lethality and seizures [19,36,37]. In contrast to p35 knockout mice [8], Cresyl Echt Violet stains of Nissl Substance have revealed no gross changes in basic hippocampal cytoarchitecture 2-4 weeks [9] and 4-6 weeks (data not shown) after loss of Cdk5. Several reports indicate that recurrent seizures can cause functional impairments in neurotransmission [126-128]. Consistently, we found that excitatory synaptic transmission in Cdk5 KO mice displaying recurrent seizures was drastically reduced in magnitude when compared to controls. Recurrent seizures in several models of seizures have been suggested to lead to neuronal sprouting and cell death [109]. It will be worthwhile to assess whether the increase in neuronal

excitability following prolonged Cdk5 KO has any effects on fiber sprouting and cell survival.

Very prolonged loss of Cdk5 in mice was associated with abnormal EEGs readings and reduced brain weight. EEGs revealed the presence of a prolonged generalized slow waves in chronic Cdk5 KO mice. Although generalized slow waves may be seen in epilepsy patients [130] and rhythmic delta activity has some specificity for epilepsy [135-137], the EEGs observed after very prolonged loss of Cdk5 KO are also commonly seen following pathologic gliosis and neuronal loss in chronic epilepsy [129] and in strokes, encephalopathies, and other neurodegeneration. Given that chronic loss of Cdk5 increased neuronal excitability and susceptibility to seizures, and eventually led to reduced brain mass, the generalized slow wave activity may indicate chronic epileptiform activity and/or subsequent neurodegenerative sequelae.

Genetic manipulation in rodents often leads to seizures, underscoring the delicate balance that exists to control excitation and inhibition in the nervous system and implicating relevant neuronal signaling molecules. Although, seizures manifest as aberrations in inhibitory or excitatory neurotransmission, there is a great deal of evidence that intracellular signaling molecules play critical roles in epilepsy. Cdk5 has already been shown to control synaptic plasticity and excitatory neurotransmission via modulation of glutamate receptor subunits in the post-synaptic density [9]. The results presented here show that Cdk5 regulates neuronal excitability and seizure susceptibility and may serve as a therapeutic target for pathological neuronal discharges and seizures.

Acknowledgments

I would like to thank Della Koovakkattu, Shiori Ogawa, Kanehiro Hayashi, Christopher Sinton (UT Southwestern Medical Center) and Stephan J. Gold (Merck Research Laboratories) for help with experiments, and Anne E.

Anderson (Baylor College of Medicine), Donald C. Cooper, and James A. Bibb for training, and supervision. I would also like to thank David Benavides, Wai Ling Lee, Janice Kansy, Jennifer Pick, Bryan Potts, Craig Powell, Shari Birnbaum, and Cathy Steffen. This work was made possible by a NIDA training grant, NARSAD Young Investigator award, and grant funding from the National Institutes on Drug Abuse and Mental Health.

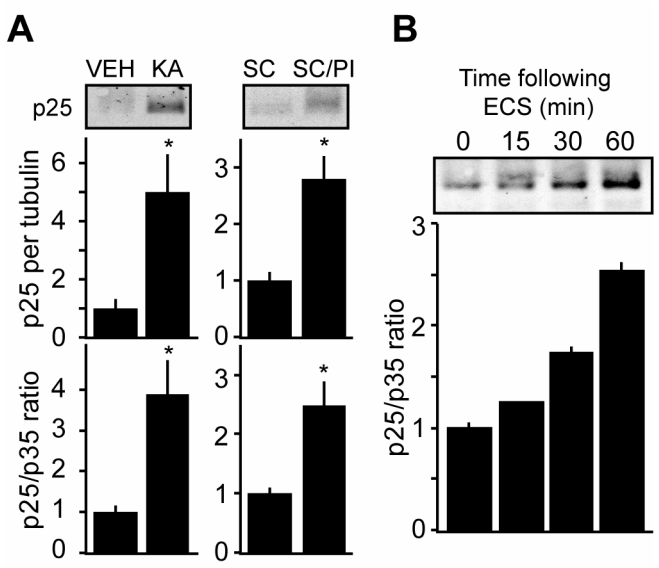

Figure 4.1. p25 generation in the hippocampus after pharmacologically-induced status epilepticus and electroconvulsive shock. (***A***) Representative immunoblots (top) and quantitation of p25 per tubulin (middle) and p25/35 ratio (bottom) after treatment with kainate and pilocarpine. VEH = saline; KA = kainate (50 mg/kg); SC = scopolamine (2 mg/kg)/saline; and SC/PI = scopolamine (2 mg/kg)/pilocarpine (280 mg/kg). n = 4; *P < 0.05 vs. VEH and SC in; Student's *t*-test. ***B,*** Representative immunoblots and quantitation of p25/p35 ratio 15, 30, and 60 min following electroconvulsive shock administration compared to unshocked controls (time = 0); n = 2. Data represents mean ± s.e.m.

Table 4.1. Long-term conditional Cdk5 knockout increases susceptibility to seizures

Handling-induced seizures and lethality

	Morbidity	Seizure latency (wks[1])	Mortality[2]
WT	0% (0/12)	N/A	0% (0/12)
KO	80% (8/10)	5.63 ± 0.53	40% (4/10)

Chemically-induced seizures[3]

	Clonus	Status epilepticus	Tonus & death
WT	71% (5/7)	57% (4/7)	42% (3/7)
KO	100% (7/7)	100% (7/7)	85% (6/7)

Audiogenically-induced seizures

	Wild running		Tonic-clonic seizure		Tonus & death	
	Morbidity	Latency (s)	Morbidity	Latency (s)	Morbidity	Latency (s)
WT	0% (0/10)	N/A	0% (0/10)	N/A	0% (0/10)	N/A
KO	27% (3/11)	32.3 ± 6.7	18% (2/11)	50.0 ± 11.0	18% (2/11)	56.0 ± 6.0

[1] Weeks after last dose of hydroxytamoxifen
[2] Within 8 wks
[3] 325 mg/kg pilocarpine, *i.p.* / 2.5 mg/kg scopolamine, *s.c.*

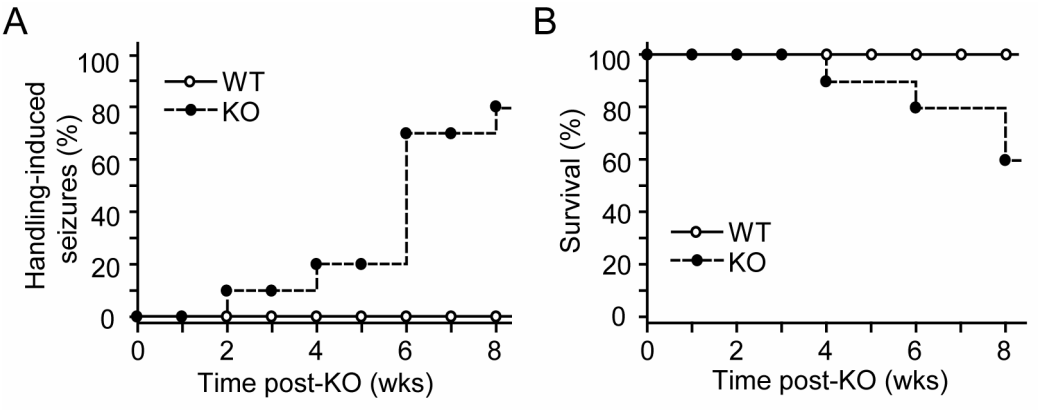

Figure 4.2. Increased seizure susceptibility and lethality after chronic conditional Cdk5 loss. ***A***,***B*** Kaplan-Meier seizure morbidity and survival curves. Percent of animals observed to have handling-induced seizures and percent survival are plotted against weeks post-KO; n = 10—14; differences between WT and KO for morbidity and mortality were statistically significant, $P < 0.01$, log-rank test.

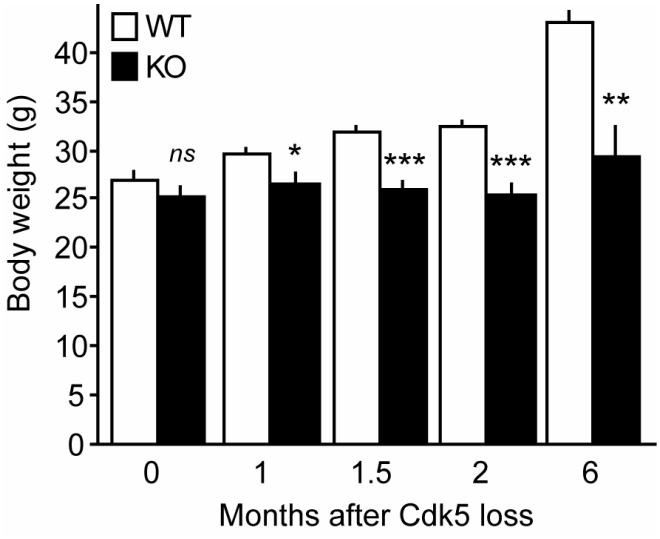

Figure 4.3. Loss of Cdk5 prevents age-dependent weight gain. Mice were weighed after indicated periods of Cdk5 knockout. Animals were treated with hydroxytamoxifen at 6-8 weeks of age. Untreated age-matched mice weighed similarly to hydroxytamoxifen-treated control mice (WT) mice. *ns* indicates $P > 0.2$. *$P < 0.05$, **$P < 0.005$, and ***$P < 0.00005$ vs. WT; *post hoc* Student's *t*-test; n = 4-16.

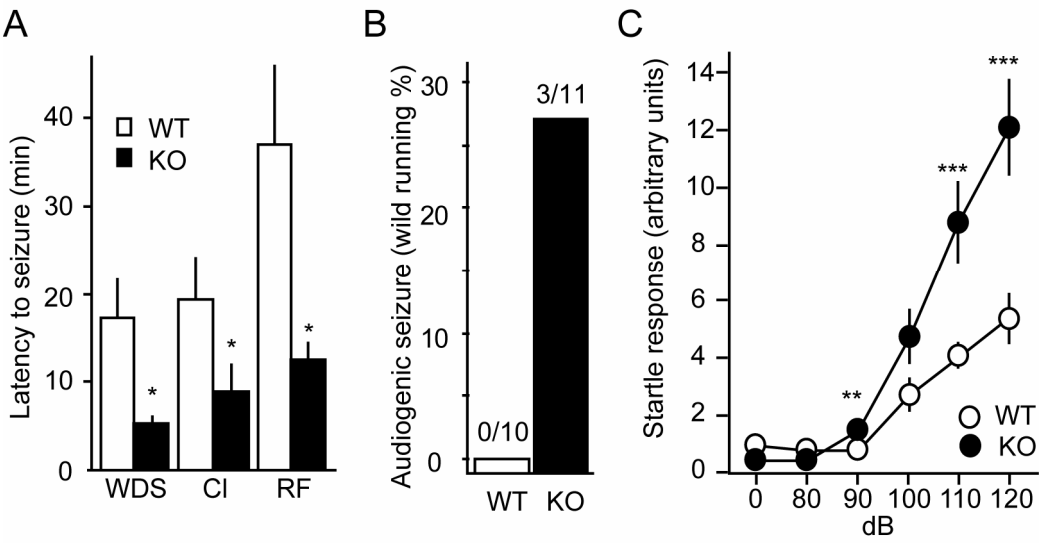

Figure 4.4. Elevated seizure susceptibility after chronic conditional Cdk5 loss. ***A***, Latency to pilocarpine-induced wet-dog shakes (WDS), clonus (Cl), and falling/rearing (RF) seizures in mice 8 weeks post-KO (n = 7—10). ***B***, Percent of animals displaying wild-running seizures following audiogenic induction (8 wk post-KO; n = 10—11). Data is representative of 3 separate experiments. ***C,*** Acoustic startle reactivity in mice 3-6 weeks post-KO (n = 17—21). Vehicle-treated animals behaved similarly to WT in all experiments. *P < 0.05 vs. WT, Student's *t*-test; **P < 0.05, ***P < 0.01 vs. WT, *post hoc* Student's *t*-test. Data represents mean ± s.e.m.

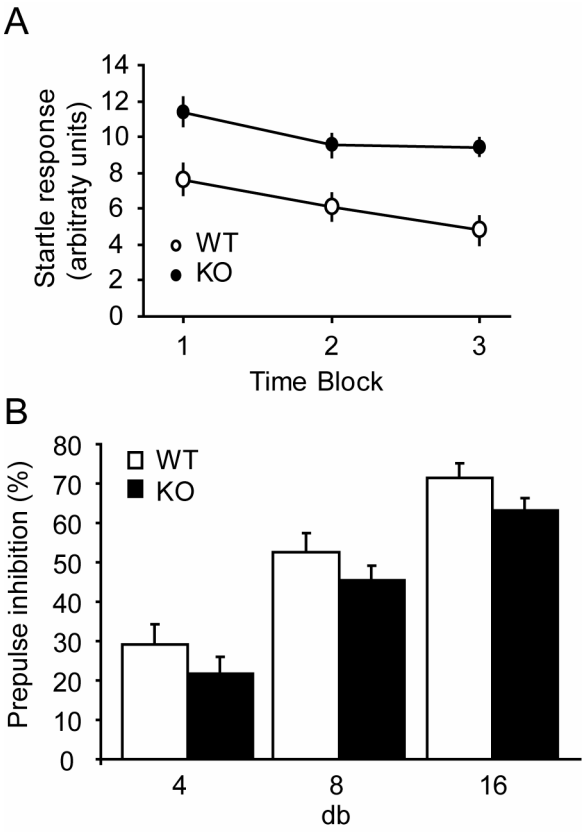

Figure 4.5. Short term habituation and prepulse inhibition in Cdk5 KO mice. (**A**) Habituation to a 120 db sound is shown as startle reactivity in three consecutive time blocks. Genotype and time blocks individually produced significant effects on startle responses ($P < 0.01$), but there was *no* significant interaction between genotype and time block ($P > 0.2$, 2-way ANOVA). n = 9-23. (**B**) Prepulse inhibition in Cdk5 KO mice. Prepulse at indicated decibels were given 5 ms prior to a 120 db sound. Prepulse inhibition is represented as percent decrease compared to an isolated 120 db sound. $P > 0.4$, 2-way ANOVA; n = 20-23. Vehicle-treated animals behaved similarly to WT.

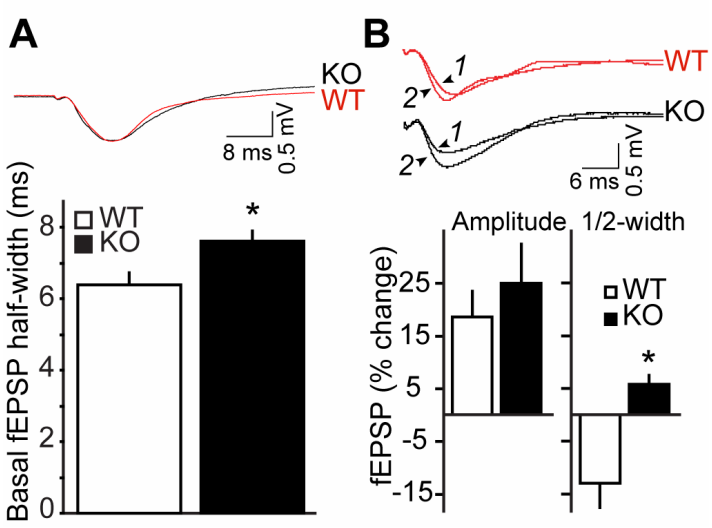

Figure 4.6. Increased fEPSP half-width after conditional Cdk5 loss. ***A***, Increased basal fEPSP half-width in SC/CA1 pathway of KO hippocampus. Representative fEPSPs traces from WT (red) and KO (black) are shown with quantitation (n = 10—12). ***B***, Representative fEPSPs traces before and after $GABA_A$ blockade (top) are shown with quantitation (bottom). Histograms show the changes in amplitude and half-width following treatment with 2 μM SR95531 (n = 8). *1* and *2* indicate traces before and after treatment with SR95531, respectively. SR95531 had similar effects on fEPSP slope measurement. *P < 0.05 vs. WT; Student's *t*-test in ***A*** and *post hoc t*-test in ***B***. Data represents mean ± s.e.m.

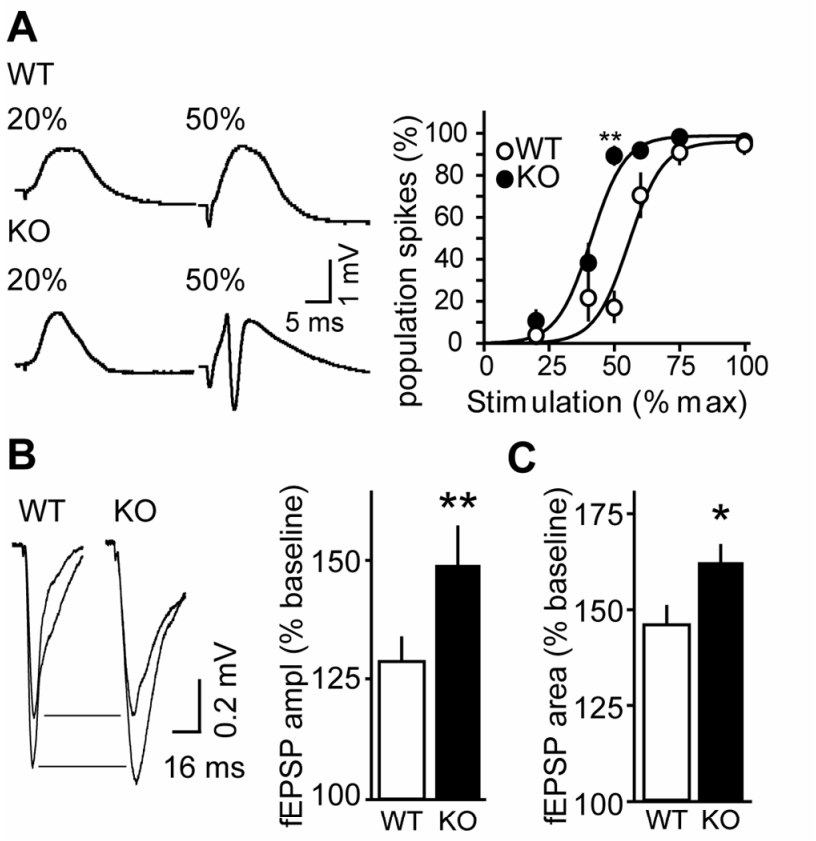

Figure 4.7. Epileptiform activity and elevated Mg^{2+}-sensitive currents in the hippocampal SC/CA1 pathway after conditional Cdk5 loss. ***A***, Representative traces and quantitation showing reduced threshold for population spikes in the *stratum pyramidale* of KO slices. Quantitation shows % of slices displaying population spikes at indicated stimulation intensities (% of maximum); n = 16-18. ***B***, Representative traces (inset) and quantitation of fEPSP amplitude in the *stratum radiatum* relative to baseline following Mg^{2+} wash-out (n = 12). ***C,*** Quantitation of fEPSP area in the *stratum radiatum* relative to baseline following Mg^{2+} wash-out (n = 6). Recordings were performed 4—8 weeks post-knockout. *P < 0.05, **P < 0.01 vs. WT, *post hoc* Student's *t*-test. Data represents mean ± s.e.m.

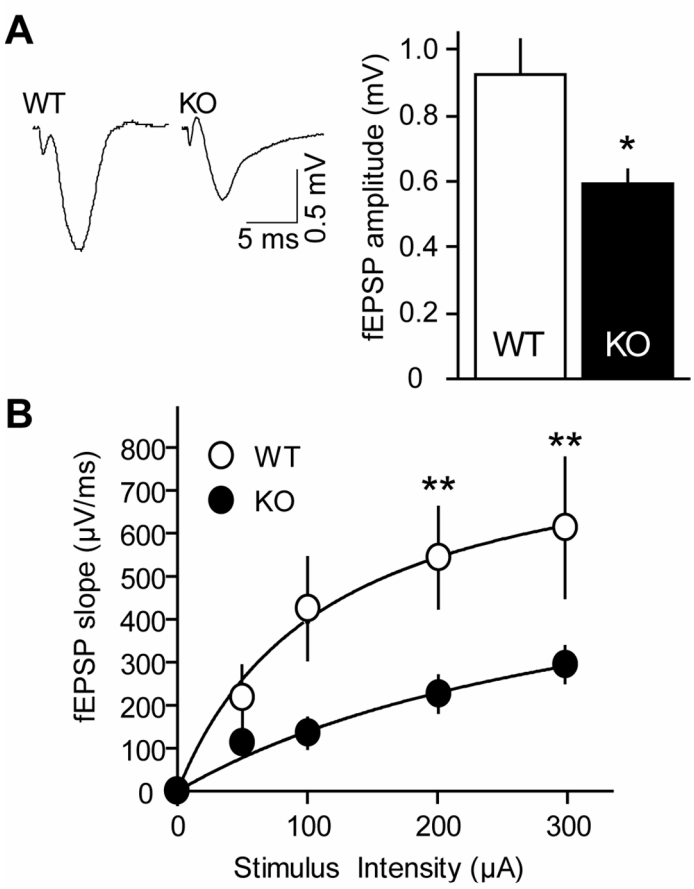

Figure 4.8. Recurrent seizures in chronic conditional Cdk5 KO mice are associated with impaired excitatory synaptic transmission in the SC/CA1 pathway. Representative traces and quantitation of fEPSPs following 30%-maximal synaptic stimulation (***A***) are shown with input/output analysis of synaptic transmission (***B***). Recordings were performed on Cdk5 KO mice displaying recurrent Racine scale 2 or greater behavioral seizures and littermate controls; n = 6—9 ; 8—10 weeks post-KO; *P < 0.05, **P < 0.05 *post hoc* vs. WT, Student's *t*-test. Data represents mean ± s.e.m.

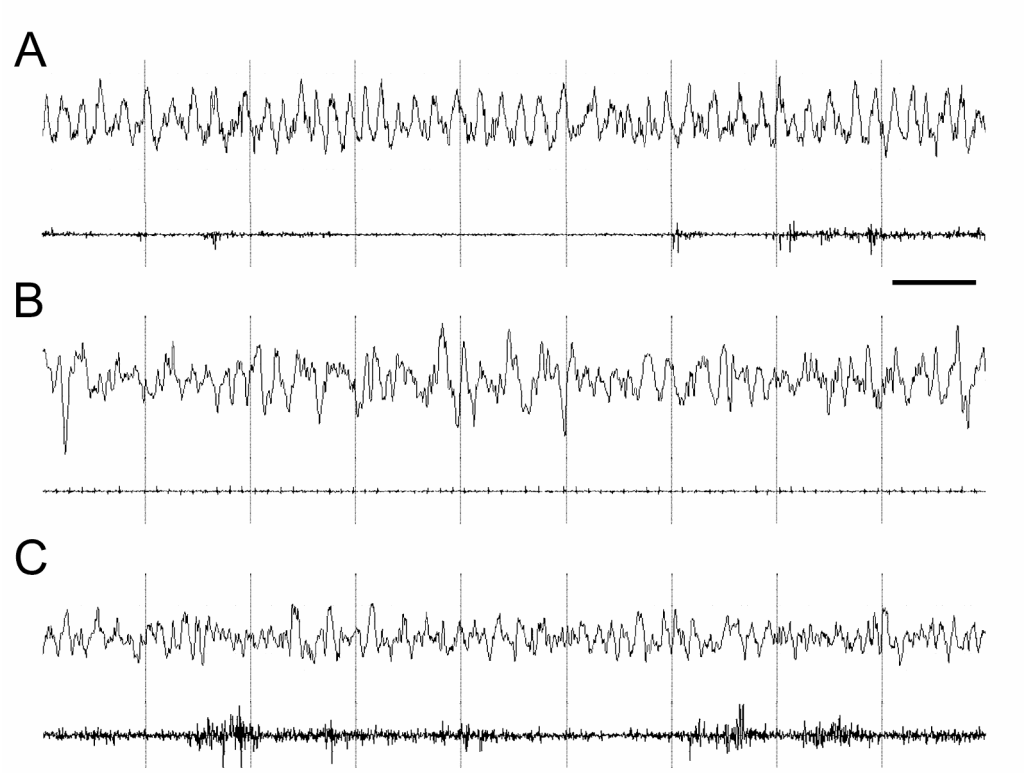

Figure 4.9. Generalized slow waves in exemplar EEG/EMG recordings from a Cdk5 knockout mouse. (***A***) Representative EEG (top) and EMG (bottom) traces of generalized slow wave phenotype which was marked by prolonged periods of generalized irregular EEG slow waves, associated with low EMG activity, interspersed with occasional movement. (***B***) Representative EEG/EMG during a period of non rapid eye movement (NREM) sleep, showing the typical low frequency, high amplitude waves on the EEG associated with this state and the minimal EMG activity, with only the heart rhythm evident against the low background muscle tonus. Some delta (1-4 Hz) activity is also evident on this recording. (***C***) EEG/EMG in an awake mouse is characterized by mixed frequency, low amplitude waves on the EEG and high EMG activity as displayed here. The scale bar represents 1 sec.

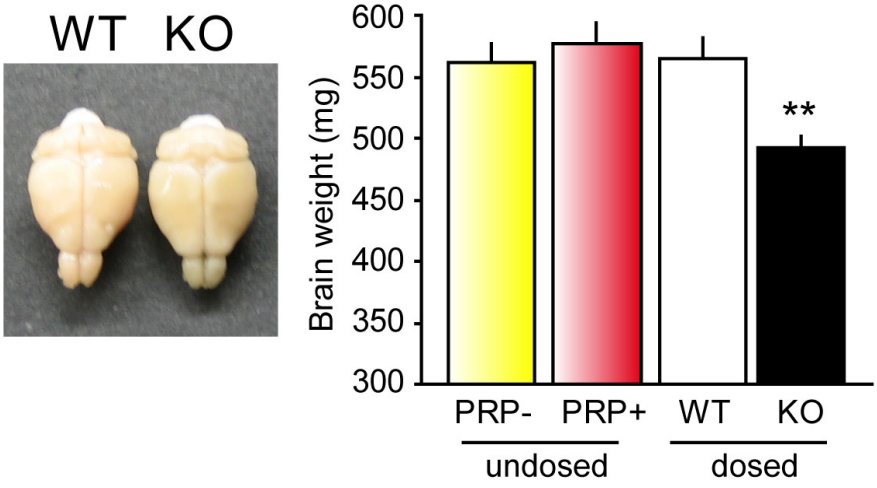

Figure 4.10. Decrease in brain mass after 6 months of Cdk5 loss. Whole brains were dissected and weighed from mice which were intracardially perfused. PRP+ and PRP- indicate hydroxytamoxifen-untreated control animals with or without the Cre transgene. **P < 0.008 vs. WT and undosed controls, determined using a two-tailed, non-parametric Student's *t*-test; n = 4-6.

CHAPTER FIVE

CYTOPLASTIC TAIL OF THE NR2B NMDA RECEPTOR SUBUNIT INHIBITS CYCLIN-DEPENDENT KINASE 5 IN VITRO

Summary

Cyclin-dependent kinases (Cdks) have been therapeutic targets for the treatment of infection diseases, cancer, and neurodegeneration. There exist a handful of potent inhibitors with selectivity for Cdk5[138], including roscovitine, butyrolactone, flavopiridol, and olomoucine. However, as mentioned before, these Cdk5 inhibitors have a variety of non-specific effects independent of Cdk5[32-34]. Nonetheless, the commonly used and novel inhibitors of Cdk5 serve as useful tools in the study of Cdk5 and may have therapeutic potential. Several experimental conditions *in vivo* will produce decreases in the phosphorylation state of Cdk5 sites. Such phenomena suggest there likely exist mechanisms to inhibit Cdk5 activity within the neuron. Cdk5 was shown to directly bind with the cytoplasmic domain of the NR2B NMDAR subunit. Interestingly, recombinant NR2B cytoplasmic tail inhibited the Cdk5-dependent phosphorylation of protein phosphatase inhibitor-1 (I-1) and post-synaptic density protein-95 (PSD-95) during a time-course kinase reaction *in vitro*. NR2B inhibited Cdk5 phosphorylation in a dose-dependent manner. Finally, kinetic analysis revealed the NR2B cytoplasmic tail noncompetitively inhibited Cdk5 with a K_i of approximately 13 μM. It would be interesting to determine if NR2B inhibits Cdk5-dependent phosphorylation of substrates in the brain and if this inhibition is part of a feedback mechanism.

Introduction

Cyclin-dependent kinase 5 phosphorylates numerous synaptic substrates and there are intracellular mechanisms to reduced Cdk5 activity *in vivo*. Cdk5's activity is dependent on cofactors p35 [23,139] or p39 [60]. Additionally, levels of phosphorylation of Thr75 of DARPP-32 and Ser6 and Ser67 of inhibitor-1 are reduced upon treatment with NMDA[56,140], suggesting possible NMDAR-dependent regulation of Cdk5 activity. It is worthwhile to study the regulation of Cdk5, since NMDAR activation is important for both synaptic plasticity and excitotoxicity.

There are several proposed mechanisms for the regulation of Cdk5 activity by NMDA. First, activation of ionotropic glutamate receptors, including NMDA receptors, leads to cleavage of p35 to p25 [141] by the Ca^{2+} activated protease calpain [13,142,143]. Upon cleavage of p35, Cdk5 is translocated away from the membrane to phosphorylate alternative substrates implicated in a wide range of diseases (a.k.a. *aberrant* substrates)[38,98,143,144]. Cdk5 activity can also be regulated via ionotropic glutamate receptors independently of p25 generation [35]. For example, treatment of neuronal cultures with kainate or NMDA induces autophosphorylation of p35, which targets it for degradation by the proteosome, ultimately leading to a reduction in Cdk5 activity. The protein—protein interactions between Cdk5, NR2B, and calpain had important effects on calpain activity and NR2B degradation (see chapters 2 and 3). For the studies described here, we assessed whether the NR2B cytoplasmic tail affected Cdk5 activity.

Experimental Procedures

Reagents and binding assays

Unless otherwise indicated, all drugs and reagents were from Sigma. Recombinant NR2B, PSD-95, and Cdk5 were purified and binding assays were performed as described in chapter 2.

Phosphorylation assays in vitro

Time course phosphorylation reactions were conducted as described in chapter 2. Recombinant protein phosphatase inhibitor-1 (I-1, prepared by Chan Nguyen, UT Southwestern Medical Center) and PSD-95 (10 μM) were incubated with enzymatic quantities of Cdk5 (~0.035 μg/μL; prepared by Kanehiro Hayashi, UT Southwestern Medical Center) in the presence or absence of recombinant 10 μM GST-tagged NR2B or GST alone. Reactions proceeded for indicated time durations and were stopped with protein sample buffer. Incorporation of ^{32}P-ATP was assessed as previously described (see chapter 2).

Dose-response Cdk5 inhibition assays were performed under near-linear conditions. I-1 (10 μM) was incubated with enzymatic quantities of Cdk5 and varying amounts of recombinant GST-tagged NR2B or GST. The same concentration of Cdk5 was used in the dose-response assays as were used in the time course reactions. Reactions were performed for 2 minutes.

Lineweaver-Burk analyses of kinetic Cdk5 phosphorylation reactions were conducted under steady-state conditions. Reaction conditions were optimized to allow for the accurate assessment of reaction velocity. Ninety second 10 μL reactions were conducted with enzymatic amounts of Cdk5 and indicated amounts of I-1 and NR2B. Reactions were stopped by adding 10 μL of 5xPSB and incorporation of ^{32}P was assessed as previously described.

Generation of NR2B mutants

Site directed mutagenesis was performed as described in Chapter 2. A serine-to-alanine mutation was made and stop codons were added at targeted regions. Primers used to make truncation mutant 1 had the following sequences: 5'-ccattgatgggctctaagactgtgacaacccac-3' and 5'-gtgggt tgtcacagtcttagagcccatcaa tgg-3' Primers used to make the S1116A mutant had the following sequences: 5'-cgaccaccccgcgccccagaccac-3'and 5'-gtggtctggggcgcggggtggtcg-3'. Primers used to make truncation mutant 3 had the following sequences: 5'-ggtctgggggca acttctgccgcagctaaccctaaaagctgcac-3' and 3'-gtgcagcttttagggttagctgcggcagaagt tgcccccagacc-5'. Primers used to make truncation mutant 4 had the following sequences: 5'-c atgctcagcaagtcgctctaaccttaacgggtaacgcaaaaccc-3' and 3'-gggt tttgcgttacccgttaaggttagagcgacttgctgagcatg-5'. Mutant plasmids were cloned, sequenced (McDermott Sequencing Center, UT Southwestern Medical Center). Protein purification was attempted as described in chapter 2.

Results

The NR2B NMDAR subunit directly interacts with Cdk5 in vitro.

Previous results (see chapter 2) demonstrated direct interactions between Cdk5, calpain, and NR2B. Additional binding assays confirm the interactions between Cdk5 and NR2B (**Fig. 5.1**). Cdk5 directly interacted with immobilized NR2B but not GST alone. Neither protein phosphatase inhibitor-1 nor DARPP-32 interacted with immobilized NR2B (data not shown). These findings confirm a specific interaction between Cdk5 and NR2B.

The cytoplasmic tail of the NR2B NMDAR subunit inhibits Cdk5-dependent phosphorylation of inhibitor-1 and PSD-95 in vitro.

Cdk5 facilitated the degradation of NR2B through protein-protein interactions. We assessed the effects of the Cdk5—NR2B interaction on Cdk5 kinase activity in time course kinase assays *in vitro*. The recombinant NR2B cytoplasmic tail reduced the maximum stoichiometry of Cdk5-dependent phosphorylation of PSD-95 to 31.9% of control (**Fig. 5.2A**). The NR2B cytoplasmic tail also reduced the maximum stoichiometry of Cdk5-dependent phosphorylation of I-1 to 38.5% of control (**Fig. 5.2B**). Reactions containing an equimolar amount of a control protein, GST, had no effects on phosphorylation stoichiometry of I-1 and PSD-95 (**Fig. 5.2A,B**). The NR2B cytoplasmic tail was not phosphorylated by Cdk5 *in vitro* (see chapter 2). Consequently, NR2B inhibited the Cdk5-dependent phosphorylation of PSD-95 and I-1 *in vitro*.

Concentration-dependent inhibition of Cdk5 by the NR2B NMDAR subunit

The NR2B cytoplasmic tail inhibited Cdk5 in a concentration-dependent manner. Cdk5 and I-1 concentrations were held constant while NR2B and control protein, GST, concentrations were varied. The GST control protein did not inhibit Cdk5-dependent phosphorylation of I-1. In contrast NR2B inhibited Cdk5-dependent phosphorylation of I-1 with an IC_{50} of 3.86 ± 0.70 μM (**Fig 5.3**). 5 μM NR2B reduced Cdk5-dependent phosphorylation of I-1 from 27.2 ± 1.80 % to 12.24 ± 0.44 %. 20 μM NR2B reduced Cdk5-dependent phosphorylation of I-1 to 2.64 ± 0.14 %. Once again, during these reactions, there was no ^{32}P-ATP incorporation into NR2B. These results indicate that the NR2B cytoplasmic tail inhibits Cdk5-dependent phosphorylation of I-1 in a concentration-dependent manner.

Lineweaver-Burk analysis of Cdk5 inhibition by the NR2B NMDAR subunit

Kinetic analyses performed under steady-state conditions confirmed that the NR2B cytoplasmic tail inhibited the rate of Cdk5-dependent phosphorylation of I-1. After optimizing the Cdk5 kinase assay to ensure linear reaction conditions, kinetic Lineweaver-Burk analyses were performed. Velocities were plotted and fit with linear regressions ($R^2 \geq 0.91$). Increasing concentrations of NR2B decreased the velocity of the kinase reaction. Moreover, slopes of the Lineweaver-Burk linear regressions at the varying NR2B concentrations were different from one another ($P = 0.017$, **Fig. 5.4**). Consequently, NR2B reduced the velocity of the Cdk5-dependent I-1 phosphorylation.

NR2B inhibited the maximum Cdk5-dependent phosphorylation of I-1 and PSD-95 (**Fig. 5.2**). Further analysis of kinetic assays revealed that NR2B inhibited phosphorylation reaction velocity in the presence of very high substrate concentrations. This finding suggests that NR2B likely noncompetitively inhibited Cdk5-dependent phosphorylation of I-1. To better understand the mechanism by which NR2B inhibited the Cdk5-dependent phosphorylation of I-1, the apparent K_i was determined. The NR2B cytoplasmic tail inhibited Cdk5-dependent phosphorylation of I-1 with K_i of 12.90 ($R^2 = 0.94$, **Fig 5.4**, inset). Consequently, the NR2B cyotplasmic tail noncompetitively inhibited Cdk5-dependent phosphorylation of I-1.

Generation of NR2B truncation mutants and analysis in binding assays.

In order to better characterize the interaction between Cdk5 and NR2B, we attempted to generate several NR2B truncation mutants. To assess whether Cdk5 bound to its consensus site on NR2B (*i.e.,* as a pseudo-substrate), a serine 1116-to-alanine mutant was generated. To map the regions necessary for binding, several truncation mutants were generated by adding multiple stop codons at selected locations (**Fig. 5.5**). Despite using several methodologies and large

amounts of protease inhibitors, purification of the pure NR2B cytoplasmic domains proved technically difficult. Coomassie and SDS-PAGE immunoblot analyses of WT and most NR2B mutants revealed that the correct truncation mutants were not being made. For purification of truncation mutants in bacteria, it is suggested to place several *preferred* stop codons in sequence. Thus, it is likely that these mutants are not of the appropriate length. There were also multiple bands below the one of interest, suggesting incomplete transcription and/or degradation. To overcome these technical hurdles, it will be necessary to make major adjustments in purification protocol and recloning of NR2B into a an alternative expression vector. For example, it will be necessary to insert multiple TAA stop codons into the NR2B mutant sequence to ensure that the bacterial transcriptases *stop* to make the truncated mutant. Moreover, since the GST-tag was cloned into the N-terminus of the WT and mutant NR2B clones, incomplete transcription products were purified along with the desired NR2B constructs. For better biochemical analyses, it will be critical to reclone the NR2B cytoplasmic tail and place the GST tag onto the C-terminus

Discussion

Protein phosphorylation and dephosphorylation events regulate most cellular signal transduction pathways. Substrate phosphorylation/ dephosphorylation and the downstream effects have received a large amount of attention and focus among biological scientists. However, phosphorylation and dephosphorylation ultimately depend on the enzymatic activity of kinases/phosphatases involved. Cdk5 is no exception. The upstream modulation of Cdk5 and its cofactors will have significant impact on the phosphorylation states of Cdk5 target and the signaling cascades involved.

Calpain-mediated cleavage of p35 to p25 directly affects Cdk5 localization and activity *in vivo* [5,30,97,142]. Cdk5 activity can also be regulated via

glutamatergic neurotransmission independently of p25 generation [35]. Activation of NMDA and kainate receptors induces autophosphorylation of p35, which targets p35 for degradation and decreases Cdk5 activity. Cdk5 can be regulated by the availability of its cofactors [145]. For example, transfection of heterologous cells with MAP kinase 8 binding protein indirectly produced an increase in p35 levels, and consequently increased the phosphorylation of Cdk5 targets such as phosphor-Ser 6 I-1 (data not shown; personal observation). Finally, there are a number of conditions which alter Cdk5 activity independent of cofactor. Treatment of slices with PDBU or NMDA can lead to decreases in the phosphorylation of several targets. Thus, there are likely several additional levels and forms of Cdk5 activity regulation.

We first confirmed that Cdk5 directly and specifically interacted with NR2B and proceeded to ask how this interaction affected Cdk5 activity. The NR2B cytoplasmic tail noncompetitively inhibited Cdk5 phosphorylation of I-1 *in vitro*. Peptide array data (see chapter 2) offers several candidate binding sequences. Furthermore, purification of the mutants described here will aid in the study of this protein—protein interaction and the inhibition of Cdk5 by NR2B.

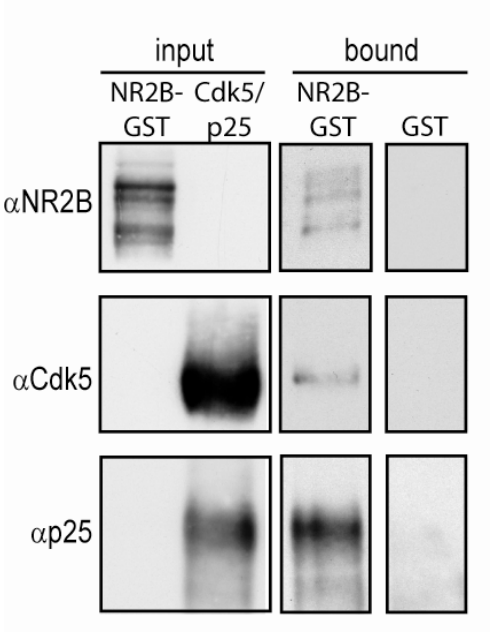

Figure 5.1. The cytoplasmic tail of the NR2B NMDAR subunit directly interacts with Cdk5/p25. Resin-conjugated recombinant NR2B C-terminus or GST were incubated with Cdk5/p25, washed, and then immunoblotted for indicated proteins. Neither NR2B-GST nor GST bound with recombinant protein phosphatase inhibitor-1. Input was 10% of amount of protein used for binding assays. Input: NR2B (1 μg), Cdk5/p25 (5 μg). The recombinant N2B cytoplasmic tail, Cdk5, and p25, ran at 60-95, 22, and 27 kDa, respectively.

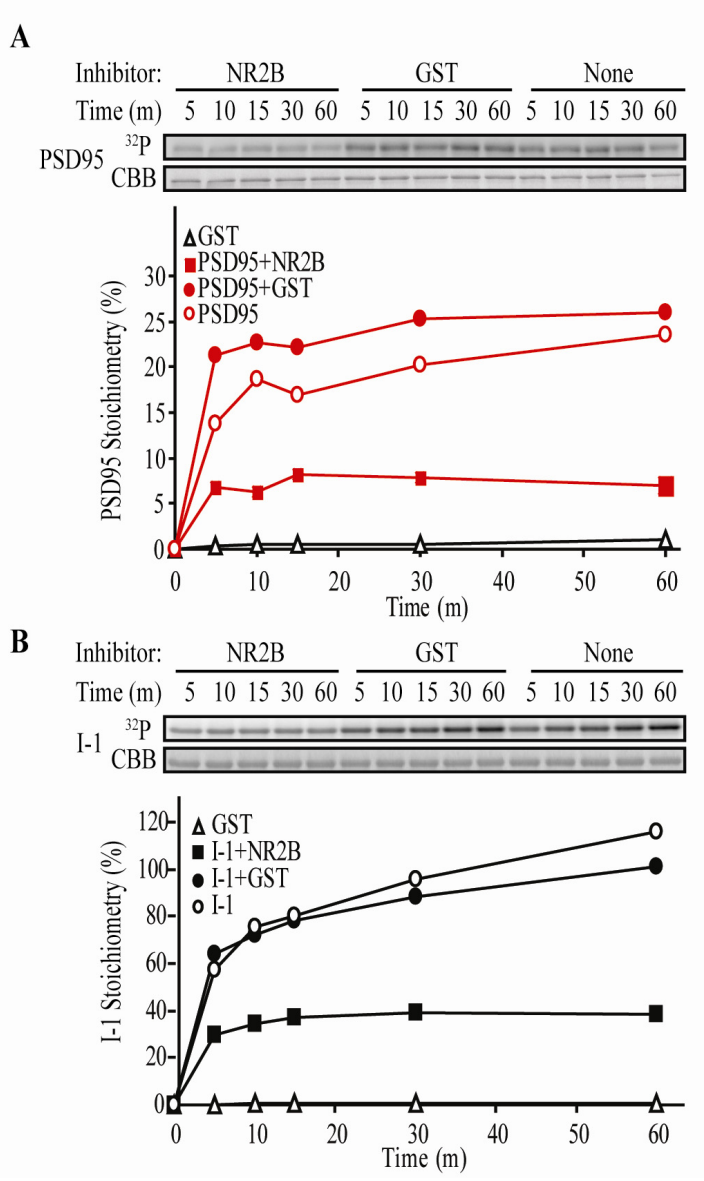

Figure 5.2. The cytoplasmic tail of the NR2B NMDAR subunit inhibits Cdk5/p25-dependent phosphorylation of I-1 and PSD-95 *in vitro*. Time course Cdk5-dependent phosphorylation reaction of PSD-95 (**A**) and protein phosphatase inhibitor-1 (**B**, I-1) with NR2B as an inhibitor. Reactions were performed for indicated times with substrate alone, substrate plus GST, or substrate plus I-1. As previously shown, NR2B was not phosphorylated. Stoichiometry was calculated as pmol ATP per pmol substrate. Data is representative of 3 experiments.

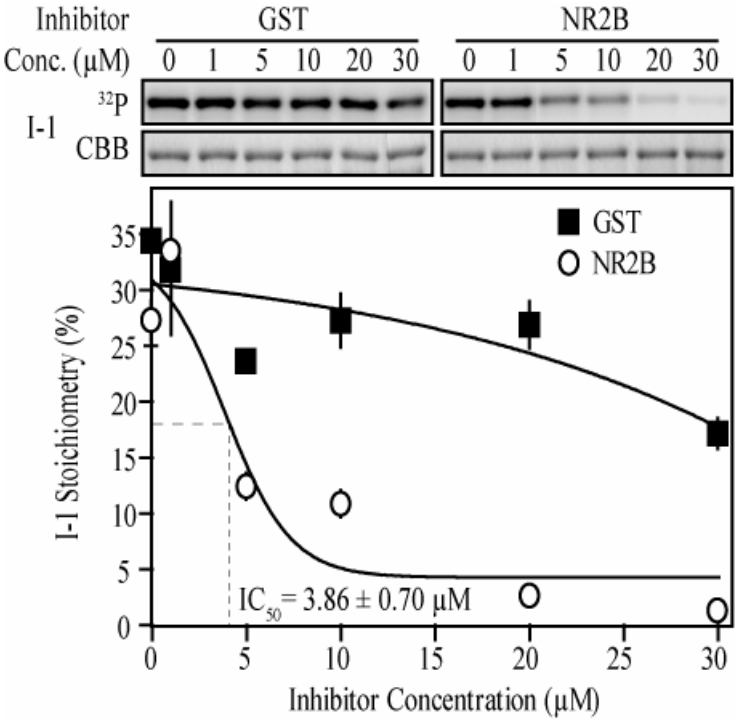

Figure 5.3. The NR2B cytoplasmic tail inhibits Cdk5 phosphorylation of I-1 in a concentration-dependent manner. Dose-dependent Cdk5 inhibition by NR2B cytoplasmic tail compared to a GST control. Cdk5 reactions were performed for 2 minutes with a constant 10 μM concentration of the Cdk5 substrate, I-1, and varying concentrations of NR2B and GST control. Sigmoidal curves and inhibition constant (IC_{50}) are shown. n = 3. $P < 0.005$, interaction between concentration and inhibitor, 2-way ANOVA. *Post hoc t*-tests indicate $P < 0.05$ at 5 μM, $P < 0.01$ at 10 and 30 μM, and $P < 0.001$ at 20 μM. Stoichiometry was calculated as pmol ATP per pmol substrate.

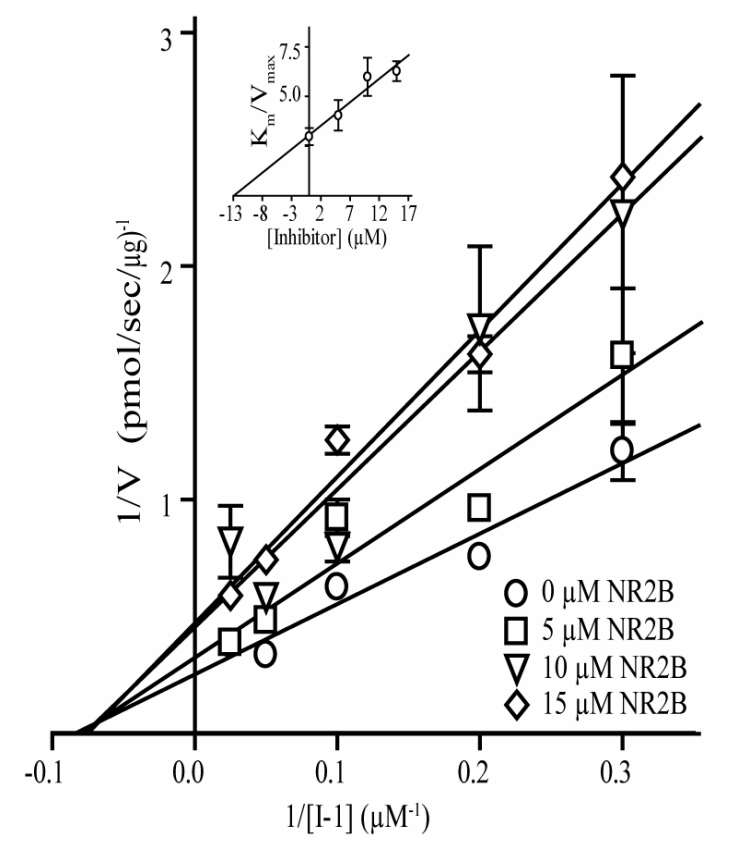

Figure 5.4. Lineweaver-Burk analysis of Cdk5-dependent phosphorylation of protein phosphatase inhibitor-1 in the presence of the NR2B NMDAR subunit cytoplasmic tail. Lineweaver-Burk analysis of Cdk5-dependent phosphorylation of I-1 in the presence of 0 (circles), 5 (squares), 10 (triangles) or 15 (diamonds) μM NR2B. Inset, secondary plot from which the Ki value was derived. The plot represents results of 3 reactions conducted under steady-state conditions. These results are also representative of 3 separate experiments.

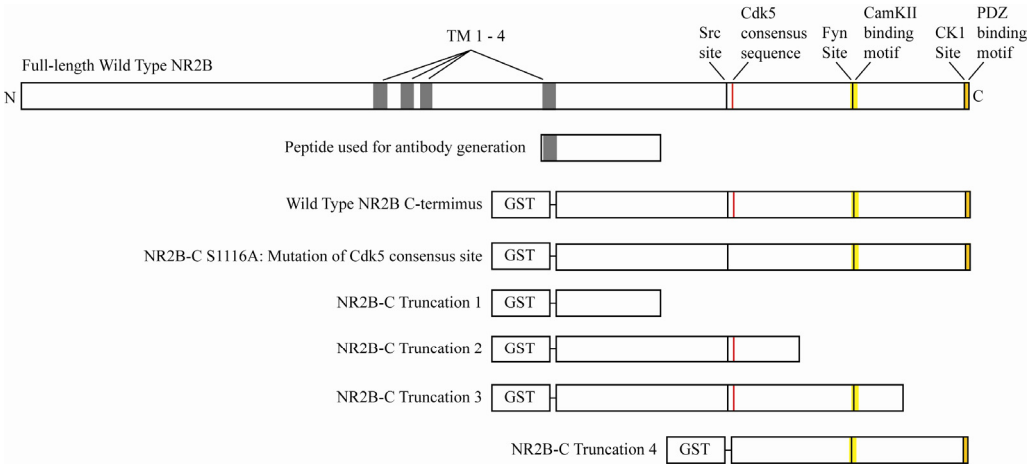

Figure 5.5. Schematic of full length NR2B and C-terminus constructs. A diagram of the full length NR2B protein is shown (top) with transmembrane domains (TM), phosphorylation sites, and binding motifs labeled. Below full length NR2B are the wild-type C-terminus construct and the mutants generated by site-directed mutagenesis.

CHAPTER SIX

EVALUATION OF PRESYNAPTIC VESICLE RELEASE IN CONDITIONAL CDK5 KO MICE

Summary

While performing experiments described in chapter 2, we also evaluated Cdk5's role in presynaptic vesicle release. Loss of Cdk5 led to an increase in post-tetanic potentiation, an impairment in short-interval paired-pulse facilitation, and greater depression in response to theta burst stimuli. Lastly, there was a NMDAR-dependent enhancement in response to low-frequency tetani. Although additional whole-cell patch-clamp studies are necessary to confirm these observations, the results suggest that loss of Cdk5 may produce an increase in the probability of presynaptic vesicle release due to increased vesicle number in the readily releasable pool or an increased sensitivity to presynaptic Ca^{2+}.

Introduction

Synaptic transmission, plasticity, and learning are all dependent on presynaptic vesicle release and recycling. Thus, impairments which affect presynaptic functions will likely have major effects on the nervous system. For example, mutations in RIM1α, a presynaptic active zone protein, leads to aberrations in presynaptic vesicle release, synaptic plasticity, and memory[57,146,147]. Cdk5 has been implicated in neurotransmitter release and endocytosis in the adult synapse. It has been suggested to both increase [22,23] and decrease [24] neurotransmitter release via phosphorylation of presynaptic substrates. Cdk5 has specifically been implicated in exocytosis and endocytosis via phosphorylation of

numerous substrates including synapsin, amphiphysin I, and dynamin[25-27,102]. For example, the Cousin and Robinson laboratories have shown that Cdk5's phosphorylation of dynamin inhibits presynaptic vesicle endocytosis. To further evaluate Cdk5's role in synaptic vesicle endocytosis, we studied short-term post-tetanic plasticity, short-term paired pulse facilitation, and responses to theta rhythms and low frequency tetani in SC/CA1 pathway of conditional Cdk5 knockout mice.

Experimental Procedures

Presynaptic neurophysiology

Transverse hippocampal slices were prepared and extracellular SC/CA1 voltage measurements in field recordings (fEPSPs) were synaptically evoked as described in chapter 2 unless otherwise mentioned. As before, recordings were performed using the MED64 multielectrode array (**Fig. 6.1**). Basal input/output measurements were performed to determine stimulus intensity to elicit 30-50% of the maximal fEPSP amplitude. Input/output analysis, paired-pulse facilitation, and tetani were performed in the absence of any drugs unless otherwise indicated. Post-tetanic potentiation (PTP) was elicited in the presence of 75 μM AP5. Baseline was followed by a brief 100 Hz tetanus [147] and post-tetanus recordings. Theta stimulus consisted of bursts as described in chapter 2 (4 pulses per burst at 100 Hz, 5 Hz burst frequency). fEPSPs were also measured during low frequency 14 Hz stimuli [147] in the presence or absence of 75 μM AP5. Data was collected using the MED64 performer and conductor software packages and analyzed using custom macros running under Igor Pro.

Statistical analysis

All data was represented at mean ± s.e.m. Errors for fold changes were calculated using standard error propagation rules. Differences between data groups were evaluated for significance using analysis of variance with *post hoc t*-tests and statistical significance was set to $p < 0.05$.

Results

Conditional loss of Cdk5 leads to an enhancement in post-tetanic potentiation in the SC/CA1 pathway of the hippocampus.

After a high frequency tetanus, neurons exhibit a form of short-term plasticity called post-tetanic potentiation (PTP). Although relevance and details of this phenomenon are still a mystery, PTP is likely due to a tetanus-induced elevation in presynaptic Ca^{2+} which leads to a short-lived increase in vesicle release. Changes in PTP could result from alterations in presynaptic Ca^{2+} channel properties or the size of the readily releasable pool of vesicles. Conditional loss of Cdk5 led to an enhancements in PTP following a 100 Hz tetanus (**Fig. 6.2A**) and following a theta burst stimulus (see chapter 2). In the presence of a NMDAR antagonist, a 100 Hz tetanus produced 142.4 ± 9.7 % of fEPSP baseline PTP in KO but only 120.7 ± 4.3 % PTP in WT slices. These findings suggest that loss of Cdk5 enhanced short-term presynaptic plasticity in addition to the post-synaptic phenotypes described in chapter 2.

Presynaptic aberrations in the Cdk5 KO SC/CA1 pathway

Presynaptic plasticity is dependent on the probability of vesicle release (P_r)[148]. Relative P_r is measured by examining paired pulse facilitation (PPF). As shown in chapter 2, conditional loss of Cdk5 did not lead to any significant differences in PPF with inter-stimulus intervals (ISIs) between 25 and 800 ms.

However, a paired-pulse stimulus protocol with an ISI of 10 ms produced a 8.1 ± 6.3 % facilitation in WT slices but 12.9 ± 4.7 % depression in KO slices (**Fig. 6.2B**). Although increases in P_r are usually characterized by decreases in PPF at several ISIs, Cdk5 KO mice only displayed decreased PPF with the 10 ms ISI. fEPSP NMDAR use-dependent blockade analyses were attempted but unsuccessful due to technical limitations. Although, additional whole cell experiments are necessary for definitive confirmation, these results are consistent with an increase in the P_r.

Theta burst topography aberration in the Cdk5 KO SC/CA1 pathway

Theta burst fEPSP topography was also altered in Cdk5 KO mice. In WT slices, theta bursts briefly led to facilitation followed by moderate depression. Meanwhile, in KO slices, a theta burst stimulus produced an immediate depression. This was followed by subsequent depression of much larger magnitude than controls (**Fig. 6.2C**). The difference between WT and KO in short-interval paired-pulse response was not NMDAR-dependent (**Fig. 6.3**). It is unclear, however, whether the aberration in theta burst topography is due to the previously described change in NMDAR-mediated EPSCs.

Loss of Cdk5 prevents synaptic depression during low frequency tetani.

fEPSPs during low frequency tetani are often measured to assess the state of the presynaptic reserve vesicle pool. In WT animals, 14 Hz train elicited fEPSP facilitation followed by vesicle depletion and consequently fEPSP depression. This was not the case in Cdk5 KO slices, which displayed a prolonged fEPSP facilitation and no significant depression (**Fig. 3.7A**). This interesting phenomenon was entirely attributed to NMDARs, as treatment with AP5, reversed the phenotype (**Fig. 3.7B**). These data show no detectable aberration in the reserve vesicle pool due to Cdk5 loss. Although unclear, the NMDAR-

dependent phenomenon may be due to an undiscovered NMDAR-mediated mechanism in the presynapse or the increased NMDAR-mediated transmission in the post-synapse. If the latter case is true, the finding is consistent with the data presented in chapter 2 showing an increase in post-synaptic NMDAR-mediated signaling. Thus, it would be informative to repeat the low frequency stimulation in the presence of ifenprodil, an antagonist which is selective for NR2B-containing receptors NMDARs.

Evaluation of Ca^{2+}-activated K^+-channels in Cdk5 KO slices

Repolarization after a theta burst stimulus is dependent on Ca^{2+}-activated K^+-channels and modulated by brain-derived neurotrophic factor[149]. These factors also lead to a voltage "*rebound*" that occurs following a large depolarizing stimulus such as a theta burst. To assess whether the presynaptic findings (and post-synaptic findings in chapter 2) were due to aberrations in Ca^{2+}-activated K^+-channels, burst duration and after-positivity were examined. Analysis revealed no differences between KO and WT in both burst duration and after-positivity following 10 theta burst stimuli (**Fig. 3.8**), decreasing the likelihood that presynaptic and post-synaptic phenotypes in Cdk5 KO mice were due to aberrations in Ca^{2+}-activated K^+-channels.

Discussion

Although several studies implicate Cdk5 in vesicle release and recycling, the exact nature of Cdk5's role in the presynaptic compartment is still unclear. Cdk5 has been implicated in the phosphorylation of numerous presynaptic substrates[25-27,102]. The data presented here show that loss of Cdk5 increases presynaptic short-term plasticity and may increase P_r in the SC/CA1 pathway of the hippocampus. Cdk5 could confer these changes by (1) increasing the number

of presynaptic vesicles, (2) increasing presynaptic Ca^{2+} influx, and/or (3) increasing sensitivity to presynaptic Ca^{2+}.

It is worthwhile to mention three potentially useful and relevant observations which complement the presynaptic findings presented in this chapter. First, preliminary electron microscopy studies of Cdk5 KO mice revealed an insignificant but trend towards increased numbers of cerebellar presynaptic vesicles (personal communication; Kanehiro Hayashi, University of Texas Southwestern Medical Center). Secondly, genetic deletion of Cdk5 in the *Caenorhabditis elegans* led to an uncoordinated behavioral phenotype consistent with an increase in neurotransmitter release (personal observation). Lastly, it has previously been shown that enhancements in neurotransmitter release produces resistance to volatile anesthetics [150]. Cdk5 KO mice required a larger volume of and more time under volatile anesthesia (*e.g.,* halothane or isoflurane) to lose consciousness (personal observation; data not shown). These three findings are consistent with the hypothesis that loss of Cdk5 leads to an increase in neurotransmitter release.

Traditionally, changes in P_r are accompanied by broad impairments in PPF. Thus, it is suspicious that loss of Cdk5 did not affect PPF between 25 and 800 ms. Cdk5 KO only affected PPF at a very short ISI. Consequently, it will be necessary to measure use-dependent NMDAR-blockade and miniature spontaneous synaptic events using whole-cell recording techniques. Ca^{2+}-caging/uncaging techniques would allow for study of Ca^{2+}-sensitivty. Immuno-staining for the presynaptic marker protein synaptophysin would allow for semiquantitation of hippocampal synapses. Electron microscopy would allow for visualization of hippocampal synapses and quantitation of the readily releasable vesicle pool. Lastly, assessment of presynaptic Cdk5 phosphorylation sites in the Cdk5 KO mice could implicate the relevant pathways to the phenotypes observed.

This study adds to the growing body of information on Cdk5's role in presynaptic plasticity and neurotransmitter release.

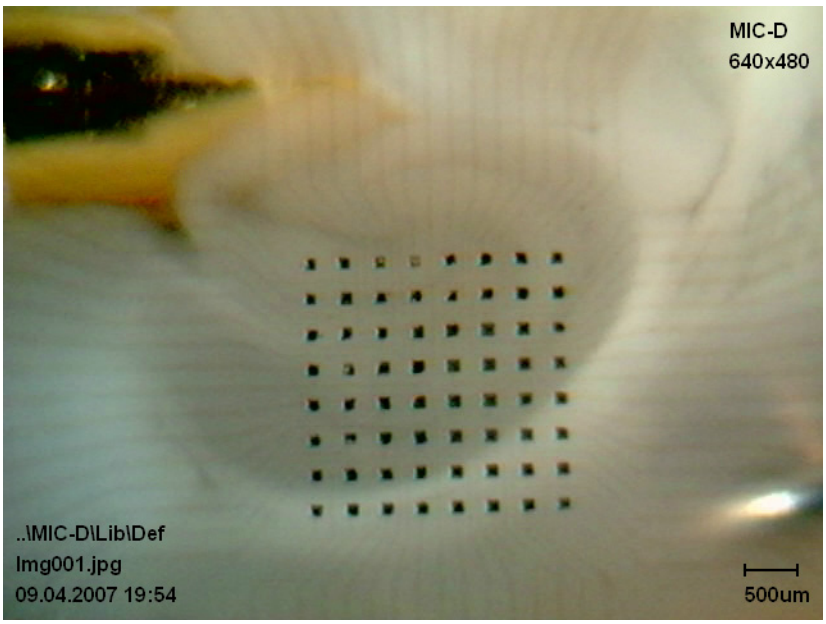

Figure 6.1. Image of a hippocampal slice on the MED64 multielectrode array. Freshly-prepared slice of dorsal hippocampus was placed onto an MED64 probe with 150 μm inter-polar spacing. The image was captured with a Olympus MIC-D camera.

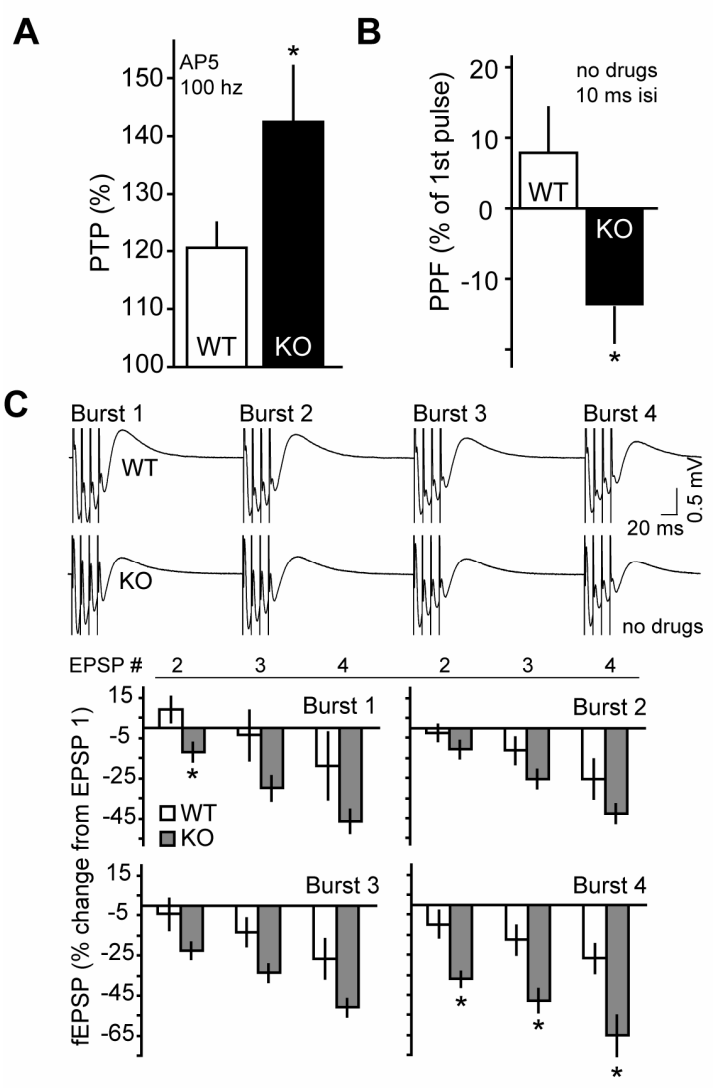

Figure 6.2. Enhanced short-term presynaptic plasticity and increased probability of release in the SC/CA1 pathway of Cdk5 KO mice. (**A**) Post-tetanic potentiation after a 100 Hz stimulus. fEPSP amplitudes were measured and plotted relative to baseline (75 μM AP5). (**B**) Paired-pulse facilitation (PPF) with 10 ms inter-stimulus interval (isi). PPF is plotted as percentage change of amplitude from 1st fEPSP. (**C**) Effects of Cdk5 KO on theta-burst responses. Traces and percentage change in amplitude (relative to the 1st fEPSP) of the 2nd, 3rd, and 4th field EPSP within a single stimulus train of 4 pulses at 100 Hz in control and KO slices. The measures are shown for bursts 1–4 of a train. Similar results were obtained with slope calculations. *P < 0.05 vs. WT, Student's *t*-test. n = 5-8. Data represent means ± s.e.m.

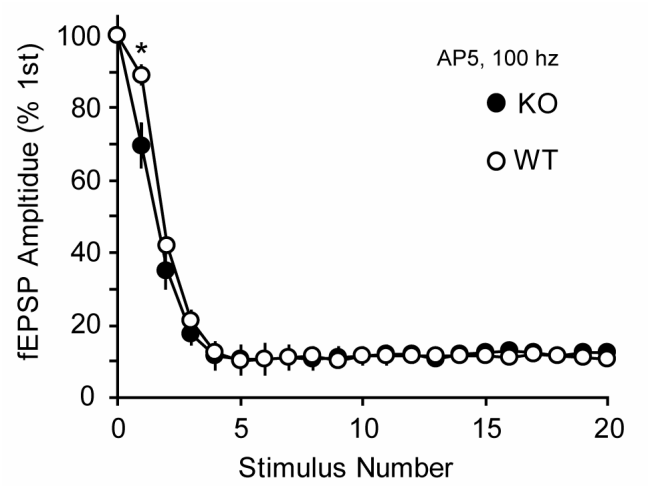

Figure 6.3. Effects of Cdk5 KO on fEPSPs during a 100 Hz tetanus. fEPSPs in response to a 100 Hz tetanus are plotted relative to the 1st response in the presence of 75 μM AP5. *P < 0.05 vs. WT, Student's *t*-test. n = 5-6 Data represent means ± s.e.m.

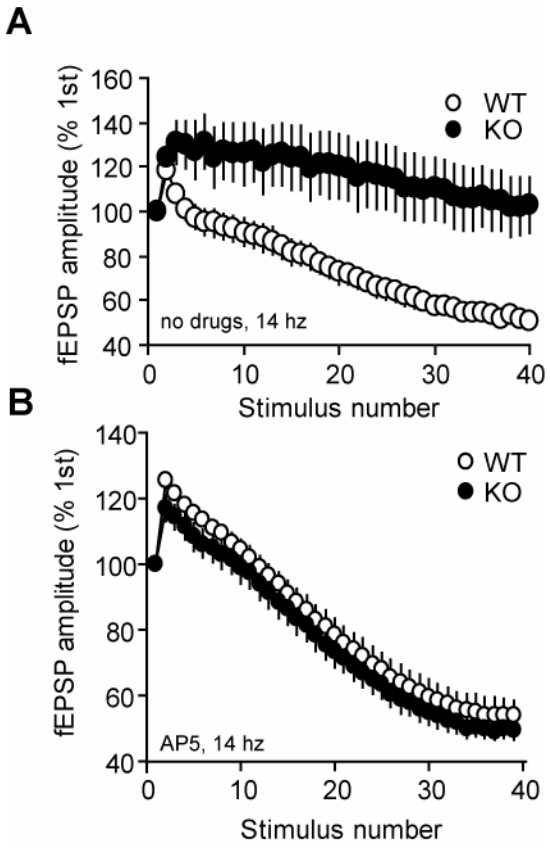

Figure 6.4. Effects of Cdk5 KO on fEPSPs during low frequency tetanus. fEPSPs amplitudes during 14 Hz tetani are plotted relative to the 1st response in the absence (**A**) or presence (**B**) of 75 μM AP5. For **A**, KO is significantly different from WT; $P < 0.001$, 2-way ANOVA. n = 4-8. Similar results were obtains with fEPSP slope measurements. Data represent means ± s.e.m.

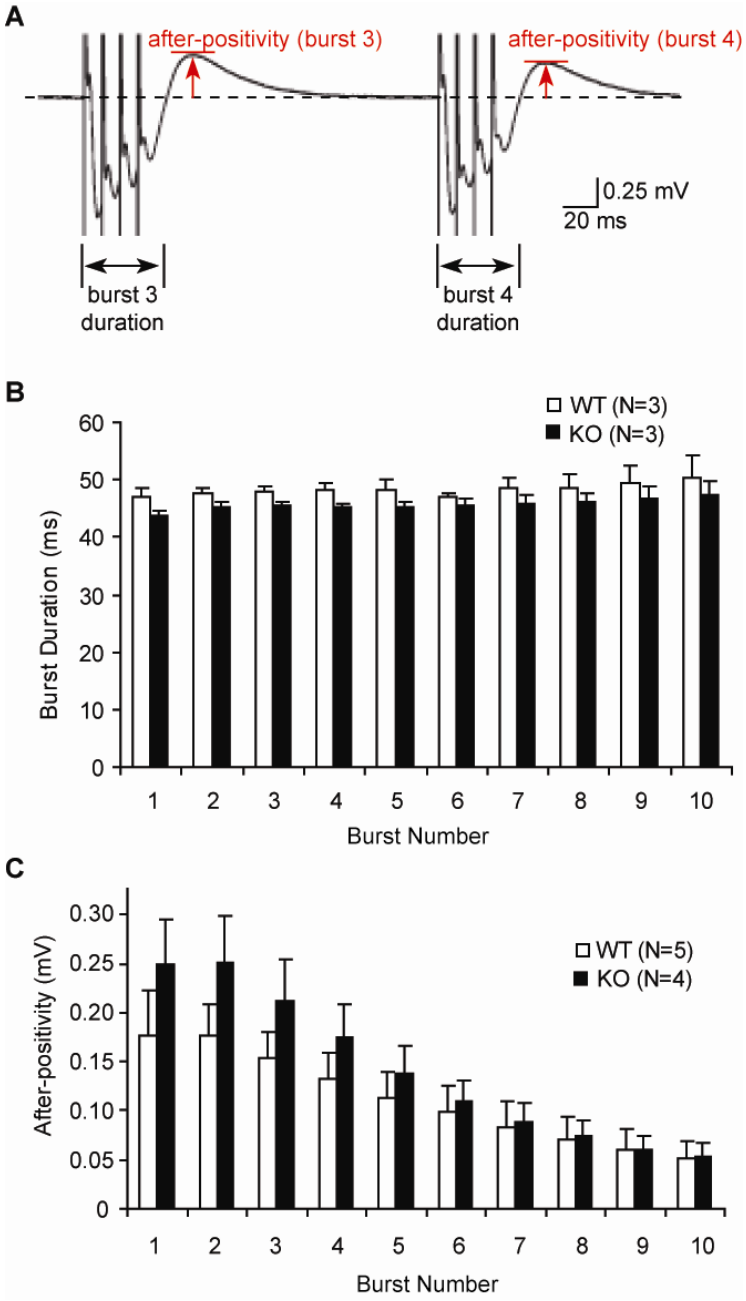

Figure 6.5 Effects of Cdk5 KO on theta burst-response parameters.
(**A**) fEPSPs during theta burst trains with burst duration and after-postivitiy measurements indicated. (**B**) Comparison of the duration of the burst responses (measured as the time required for the response to return to the prestimulation baseline) in WT and KO slices. (**C**) Maximum amplitudes of the afterpotential

following a theta burst for WT and KO slices. The amplitude for bursts 2–10 was similar for both genotypes Percentage increase in response area across a series of 10 theta bursts was also similar in WT and KO slices. Data represent means ± s.e.m.

CHAPTER SEVEN

CONDITIONAL KNOCKDOWN OF CDK5 USING VIRAL VECTORS AND AN ALTERNATIVE TRANSGENIC APPROACH

Summary

Conditional knockout technology has allowed for the study of developmentally-important proteins in the adult animal. Since Cyclin-dependent kinase 5 (Cdk5) is critical for cortical lamination, traditional Cdk5 KO die shortly after birth. Therefore, to study the roles of Cdk5 in the adult brain, we have developed several conditional Cdk5 KO models. In all three models, the same critical exons were flanked with *loxP* elements. Cre was introduced via the PRP-Cre-ER transgene, the CamKII-Cre transgene, and adeno-associated viral (rAAV) vectors. The PRP-Cre-ER transgenic allowed for a drug-inducible Cdk5 KO line with dramatic knockdown throughout the forebrain. Meanwhile, the CamKII-Cre transgenic allowed for moderate forebrain knockdown in the adult animal. Lastly, rAAV transduction with Cre allowed for Cdk5 knockdown in target regions such as the hippocampus and striatum.

Introduction

The first knockout mice were produced by Mario Capecchi, Martin Evans and Oliver Smithies in 1987-1989 and licensed to Lexicon Genetics. Between the pharmacological reagents and knockout mice, we have had the opportunity to ask fundamental biological questions. Although a major advance in the biological sciences, traditional knockout mice present their own set of caveats. For example, traditional knockout mice have a targeted genetic deletion from conception. Therefore, knockout of targeted gene/protein which has a role in development

may have post-developmental consequences. Consequently, we may not be able to accurately study developmentally-important genes/proteins in the adult brain of *null* mutants.

Cyclin-dependent kinase 5 (Cdk5) is critical for cortical lamination during development as it regulates neuronal migration, differentiation, and connectivity [15]. Traditional Cdk5 and p35/p39 double cofactor knockout mice exhibited severe disruptions in cortical lamination as neurons failed to migrate to the appropriate layers. The appearance of an inverted cortex was accompanied by aberrations in the cytoarchitecture of other structures including the hippocampus, brainstem, and cerebellum[16-18]. Thus, the study of Cdk5 function in the adult brain has been limited by lethality and congenital abnormalities in constitutive knockout mice[8] as well as by pharmacological non-specificity[33].

To address these concerns, we developed three conditional Cdk5 knockout model systems. As described in chapter 2, all 3 strategies rely on mice in which both Cdk5 alleles were flanked with *loxP* sequences. In the 1st conditional knockout line described in chapters 2-4, Cdk5 deletion was mediated by the Cre-ER recombinase. This allowed for a drug-induced knockdown of Cdk5 throughout the mouse forebrain, especially the hippocampus. As an alternative strategy, Cdk5 expression was knocked down in forebrain, especially in the striatum, using a recombinase under direct control of the CaMKII promoter. Lastly, we have used adeno-associated viral vectors to express the recombinase in target regions.

Experimental Procedures

Reagents and materials

All drugs and reagents were from Sigma, except where indicated. Animals were maintained as described in chapter 2.

Generation and application of recombinant adeno-associated viral vectors

rAAV viral vectors were generated in 15 cm plates or roller bottles essentially as described [52,151-153]. HEK-293T cells (ATCC) were grown in Dulbecco's Modified Eagle's Medium (DMEM) containing 10% fetal bovine serum and antibiotics/antifungal agents (Invtirogen)[154]. At 85% confluency or after media in bottles had reached glucose concentration of 160 mg/dl (Accu-Chek), cells were transfected with selected plasmids in a calcium chloride solution. To generate rAAV 2/2, cells were cotransfected with 3 plasmids: pHelper (11.6 Kb, Stratagene), pAAV-RC (7.3 Kb, Stratagene), and a plasmid containing enhanced GFP (eGFP) or eGFP-Cre inserted into the multiple cloning site (cloned into pAAV-MCS by Ralph DiLeone, Yale University). To generate rAAV 2/5, cells were cotransfected with transfected with the pAAV-MCS plasmid containing eGFP or eGFP-Cre and the pDP5rs plasmid (23.7 Kb, provided by Dr. Corinna Burger, University of Wisconsin). Seventy-two hours after transfection, HEK293T cells were examined under a microscope to ensure efficient transfection with plasmids. Efficient transfection was confirmed by the presence of aggregates/plaques and fluorescence upon excitation. Following freeze-thaw lysis, nucleic acids were digested with benzonase (Novagen). Clarified lysate was added to a iodixanol gradient (with 15%, 25%, 40%, and 60% layers) and centrifuged at 350,000 g for 2 hours (10 ºC). Purified virus, which was located in the 40% layer, was aspirated off with a syringe. rAAV 2/2 was further purified by heparin column chromatography using heparin-agarose and a NaCl elution gradient. Lastly, rAAV vectors were dialyzed into phosphate buffered saline (containing 2.5 mM KCl and 1mM $MgCl_2$) and concentrated to < 100 μL using a centrifuge concentrator (Biomax).

rAAV vectors were analyzed for capsid proteins and purity by 8% SDS-PAGE followed by silver staining (SilverExpress, Invitrogen). PC12 heterologous

cells (kindly provided by Eric Nestler, UT Southwestern Medical Center) were transfected with dilutions of rAAV preparations and viral titer was determined and adjusted to 10^{11}-10^{12} pfu/mL by comparing new preparations to previously established ones (kindly provided by Ralph DiLeone). The rAAV particles transduced neurons with high efficiency *in vivo* and maintain detectable levels of expression in the brain for up to 12 months after infection (personal communication, David Benavides). Adult male homozygous Cdk5 *floxed* mice were utilized for bilateral stereotaxic delivery of rAAV (~$4x10^8$ particles, 0.4 µL/hemisphere) to the hippocampus (coordinates from Bregma at skull surface: A/P -1.9 to -2.0 mm, Lat +1.2 to 1.5 mm, D/V -0.12 to -1.4 to -2.0 mm; 10^o angle of entry) or the nucleus accumbens core (coordinates from Bregma at skull surface: A/P +1.6 to +1.9mm, Lat +1.5mm, D/V -4.5mm; 10^o angle of entry; striatal surgeries performed by David Benavides). Aseptic surgical procedures were performed after anesthesia with Avertin (240 mg/kg).

Cre expression was analyzed by examining the eGFP fluorescence in 350 µm transverse acute hippocampal slices under an epifluorescent microscope or via *in situ* hybridizations for Cre mRNA in coronal cryosections (see chapter 2).

Generation and study of CamKII-Cre Cdk5 knockdown mice

CamKII-Cre Cdk5 conditional knockdown mice were generated by breeding homozygous *floxed* Cdk5 mice with mice expressing Cre recombinase under the control of the αCaMKII promoter [155,156]. The CaMKII-Cre line was chosen in order to mediate recombination in the postnatal forebrain as previously reported for this transgenic (T70) line [155,157]. Littermate, homozygous *floxed* Cdk5 mice lacking the Cre transgene served as controls. Adult male mice (≥ 6 weeks old) were utilized for all experiments. *Floxed* alleles were identified as described in chapter 2. Transgenic alleles were identified by a polymerase chain reaction (PCR)-based genotyping strategy as described[156]. *In situ* hybridizations,

immunoblots, fear conditioning, and electrophysiology were performed as described in chapter 2.

Results

Generation and application of viral vectors for the regional knockdown of Cdk5

To allow for region-specific studies of Cdk5, recombinant adeno-associated viral vectors (rAAV) were generated. For additional control of transduction field size and regional efficiency, serotypes 2 and 5 (*i.e.,* rAAV 2/2 and 2/5, respectively) were purified. SDS-PAGE analysis was used to assess for purity and the presence of AAV capsid proteins (**Fig. 7.1A**). Viral vectors contained DNA for eGFP or eGFP-Cre. Transduction of heterologous cells with eGFP resulted in expression of cytoplasmic eGFP in culture (**Fig. 7.1B**, left). Transduction of heterologous cells with eGFP-Cre led to expression of an eGFP-Cre fusion protein that was localized to the nucleus (**Fig. 7.1B**, right).

Injection of purified rAAV 2/2 into the striatum or CA1 region of the hippocampus of an anesthetized animal allowed for transduction of 0.5-1 mm^3 of tissue. Meanwhile, serotype 5 spread to allow transduction of >1 mm^3 (data not shown; surgeries performed by David Benavides, UT Southwestern Medical Center). Consequently, rAAV serotype 2 allowed for very precise targeting of small regions such as the nucleus accumbens, while serotype 5 allow for additional spread and transduction of larger regions, such as the dorsal striatum.

Transduction of hippocampus neurons with rAAV 2/2 eGFP-Cre led to epifluorescence upon excitation in acute slice preparations (**Fig. 7.1C**). This allowed for *post hoc* localization of the target region. *In situ* hybridizations in cryosections from virally-targeted brains also confirmed region-specific expression of Cre (**Fig. 7.1D**). Expression of Cre in the hippocampus and striatum following viral transduction ultimately produced a region-specific > 50%

knockdown of Cdk5[156] (personal communication, David Benavides, UT Southwestern Medical Center). Thus, generation and application of viral vectors allowed for regional expression of Cre and knockdown of Cdk5 *in vivo*.

Conditional knockdown in the adult forebrain using the CamKII-Cre transgenic mouse line

As an alternative to the PRP-Cre line described in chapter 2, *floxed* Cdk5 mice were also bred with transgenic mice bearing Cre under control of the CamKII promoter [155,157]. Previously reported CamKII-Cre lines have shown high specificity for Cre expression the hippocampus [155]. However, the extent and localization of Cre expression depends entirely on the mosaicism of the mouse line used. For our studies, the T70 CamKII line (kindly provided by Dr. Luis Parada, UT Southwestern Medical Center) was employed. Previous characterization[157] and *in situ* hybridizations revealed moderate Cre mRNA expression and corresponding Cdk5 mRNA knockdown in the hippocampus, striatum, and other regions of the brain (**Fig. 7.2A**)[156]. Western immunoblots revealed an insignificant Cdk5 knockdown in hippocampal lysates from CamKII-Cre Cdk5 KO mice (1.00 ± 0.05 and 0.78 ± 0.05 for WT and KO, respectively; **Fig. 7.2A**). This data corresponds with quantitation of the ^{35}S-UTP *in situ* hybridizations, which revealed a mild but significant decrease in hippocampal Cdk5 mRNA (personal communication, David Benavides)[156]. Unlike previously reported mice bearing the CamKII-Cre transgene, there appears to be greater Cre expression and Cdk5 knockdown in the striatum versus the hippocampus (personal communication; David Benavides)[156]. Therefore the Cdk5 floxed mice bearing the T70 CamKII-Cre transgene may not serve as a good model for hippocampal Cdk5 knockdown but likely has applications for studies on the striatum.

Analysis of NR2B levels, fear-conditioned learning, and synaptic plasticity in the Schaffer Collateral pathway of the hippocampus in the CamKII-Cre Cdk5 knockdown mice.

Since ~60% loss of hippocampal Cdk5 protein increases NR2B levels and improved fear-conditioned learning (see chapter 2), we evaluated NR2B levels and aversive learning in the CamKII-Cre Cdk5 KO mice. Hippocampal NR2B levels were the same in CamKII-Cre WT and KO mice (**Fig. 7.3A**). Furthermore, no significant differences were seen fear-conditioned learning to context or cue (**Fig. 7.3B**). Thus, a marginal reduction in hippocampal Cdk5 had no major affects on either NR2B levels or fear-conditioned memory.

A large knockdown of Cdk5 led to a NMDAR-mediated enhancement in synaptic plasticity (chapter 2). We examined long-term potentiation in the SC/CA1 hippocampal pathway of CamKII-Cre Cdk5 KO mice. No overt differences were observed in the input/output analysis suggesting intact synaptic transmission (data not shown). A 2 x TBS stimulation protocol induced equivalent LTP in both CamKII-Cre Cdk5 WT and KO slices (**Fig. 7.4**). Although additional analysis may reveal a more subtle difference in LTP threshold, the data suggests that mild knockdown of Cdk5 does not affect LTP induction in the CamKII-Cre Cdk5 KO line.

Discussion

To study the roles of Cdk5 in the adult brain, my colleagues and I developed three conditional Cdk5 KO mouse models. For all three models critical Cdk5 exons were flanked with *LoxP* sequences. The studies described throughout chapters 2-4 were performed on Cdk5 KO mice carrying a Cre-ER transgene. This Cre line allowed for a drug-inducible conditional Cdk5 knockout mouse which displayed robust knockout in the hippocampus. The recombinase was also

introduced using several targeted rAAV vectors. These allowed for regional and temporal control of Cdk5 KO. Finally, the recombinase was introduced using a transgenic line in which Cre was driven by the CamKII promoter. This line produced marginal knockdown of Cdk5 in the hippocampus and moderate knockdown in the striatum. The CamKII-Cre Cdk5 KO line did not display a significant decrease in Cdk5 protein levels. Furthermore, the CamKII-Cre Cdk5 KO line displayed normal levels of hippocampal NR2B, fear-conditioned learning, and hippocampal LTP in the SC/CA1. Each model system has provided us with the tools necessary to study the roles of Cdk5 in the adult brain.

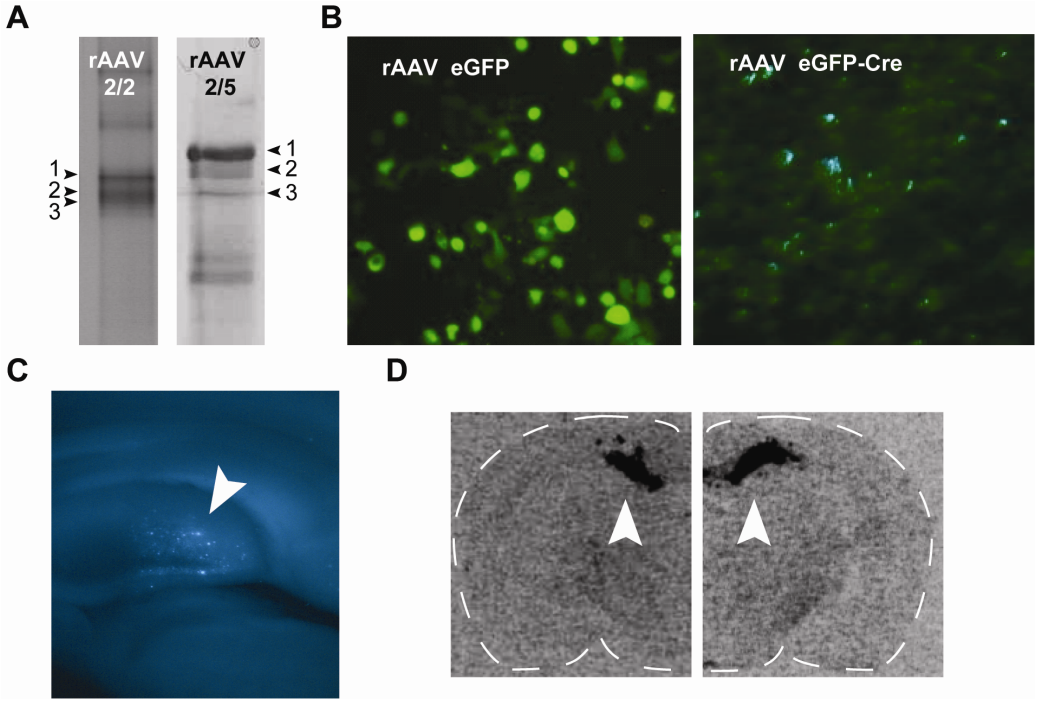

Figure 7.1. Generation and application of adeno-associated viral vectors for targeted loss of Cdk5. (**A**) Purified AAV serotypes 2/2 (left) and 2/5 (right) capsid proteins VP1, VP2, and VP3 (indicated by numbers) visualized by silver-stained 8% SDS-PAGE. (**B**) Exemplar images of cos-7 heterologous cells in culture which have been transduced with AAV 2/2 carrying eGFP (left) and eGFP-Cre (right). Image shows epifluorescence from GFP fluorophores expressed in cells. (**C**) Epifluorescence in hippocampal neurons following transduction with AAV 2/2 eGPF-Cre. (**D**) Targeted expression of Cre in the brain following injection with AAV 2/2 eGPF-Cre. Cre mRNA is detected by *in situ* hybridization using a radiolabeled probe. Dotted line demarcates the border of the brain. Arrows in **C** and **D** indicate regions expressing eGFP-Cre.

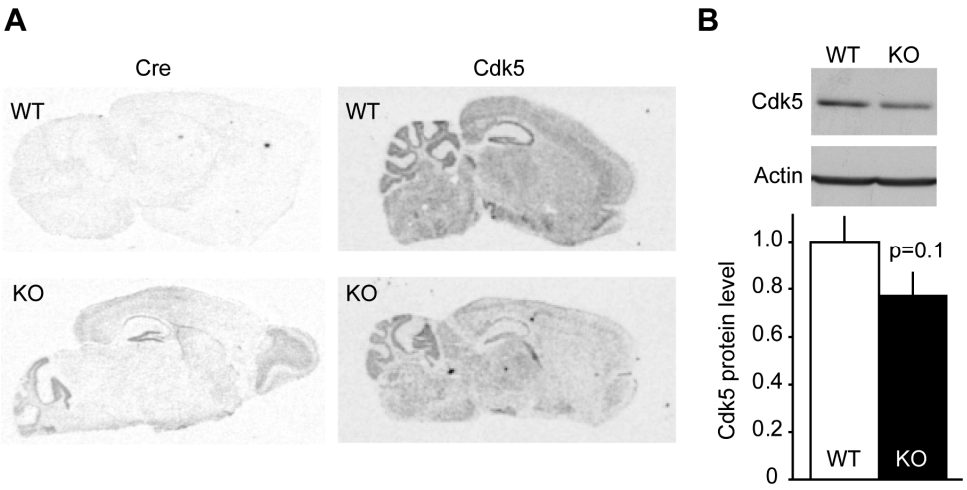

Figure 7.2. CamKII-Cre transgenic conditional Cdk5 knockdown in the adult forebrain. (**A**) Radiolabeled *in situ* hybridizations for Cre and Cdk5 mRNA. Cdk5 KO samples display Cre staining in the striatum, hippocampus, olfactory bulb, cortical layers, and cerebellum (left). Cre expression corresponded to moderate decreases in Cdk5 mRNA labeling (right). (**B**) Quantitative immunoblot analysis of hippocampal lysates. Representative immunoblots of Cdk5 and actin are shown with quantitation. Actin levels did not change relative to tubulin in hippocampal lysates from the CamKII-Cre transgenic Cdk5 knockdown mice. n = 5; P = 0.1 by Student's *t*-test and P = 0.06 by Mann-Whitney U-test. Data represents mean ± s.e.m.

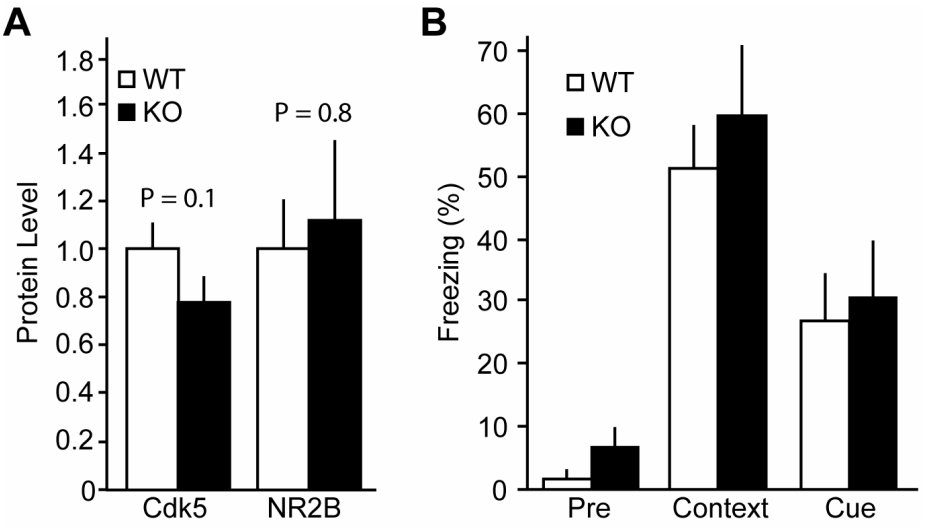

Figure 7.3. Analysis of NR2B levels and fear conditioned learning in CamKII-Cre Cdk5 knockdown mice. (**A**) Immunoblot analysis of Cdk5 and NR2B in hippocampal lysates form CamKII-Cre Cdk5 knockdown mice, n = 3, Student's *t*-test. (**B**) Freezing time before conditioning (Pre) and following context or cue re-exposure are shown; n = 12-16. Data represents mean ± s.e.m.

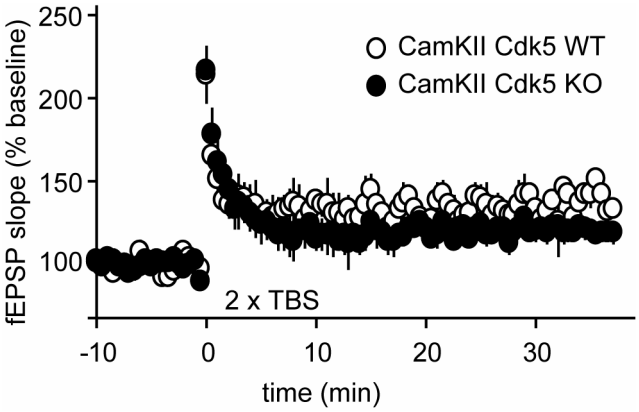

Figure 7.4. Evaluation of synaptic plasticity in the SC/CA1 pathway of CamKII-Cre Cdk5 knockdown mice. LTP in WT and CamKII Cdk5 KOs after a after a 2 x TBS (see chapter 2) presented as percent of baseline (-10—0 min); n = 3. Data represents mean ± s.e.m.

CHAPTER EIGHT

CONCLUSION

During the past decade, Cdk5 has been implicated in numerous physiological and pathological processes. These observations have been aided by pharmacological reagents, Cdk5 *null* mice, and manipulation of Cdk5 cofactors. To better understand the roles of Cdk5 in the adult brain, we developed several conditional Cdk5 knockout model systems. Loss of Cdk5 throughout the mouse forebrain led to several interesting behavioral, electrophysiological, and biochemical changes. Characterization of the Cdk5 KO mice implicated Cdk5 in several physiological processes and biochemical pathway. In conclusion, we will briefly review and discuss the relationships between the principal observations presented in this dissertation.

Conditional loss of Cdk5 in the mouse forebrain improved performance in hippocampus-dependent learning tasks such as contextual fear conditioning, contextual extinction, and reversal water maze. These behavioral phenotypes were accompanied by an enhancement in hippocampal synaptic plasticity. Specifically, conditional loss of Cdk5 reduced the threshold necessary to induce LTP in the SC/CA1 pathway. The enhancement in synaptic plasticity corresponded with increases in currents through NR2B-containing NMDARs and NR2B protein levels. Reversal experiments revealed that the increased current through NR2B-containing NMDARs accounted for the enhancement in synaptic plasticity. It is highly likely that the increase in total, synaptic, and surface NR2B levels led to the increased current through NR2B-containing NMDARs[60].

Elevated NR2B levels in Cdk5 KO mice were associated with an impairment in the calpain-dependent cleavage of NR2B. This corresponded with

data showing that recombinant Cdk5/p25 facilitated the degradation of NR2B *in vitro*. These data are consistent with the immunoblot and electrophysiological experiments described above and suggest that Cdk5 facilitates cleavage of NR2B. Interestingly, Cdk5, NR2B, and calpain all interact *in vitro* and *in vivo*. We propose that Cdk5 normally facilitates the calpain-mediated cleavage of NR2B via direct protein—protein interactions. As a consequence, it is likely that loss of Cdk5 in the mouse brain led to an increase in NR2B levels and a subsequent enhancement in synaptic plasticity.

While studying the role of Cdk5 in functional plasticity, we hypothesized that Cdk5 may also regulate spine dynamics, which is dependent on spectrin cleavage and actin depolymerization. Incidentally, we found that the levels of depolymerized actin were reduced in Cdk5 KO mice, especially in the synapse. Interestingly, Cdk5 KO mice displayed blunted generation of the cleaved spectrin following prolonged activation of calpain. In addition, recombinant Cdk5 facilitated the calpain-dependent cleavage of spectrin *in vitro*. These findings all correlate with one another and suggest that Cdk5 may facilitate the degradation of spectrin, thereby regulating actin polymerization and spine dynamics. Fascinatingly, additional evidence suggested that Cdk5 may also regulate the calpain-dependent degradation of other substrates including p35 and STEP. These independent observations suggest that Cdk5 may actually modulate the calpain-mediated degradation of many substrates.

There is strong data to suggest that modulation of NR2B cleavage by Cdk5 plays important roles in the brain. However, only Cdk5's regulation of NR2B degradation has been studied in depth. Does Cdk5's modulation of spectrin degradation play any important role in the cell? Does Cdk5's regulation of STEP degradation have any effects on synaptic plasticity? It is entirely unclear how the findings presented in chapters 2 and 3 relate to one another or if Cdk5 directly

modulates calpain regardless of substrate. These questions and many others remain unanswered and the underpinning for future research.

Initially, Cdk5 knockout led to enhancements in learning and synaptic plasticity. However, chronic loss of Cdk5 was associated with increased seizure susceptibility and neuronal excitability. Chronic loss of Cdk5 caused increased propensity to handling induced seizures which was associated with lethality. Consistently, there was a reduced threshold for pharmacologically- and audiogenically-induced seizures. Behavioral findings correlated with increased electrophysiological neuronal excitability. Cdk5 KO slices displayed impairments in neuronal repolarization and a reduced threshold for epileptiform activity. Based on the current dogma[109], the increases in neuronal excitability likely contribute to the reduction in seizure threshold. We also hypothesize that the increase in NMDAR-mediated currents may contribute to the elevated neuronal excitability. However, we did not directly assess what role NR2B played in the hyperexcitability of Cdk5 KO mice. Furthermore, it is not clear whether the increase in neuronal excitability directly affected seizure susceptibility. Consequently, these observations remain descriptive and additional investigations will be required to assess causality.

Very prolonged Cdk5 KO (beyond the time associated with increases in behavioral and neuronal excitability) ultimately led to neurodegenerative-like sequelae. Recurrent seizures were associated with impairments in synaptic transmission. Also very prolonged loss of Cdk5 led to abnormal EEG patterns and reduced brain weights. These findings indicate that loss of Cdk5 for an excess amount of time may lead to degenerative changes. Additional histology and EEG analyses are necessary to test this interesting hypothesis.

How do the findings in chapter 4 relate to those described earlier? We can place the observations from chapter 4 in a timeline relative to the phenotypes described in chapter 2: Cdk5 KO enhancements in learning, plasticity, and

NMDAR-mediated currents precede increased seizure susceptibility and neuronal excitability which precedes neurodegenerative-like sequelae. Other than this timeline, there is no data to directly link the observations in chapter 4 to those described in earlier chapters. Any relationship between the findings in these chapters in entirely speculative. Thus, unless additional information is derived, it would be wise to consider the studies presented in chapters 2, 3, and 4, and independent investigations.

During the course of my studies, it became apparent that the NR2B cytoplasmic tail inhibited Cdk5 activity *in vitro*. One could hypothesize that NR2B inhibits Cdk5 as a feedback loop for the mechanisms described in chapter 2. However, there is no data to support or refute this hypothesis or even suggest that this inhibition occurs *in vivo*. Additional electrophysiological analyses also revealed that loss of Cdk5 had distinct effects on presynaptic function. Specifically, conditional loss of CDk5 led to an enhancement in post-tetanic short-term potentiation and an aberration in short inter-stimulus interval paired-pulse facilitation. Although unclear, these presynaptic phenotypes may implicate Cdk5 in presynaptic vesicle release, vesicle recycling, or Ca^{2+} sensitivity. The final data chapter describes the development of alternative strategies to achieve conditional Cdk5 KO. It is important to recognize that except for the use of similar reagents and model systems, there is not substantiated link between these studies and those described in earlier chapters. Therefore, as is, the studies presented in chapters 5, 6, and 7 should once again be considered as independent and interesting observations which may guide and serve as a foundation for future studies.

In conclusion, these studies provide us with information about Cdk5's role in the central nervous system. Data from transgenic mice show that loss of Cdk5 leads to enhancements in learning and plasticity which are mediated by increases in NR2B levels. In correlation, Cdk5 facilitated NR2B degradation and directly

interacted with NR2B and calpain. Interestingly, Cdk5 was separately found to modulate the degradation of other calpain substrates. This raises the possibility that Cdk5 *may* modulate calpain independent of substrate or play a role in the degradation of several proteins. Cdk5 was also separately shown to regulate behavioral and neuronal excitability. It is, however, unclear whether or not this phenomenon is related to Cdk5's regulation of NR2B degradation. Through the experiments described herein, we have implicated Cdk5 in several interesting and likely separate physiological processes and biochemical pathways in the central nervous system. It is my hope that these studies on the regulation of excitatory neurotransmission, synaptic plasticity, and learning by Cdk5 further our understanding of the nervous system and offer a foundation for additional research.

APPENDIX

DATA ANALYSIS MACROS FOR IGOR PRO

```
// Use modern global access method.
// Field analysis macro for analysis of  EPSP amplitude, slope , time constant, rise rate and fiber volley size from 2 channels .
// All times are adjusted to start from the onset of the artifact
// Written by Ammar Hawasli and Don Cooper
```

Averaging fEPSP waves macro 1

```
Macro averagewaves()
//assumes that waves are saved in the following way
//a is followed by the io curve stimulus intensity order and then by the sweep number
//so a32 means it came from the 3rd stimulus intensity in the IO curve and it is the 2nd sweep
//this number is given to a curve when the text file is loaded into IGOR
duplicate/o a11 IO_1_avg
duplicate/o a21 IO_2_avg
duplicate/o a31 IO_3_avg
duplicate/o a41 IO_4_avg
duplicate/o a51 IO_5_avg
duplicate/o a61 IO_6_avg
duplicate/o a71 IO_7_avg
duplicate/o a81 IO_8_avg
IO_1_avg= (a11+a12+a13)/3
IO_2_avg=(a21+a22+a23)/3
IO_3_avg= (a31+a32+a33)/3
IO_4_avg=(a41+a42+a43)/3
IO_5_avg= (a51+a52+a53)/3
IO_6_avg=(a61+a62+a63)/3
IO_7_avg= (a71+a72+a73)/3
IO_8_avg=(a81+a82+a83)/3
Display/w=(5.25,42.5,762,262.25)
IO_1_avg,IO_2_avg,IO_3_avg,IO_4_avg,IO_5_avg,IO_6_avg,IO_7_avg,IO_8_avg
        SetAxis left -1.8,1.8
        SetAxis bottom 0,500
end
```

Averaging fEPSP waves macro 2

```
macro
Averagewaves1to3(io1wave1,io1wave2,io1wave3,io2wave1,io2wave2,io2wave3
,io3wave1,io3wave2,io3wave3)
string
io1wave1,io0wave2,io1wave3,io2wave1,io2wave2,io2wave3,io3wave1,io3wave
2,io3wave3
//this macro requires me to enter file names for the waves
duplicate/o $io1wave1 IO_1_wave1
duplicate/o $io1wave2 IO_1_wave2
duplicate/o $io1wave3 IO_1_wave3
duplicate/o $io1wave1 IO_1_avg
IO_1_avg= (IO_1_wave1+IO_1_wave2+IO_1_Wave3)/3
duplicate/o $io2wave1 IO_2_wave1
duplicate/o $io2wave2 IO_2_wave2
duplicate/o $io2wave3 IO_2_wave3
duplicate/o $io2wave1 IO_2_avg
IO_2_avg= (IO_2_wave1+IO_2_wave2+IO_2_Wave3)/3
duplicate/o $io3wave1 IO_3_wave1
duplicate/o $io3wave2 IO_3_wave2
duplicate/o $io3wave3 IO_3_wave3
duplicate/o $io3wave1 IO_3_avg
IO_3_avg= (IO_3_wave1+IO_3_wave2+IO_3_Wave3)/3
display IO_1_avg,IO_2_avg,IO_3_avg
end
```

Analysis of paired pulse facilitation

```
Macro PairedPulse(Firstwave,start, fvinterval,ppinterval)
string firstwave, secondwave
variable start,fvinterval,ppinterval
Variable,slope1,Slope2,MinFV1,MaxFV1,sint,PeakPP1,PeakPPloc1,PeakPP2,Pe
akPPloc2,MinFV2,MaxFV2,FVmaxloc1,FVmaxloc2
variable
fitstart1,fitstart2,tau1,tau2,PP1derivative,PP2derivative,FVminloc1,FVminloc2,a
rtifact1,artifact2,FVamp1,FVamp2,peaktopeak1, peaktopeak2
Make/o/n=10 PP1,PP2
Make/o/t/n=10 PPlabels
PPlabels[0]="PeakPP"
PPlabels[1]="Slope"
PPlabels[2]="peaktopeak amp"
PPlabels[3]="Derivative"
PPlabels[4]="Fiber Volley amp"
PPlabels[5]="Fiber Volley start"
```

```
PPlabels[6]="Fiber Volley stop"
PPlabels[7]="PP peak location"
PPlabels[8]="PPinterval"
wavestats/q $firstwave
artifact1=v_maxloc-0.1
//wavestats/q/r=(20,)$firstwave
artifact2=artifact1+ppinterval
//PPinterval=artifact2-artifact1
Display /W=(5.25,42.5,762,262.25) $firstwave
duplicate/o $firstwave '2ndwave'
        ModifyGraph rgb($firstwave)=(0,0,0)
appendtograph '2ndwave'
        ModifyGraph offset('2ndwave')={-PPinterval,0}
        wavestats/q/r=(artifact1-5,artifact1-0.1) $firstwave
        $firstwave-=(v_avg)
        wavestats/q/r=(artifact2-5,artifact2-0.1) '2ndwave'
        '2ndwave'-=(v_avg)
        SetAxis left -1,1
        SetAxis bottom 0,30
        Dowindow/K FieldPPGraph
        Dowindow/C FieldPPGraph
        sint=0.05 // sets the sampline interval
Setscale /P x, 0, sint, "ms", $firstwave //scales the wave
wavestats/q/r=(start,start+fvinterval) $firstwave //establishes a window to look
for the Fiber Volley
        MinFV1 =v_min//minimum of the FV
        maxFV1=v_max //peak of the FV
        FVmaxloc1=v_maxloc-artifact1
        FVminloc1=v_minloc-artifact1
        FVamp1=MaxFV1-minFV1
Tag/C/N=text1/F=0/X=0.00/Y=0.00 $firstwave,start,"\\W523"
Tag/C/N=text2/F=0/X=0.00/Y=0.00 $firstwave,start+fvinterval,"\\W523"
wavestats/q/r=(v_maxloc,V_maxloc+20) $firstwave //Establish the window for
the EPSP
Print maxFV1-minFV1, "FV amplitude"
Tag/C/N=text3/F=0/X=0.00/Y=0.00 $firstwave,V_maxloc,"\\W524"
Tag/C/N=text4/F=0/X=0.00/Y=0.00 $firstwave,V_minloc,"\\W524"
        PeakPP1= -v_min
        PeakPPloc1=V_minloc-artifact1
        fitstart1=(PeakPPloc1-FVmaxloc1)*.1
CurveFit/q line  $firstwave(V_maxloc+fitstart1,v_minloc-fitstart1) /D
        slope1=w_coef[1]
        CurveFit/q exp  $firstwave(V_maxloc+fitstart1,v_minloc-fitstart1) /D
        tau1=1/k2
Duplicate/o/r=(V_maxloc+fitstart1,v_minloc-fitstart1)$firstwave PPdiff1
```

```
differentiate PPdiff1
wavestats/q/r=[0,5] PPdiff1
PPdiff1=PPdiff1-v_avg
wavestats/q PPdiff1
Smooth/B 9, PPdiff1
PP1derivative=v_max
peaktopeak1=MaxFV1+PeakPP1
//Second pulse begins here
wavestats/q/r=(artifact2+start-5,artifact2+start-5+fvinterval) '2ndwave'
//Assumes a 5 ms baseline before the first Pulse
        MinFV2 =v_min//minimum of the FV
        maxFV2=v_max //peak of the FV
        FVmaxloc2=v_maxloc-artifact2
        FVminloc2=v_minloc-artifact2
        FVamp2=MaxFV2-minFV2
        Tag/C/N=text11/F=0/X=0.00/Y=0.00  '2ndwave' ,artifact2+start-
5,"\\W523"  //assumes 5.7 start time window
Tag/C/N=text12/F=0/X=0.00/Y=0.00  '2ndwave' ,artifact2+start-
5+fvinterval,"\\W523"
wavestats/q/r=(v_maxloc,V_maxloc+20) '2ndwave'
Tag/C/N=text13/F=0/X=0.00/Y=0.00 '2ndwave' ,V_maxloc,"\\W524"
Tag/C/N=text14/F=0/X=0.00/Y=0.00 '2ndwave' ,V_minloc,"\\W524"
        PeakPP2= -v_min
        PeakPPloc2=V_minloc-artifact2
        fitstart2=(PeakPPloc2-FVmaxloc2)*.1
CurveFit/q line '2ndwave' (V_maxloc+fitstart2,v_minloc-fitstart2) /D
Slope2=W_coef[1]
//CurveFit/q exp '2ndwave' (V_maxloc+fitstart2,v_minloc-fitstart2)/D
//Tau2=1/k2
Duplicate/o/r=(V_maxloc+fitstart2,v_minloc-fitstart2)'2ndwave'  PPdiff2
differentiate PPdiff2
wavestats/q/r=[0,5] PPdiff2
PPdiff2=PPdiff2-v_avg
wavestats/q PPdiff2
PP2derivative=v_max
Smooth/B 9, PPdiff2
print PP1derivative,pp2derivative
peaktopeak2=MaxFV2+PeakPP2
PP1[0]=PeakPP1
PP1[1]=Slope1
PP1[2]=peaktopeak1
PP1[3]=PP1derivative
PP1[4]=FVamp1
PP1[5]=FVminloc1
PP1[6]=FVmaxloc1
```

```
PP1[7]=PeakPPloc1
PP1[8]=PPinterval
PP2[0]=PeakPP2
PP2[1]=Slope2
PP2[2]=peaktopeak2
PP2[3]=PP2derivative
PP2[4]=FVamp2
PP2[5]=FVminloc2
PP2[6]=FVmaxloc2
PP2[7]=PeakPPloc2
PP2[8]=PPinterval
Edit/W=(430.5,320,765,516.5) PPlabels,PP1,PP2
dowindow/k PPtable
dowindow/c PPtable
If(FVmaxloc1<FVminloc1)
        print "Increase the Start window time PP1"
        TextBox/C/N=text10/F=0/A=MC "ERROR: Increase start time
window\\Z14"
endif
if (FVmaxloc2<FVminloc2)
        print "Increase the Start window time for PP2"
        TextBox/C/N=text10/F=0/A=MC "ERROR: Increase start time
window\\Z14"
        endif
end
```

fEPSP slope, amplitude, and fiber volley measurements for two waves

```
Macro FieldEPSP(firstwave,secondwave,start, fvinterval) //Start is 5.7ms
string firstwave,secondwave
variable start, fvinterval
String/g firstwave1, secondwave
Variable/G,slope1,Slope2,MinFV1,MaxFV1,sint,PeakEPSP1,PeakEPSPloc1,Pea
kEPSP2,PeakEPSPloc2,MinFV2,MaxFV2,FVmaxloc1,FVmaxloc2
variable/G
fitstart1,fitstart2,tau1,tau2,EPSP1derivative,EPSP2derivative,FVminloc1,FVminl
oc2,artifact1,artifact2,FVamp1,FVamp2
Make/o/n=10 EPSP1,EPSP2
Make/o/t/n=10 EPSPlabels
EPSPlabels[0]="PeakEPSP"
EPSPlabels[1]="Slope"
EPSPlabels[2]="tau"
EPSPlabels[3]="Derivative"
EPSPlabels[4]="Fiber Volley amp"
EPSPlabels[5]="Fiber Volley start"
```

```
EPSPlabels[6]="Fiber Volley stop"
EPSPlabels[7]="EPSP peak location"
EPSPlabels[8]="Artifactloc"
wavestats/q $firstwave
artifact1=v_maxloc-0.1
wavestats/q $secondwave
artifact2=v_maxloc-0.1
Display /W=(5.25,42.5,762,262.25) $firstwave,$secondwave
        ModifyGraph rgb($firstwave)=(0,0,0)//,rgb(fit_$firstwave)=(0,0,0)
        SetAxis left -1.2,1.2
        SetAxis bottom 0,30
        Dowindow/K FieldEPSPGraph
        Dowindow/C FieldEPSPGraph
        sint=0.05 // sets the sampline interval
Setscale /P x, 0, sint, "ms", $firstwave //scales the wave
wavestats/q/r=(start,start+fvinterval) $firstwave //establishes a window to look
for the Fiber Volley
        MinFV1 =v_min//minimum of the FV
        maxFV1=v_max //peak of the FV
        FVmaxloc1=v_maxloc-artifact1
        FVminloc1=v_minloc-artifact1
FVamp1=MaxFV1-minFV1
Tag/C/N=text1/F=0/X=0.00/Y=0.00 $firstwave,start,"\\W523"
Tag/C/N=text2/F=0/X=0.00/Y=0.00 $firstwave,start+fvinterval,"\\W523"
wavestats/q/r=(v_maxloc,V_maxloc+20) $firstwave //Establish the window for
the EPSP
Print maxFV1-minFV1, "FV amplitude"
Tag/C/N=text3/F=0/X=0.00/Y=0.00 $firstwave,V_maxloc,"\\W524"
Tag/C/N=text4/F=0/X=0.00/Y=0.00 $firstwave,V_minloc,"\\W524"
        PeakEPSP1= -v_min
        PeakEPSPloc1=V_minloc-artifact1
        fitstart1=(PeakEPSPloc1-FVmaxloc1)*.1
CurveFit/q line  $firstwave(V_maxloc+fitstart1,v_minloc-fitstart1) /D
        slope1=w_coef[1]
        CurveFit/q exp  $firstwave(V_maxloc+fitstart1,v_minloc-fitstart1) /D
        tau1=1/k2
Duplicate/o/r=(V_maxloc+fitstart1,v_minloc-fitstart1)$firstwave EPSPdiff1
differentiate EPSPdiff1
wavestats/q/r=[0,5] EPSPdiff1
EPSPdiff1=EPSPdiff1-v_avg
wavestats/q EPSPdiff1
EPSP1derivative=v_max
Smooth/B 9,EPSPdiff1
setscale /P x, 0, sint, "ms", $secondwave
wavestats/r=(start,start+fvinterval) $secondwave
```

```
		MinFV2 =v_min//minimum of the FV
		maxFV2=v_max //peak of the FV
		FVmaxloc2=v_maxloc-artifact2
		FVminloc2=v_minloc-artifact2
		print FVminloc2,FVmaxloc2
		print v_minloc,v_maxloc
		FVamp2=MaxFV2-minFV2
appendtograph $secondwave
ModifyGraph rgb($secondwave)=(0,0,0)
Tag/C/N=text5/F=0/X=0.00/Y=0.00 $secondwave,start,"\\W523"
Tag/C/N=text6/F=0/X=0.00/Y=0.00 $secondwave,start+fvinterval,"\\W523"
wavestats/q/r=(v_maxloc,V_maxloc+20) $secondwave
Tag/C/N=text7/F=0/X=0.00/Y=0.00 $secondwave,V_maxloc,"\\W524"
Tag/C/N=text8/F=0/X=0.00/Y=0.00 $secondwave,V_minloc,"\\W524"
		PeakEPSP2= -v_min
		PeakEPSPloc2=V_minloc-artifact2
		fitstart2=(PeakEPSPloc2-FVmaxloc2)*.1
CurveFit/q line  $secondwave(V_maxloc+fitstart2,v_minloc-fitstart2) /D
Slope2=W_coef[1]
CurveFit/q exp  $secondwave(V_maxloc+fitstart2,v_minloc-fitstart2) /D
Tau2=1/k2
Duplicate/o/r=(V_maxloc+fitstart2,v_minloc-fitstart2)$secondwave EPSPdiff2
differentiate EPSPdiff2
wavestats/q/r=[0,5] EPSPdiff2
EPSPdiff2=EPSPdiff2-v_avg
wavestats/q EPSPdiff2
EPSP2derivative=v_max
Smooth/B 9,EPSPdiff2
EPSP1[0]=PeakEPSP1
EPSP1[1]=Slope1
EPSP1[2]=tau1
EPSP1[3]=EPSP1derivative
EPSP1[4]=FVamp1
EPSP1[5]=FVminloc1
EPSP1[6]=FVmaxloc1
EPSP1[7]=PeakEPSPloc1
EPSP1[8]=Artifact1
EPSP2[0]=PeakEPSP2
EPSP2[1]=Slope2
EPSP2[2]=tau2
EPSP2[3]=EPSP2derivative
EPSP2[4]=FVamp2
EPSP2[5]=FVminloc2
EPSP2[6]=FVmaxloc2
EPSP2[7]=PeakEPSPloc2
```

```
EPSP2[8]=Artifact2
Edit/W=(430.5,320,765,516.5) EPSPlabels,EPSP1,EPSP2
dowindow/k EPSPtable
dowindow/c EPSPtable
If(FVmaxloc1<FVminloc1)
        print "Increase the Start window time for EPSP1"
        TextBox/C/N=text10/F=0/A=MC "ERROR: Increase start time
window\\Z14"
endif
if (FVmaxloc2<FVminloc2)
        print "Increase the Start window time for EPSP2"
        TextBox/C/N=text11/F=0/A=MC "ERROR: Increase start time
window\\Z14"
        endif
end
Window IOlayout() : Layout
        PauseUpdate; Silent 1           // building window...
        Layout/C=1/W=(58.5,71.75,559.5,498.5)
Graph0(72,72,531.75,251.25)/O=1/F=0/T,Graph1(75.75,236.25,548.25,381.75)/
O=1/F=0/T
        Append
FieldEPSPGraph(62.25,380.25,528.75,601.5)/O=1/F=0/T,Table0(57.75,603.75,5
36.25,717.75)/O=2
EndMacro
```

fEPSP slope, amplitude, and fiber volley measurements for a full input/output analysis

```
Macro
IOCurveFieldEPSP(firstwave,secondwave,thirdwave,fourthwave,fifthwave,sixth
wave,seventhwave,start,fvinterval) //Start is 5.7ms
string
firstwave,secondwave,thirdwave,fourthwave,fifthwave,sixthwave,seventhwave
variable start, fvinterval
String/g firstwave,
secondwave,thirdwave,fourthwave,fifthwave,sixthwave,seventhwave
Variable/G
slope1,Slope2,slope3,slope4,slope5,slope6,slope7,MinFV1,MaxFV1,sint,PeakEP
SP1,PeakEPSPloc1,FVmaxloc1,PeakEPSP2,PeakEPSPloc2,MinFV2,MaxFV2,F
Vmaxloc2
Variable/G
PeakEPSP3,PeakEPSPloc3,MinFV3,MaxFV3,FVmaxloc3,PeakEPSP4,PeakEPS
Ploc4,MinFV4,MaxFV4,FVmaxloc4,PeakEPSP5,PeakEPSPloc5,MinFV5,MaxF
V5,FVmaxloc5
```

```
Variable/G
PeakEPSP6,PeakEPSPloc6,MinFV6,MaxFV6,FVmaxloc6,PeakEPSP7,PeakEPS
Ploc7,MinFV7,MaxFV7,FVmaxloc7,
variable/G
fitstart1,fitstart2,tau1,tau2,EPSP1derivative,EPSP2derivative,FVminloc1,FVminl
oc2,artifact1,artifact2,FVamp1,FVamp2,fitstart3,fitstart4,tau3,tau4,EPSP3derivat
ive,EPSP4derivative,FVminloc3,FVminloc4,artifact3,artifact4,FVamp3,FVamp4
Variable/G
fitstart5,fitstart6,tau5,tau6,EPSP5derivative,EPSP6derivative,FVminloc5,FVminl
oc6,artifact5,artifact6,FVamp5,FVamp6,fitstart7,tau7,EPSP7derivative,FVminlo
c7,artifact7,FVamp7
Variable/G EPSPamp1, EPSPamp2,EPSPamp3,
EPSPamp4,EPSPamp5,EPSPamp6,EPSPamp7
Make/o/n=10 EPSP1,EPSP2,EPSP3,EPSP4,EPSP5,EPSP6,EPSP7
Make/o/t/n=10 EPSPlabels
EPSPlabels[0]="PeakEPSP"
EPSPlabels[1]="Slope"
EPSPlabels[2]="tau"
EPSPlabels[3]="Derivative"
EPSPlabels[4]="Fiber Volley amp"
EPSPlabels[5]="Fiber Volley start"
EPSPlabels[6]="Fiber Volley stop"
EPSPlabels[7]="EPSP peak location"
EPSPlabels[8]="Artifactloc"
EPSPlabels[9]="PeakEPSP+FV"
wavestats/q $firstwave
artifact1=v_maxloc-0.1
wavestats/q $secondwave
artifact2=v_maxloc-0.1
wavestats/q $thirdwave
artifact3=v_maxloc-0.1
wavestats/q $fourthwave
artifact4=v_maxloc-0.1
wavestats/q $fifthwave
artifact5=v_maxloc-0.1
wavestats/q $sixthwave
artifact6=v_maxloc-0.1
wavestats/q $seventhwave
artifact7=v_maxloc-0.1
Display /W=(21.75,220.25,794.25,446.7)
$firstwave,$secondwave,$thirdwave,$fourthwave,$fifthwave,$sixthwave,$sevent
hwave
        ModifyGraph rgb($firstwave)=(0,0,0)//,rgb(fit_$firstwave)=(0,0,0)
        SetAxis left -1.8,1.8
        SetAxis bottom 0,30
```

```
	Dowindow/K FieldEPSPGraph
	Dowindow/C FieldEPSPGraph
	sint=0.05 // sets the sampline interval
Setscale /P x, 0, sint, "ms", $firstwave //scales the wave
wavestats/q/r=(start,start+fvinterval) $firstwave //establishes a window to look
for the Fiber Volley
	MinFV1 =v_min//minimum of the FV
	maxFV1=v_max //peak of the FV
	FVmaxloc1=v_maxloc-artifact1
	FVminloc1=v_minloc-artifact1
FVamp1=MaxFV1-minFV1
Tag/C/N=text1/F=0/X=0.00/Y=0.00 $firstwave,start,"\\W523"
Tag/C/N=text2/F=0/X=0.00/Y=0.00 $firstwave,start+fvinterval,"\\W523"
wavestats/q/r=(v_maxloc,V_maxloc+20) $firstwave //Establish the window for
the EPSP
Print maxFV1-minFV1, "FV amplitude"
Tag/C/N=text3/F=0/X=0.00/Y=0.00 $firstwave,V_maxloc,"\\W524"
Tag/C/N=text4/F=0/X=0.00/Y=0.00 $firstwave,V_minloc,"\\W524"
	PeakEPSP1= -v_min
	PeakEPSPloc1=V_minloc-artifact1
	fitstart1=(PeakEPSPloc1-FVmaxloc1)*.1
CurveFit/q line  $firstwave(V_maxloc+fitstart1,v_minloc-fitstart1) /D
	slope1=-1*w_coef[1]
	CurveFit/q exp  $firstwave(V_maxloc+fitstart1,v_minloc-fitstart1) /D
	tau1=1/k2
Duplicate/o/r=(V_maxloc+fitstart1,v_minloc-fitstart1)$firstwave EPSPdiff1
differentiate EPSPdiff1
wavestats/q/r=[0,5] EPSPdiff1
EPSPdiff1=EPSPdiff1-v_avg
wavestats/q EPSPdiff1
EPSP1derivative=v_max
Smooth/B 9,EPSPdiff1
EPSPamp1=maxFV1+peakEPSP1
//second wave below
setscale /P x, 0, sint, "ms", $secondwave
wavestats/r=(start,start+fvinterval) $secondwave
	MinFV2 =v_min//minimum of the FV
	maxFV2=v_max //peak of the FV
	FVmaxloc2=v_maxloc-artifact2
	FVminloc2=v_minloc-artifact2
	print FVminloc2,FVmaxloc2
	print v_minloc,v_maxloc
	FVamp2=MaxFV2-minFV2
appendtograph $secondwave
ModifyGraph rgb($secondwave)=(0,0,0)
```

```
Tag/C/N=text5/F=0/X=0.00/Y=0.00 $secondwave,start,"\\W523"
Tag/C/N=text6/F=0/X=0.00/Y=0.00 $secondwave,start+fvinterval,"\\W523"
wavestats/q/r=(v_maxloc,V_maxloc+20) $secondwave
Tag/C/N=text7/F=0/X=0.00/Y=0.00 $secondwave,V_maxloc,"\\W524"
Tag/C/N=text8/F=0/X=0.00/Y=0.00 $secondwave,V_minloc,"\\W524"
	PeakEPSP2= -v_min
	PeakEPSPloc2=V_minloc-artifact2
	fitstart2=(PeakEPSPloc2-FVmaxloc2)*.1
CurveFit/q line  $secondwave(V_maxloc+fitstart2,v_minloc-fitstart2) /D
Slope2=-1*W_coef[1]
CurveFit/q exp  $secondwave(V_maxloc+fitstart2,v_minloc-fitstart2) /D
Tau2=1/k2
Duplicate/o/r=(V_maxloc+fitstart2,v_minloc-fitstart2)$secondwave EPSPdiff2
differentiate EPSPdiff2
wavestats/q/r=[0,5] EPSPdiff2
EPSPdiff2=EPSPdiff2-v_avg
wavestats/q EPSPdiff2
EPSP2derivative=v_max
Smooth/B 9,EPSPdiff2
EPSPamp2=maxFV2+peakEPSP2
//wave3below
setscale /P x, 0, sint, "ms", $thirdwave
wavestats/r=(start,start+fvinterval) $thirdwave
	MinFV3 =v_min//minimum of the FV
	maxFV3=v_max //peak of the FV
	FVmaxloc3=v_maxloc-artifact3
	FVminloc3=v_minloc-artifact3
	print FVminloc3,FVmaxloc3
	print v_minloc,v_maxloc
	FVamp3=MaxFV3-minFV3
appendtograph $thirdwave
ModifyGraph rgb($thirdwave)=(0,0,0)
Tag/C/N=text9/F=0/X=0.00/Y=0.00 $thirdwave,start,"\\W523"
Tag/C/N=text10/F=0/X=0.00/Y=0.00 $thirdwave,start+fvinterval,"\\W523"
wavestats/q/r=(v_maxloc,V_maxloc+20) $thirdwave
Tag/C/N=text11/F=0/X=0.00/Y=0.00 $thirdwave,V_maxloc,"\\W524"
Tag/C/N=text12/F=0/X=0.00/Y=0.00 $thirdwave,V_minloc,"\\W524"
	PeakEPSP3= -v_min
	PeakEPSPloc3=V_minloc-artifact3
	fitstart3=(PeakEPSPloc3-FVmaxloc3)*.1
CurveFit/q line  $thirdwave(V_maxloc+fitstart3,v_minloc-fitstart3) /D
Slope3=-1*W_coef[1]
CurveFit/q exp  $thirdwave(V_maxloc+fitstart3,v_minloc-fitstart3) /D
Tau3=1/k2
```

```
Duplicate/o/r=(V_maxloc+fitstart3,v_minloc-fitstart3)$thirdwave EPSPdiff3
differentiate EPSPdiff3
wavestats/q/r=[0,5] EPSPdiff3
EPSPdiff3=EPSPdiff3-v_avg
wavestats/q EPSPdiff3
EPSP3derivative=v_max
Smooth/B 9,EPSPdiff3
EPSPamp3=maxFV3+peakEPSP3
//wave 4 below
setscale /P x, 0, sint, "ms", $fourthwave
wavestats/r=(start,start+fvinterval) $fourthwave
        MinFV4 =v_min//minimum of the FV
        maxFV4=v_max //peak of the FV
        FVmaxloc4=v_maxloc-artifact4
        FVminloc4=v_minloc-artifact4
        print FVminloc4,FVmaxloc4
        print v_minloc,v_maxloc
        FVamp4=MaxFV4-minFV4
appendtograph $fourthwave
ModifyGraph rgb($fourthwave)=(0,0,0)
Tag/C/N=text13/F=0/X=0.00/Y=0.00 $fourthwave,start,"\\W523"
Tag/C/N=text14/F=0/X=0.00/Y=0.00 $fourthwave,start+fvinterval,"\\W523"
wavestats/q/r=(v_maxloc,V_maxloc+20) $fourthwave
Tag/C/N=text15/F=0/X=0.00/Y=0.00 $secondwave,V_maxloc,"\\W524"
Tag/C/N=text16/F=0/X=0.00/Y=0.00 $secondwave,V_minloc,"\\W524"
        PeakEPSP4= -v_min
        PeakEPSPloc4=V_minloc-artifact4
        fitstart4=(PeakEPSPloc4-FVmaxloc4)*.1
CurveFit/q line  $fourthwave(V_maxloc+fitstart4,v_minloc-fitstart4) /D
Slope4=-1*W_coef[1]
CurveFit/q exp  $fourthwave(V_maxloc+fitstart4,v_minloc-fitstart4) /D
Tau4=1/k2
Duplicate/o/r=(V_maxloc+fitstart4,v_minloc-fitstart4)$fourthwave EPSPdiff4
differentiate EPSPdiff4
wavestats/q/r=[0,5] EPSPdiff4
EPSPdiff4=EPSPdiff4-v_avg
wavestats/q EPSPdiff4
EPSP4derivative=v_max
Smooth/B 9,EPSPdiff4
EPSPamp4=maxFV4+peakEPSP4
//fifth wave below
setscale /P x, 0, sint, "ms", $fifthwave
wavestats/r=(start,start+fvinterval) $fifthwave
        MinFV5 =v_min//minimum of the FV
        maxFV5=v_max //peak of the FV
```

```
		FVmaxloc5=v_maxloc-artifact5
		FVminloc5=v_minloc-artifact5
		print FVminloc5,FVmaxloc5
		print v_minloc,v_maxloc
		FVamp5=MaxFV5-minFV5
appendtograph $fifthwave
ModifyGraph rgb($fifthwave)=(0,0,0)
Tag/C/N=text17/F=0/X=0.00/Y=0.00 $fifthwave,start,"\\W523"
Tag/C/N=text18/F=0/X=0.00/Y=0.00 $fifthwave,start+fvinterval,"\\W523"
wavestats/q/r=(v_maxloc,V_maxloc+20) $fifthwave
Tag/C/N=text19/F=0/X=0.00/Y=0.00 $fifthwave,V_maxloc,"\\W524"
Tag/C/N=text20/F=0/X=0.00/Y=0.00 $fifthwave,V_minloc,"\\W524"
		PeakEPSP5= -v_min
		PeakEPSPloc5=V_minloc-artifact5
		fitstart5=(PeakEPSPloc5-FVmaxloc5)*.1
CurveFit/q line  $fifthwave(V_maxloc+fitstart5,v_minloc-fitstart5) /D
Slope5=-1*W_coef[1]
CurveFit/q exp  $fifthwave(V_maxloc+fitstart5,v_minloc-fitstart5) /D
Tau5=1/k2
Duplicate/o/r=(V_maxloc+fitstart5,v_minloc-fitstart5)$fifthwave EPSPdiff5
differentiate EPSPdiff5
wavestats/q/r=[0,5] EPSPdiff5
EPSPdiff5=EPSPdiff5-v_avg
wavestats/q EPSPdiff5
EPSP5derivative=v_max
Smooth/B 9,EPSPdiff5
EPSPamp5=maxFV5+peakEPSP5
//sixthwave below
setscale /P x, 0, sint, "ms", $sixthwave
wavestats/r=(start,start+fvinterval) $sixthwave
		MinFV6 =v_min//minimum of the FV
		maxFV6=v_max //peak of the FV
		FVmaxloc6=v_maxloc-artifact6
		FVminloc6=v_minloc-artifact6
		print FVminloc6,FVmaxloc6
		print v_minloc,v_maxloc
		FVamp6=MaxFV6-minFV6
appendtograph $sixthwave
ModifyGraph rgb($sixthwave)=(0,0,0)
Tag/C/N=text21/F=0/X=0.00/Y=0.00 $sixthwave,start,"\\W523"
Tag/C/N=text22/F=0/X=0.00/Y=0.00 $sixthwave,start+fvinterval,"\\W523"
wavestats/q/r=(v_maxloc,V_maxloc+20) $sixthwave
Tag/C/N=text23/F=0/X=0.00/Y=0.00 $sixthwave,V_maxloc,"\\W524"
Tag/C/N=text24/F=0/X=0.00/Y=0.00 $sixthwave,V_minloc,"\\W524"
		PeakEPSP6= -v_min
```

```
	PeakEPSPloc6=V_minloc-artifact6
	fitstart6=(PeakEPSPloc6-FVmaxloc6)*.1
CurveFit/q line  $sixthwave(V_maxloc+fitstart6,v_minloc-fitstart6) /D
Slope6=-1*W_coef[1]
CurveFit/q exp  $sixthwave(V_maxloc+fitstart6,v_minloc-fitstart6) /D
Tau6=1/k2
Duplicate/o/r=(V_maxloc+fitstart6,v_minloc-fitstart6)$sixthwave EPSPdiff6
differentiate EPSPdiff6
wavestats/q/r=[0,5] EPSPdiff6
EPSPdiff6=EPSPdiff6-v_avg
wavestats/q EPSPdiff6
EPSP6derivative=v_max
Smooth/B 9,EPSPdiff6
EPSPamp6=maxFV6+peakEPSP6
//seventh wave below
setscale /P x, 0, sint, "ms", $seventhwave
wavestats/r=(start,start+fvinterval) $seventhwave
	MinFV7 =v_min//minimum of the FV
	maxFV7=v_max //peak of the FV
	FVmaxloc7=v_maxloc-artifact7
	FVminloc7=v_minloc-artifact7
	print FVminloc7,FVmaxloc7
	print v_minloc,v_maxloc
	FVamp7=MaxFV7-minFV7
appendtograph $seventhwave
ModifyGraph rgb($seventhwave)=(0,0,0)
Tag/C/N=text25/F=0/X=0.00/Y=0.00 $seventhwave,start,"\\W523"
Tag/C/N=text26/F=0/X=0.00/Y=0.00 $seventhwave,start+fvinterval,"\\W523"
wavestats/q/r=(v_maxloc,V_maxloc+20) $seventhwave
Tag/C/N=text27/F=0/X=0.00/Y=0.00 $seventhwave,V_maxloc,"\\W524"
Tag/C/N=text28/F=0/X=0.00/Y=0.00 $seventhwave,V_minloc,"\\W524"
	PeakEPSP7= -v_min
	PeakEPSPloc7=V_minloc-artifact7
	fitstart7=(PeakEPSPloc7-FVmaxloc7)*.1
CurveFit/q line  $seventhwave(V_maxloc+fitstart7,v_minloc-fitstart7) /D
Slope7=-1*W_coef[1]
CurveFit/q exp  $seventhwave(V_maxloc+fitstart7,v_minloc-fitstart7) /D
Tau2=1/k2
Duplicate/o/r=(V_maxloc+fitstart7,v_minloc-fitstart7)$seventhwave EPSPdiff7
differentiate EPSPdiff7
wavestats/q/r=[0,5] EPSPdiff7
EPSPdiff7=EPSPdiff7-v_avg
wavestats/q EPSPdiff7
EPSP7derivative=v_max
Smooth/B 9,EPSPdiff7
```

EPSPamp7=maxFV7+peakEPSP7
EPSP1[0]=PeakEPSP1
EPSP1[1]=Slope1
EPSP1[2]=tau1
EPSP1[3]=EPSP1derivative
EPSP1[4]=FVamp1
EPSP1[5]=FVminloc1
EPSP1[6]=FVmaxloc1
EPSP1[7]=PeakEPSPloc1
EPSP1[8]=Artifact1
EPSP1[9]=EPSPamp1
EPSP2[0]=PeakEPSP2
EPSP2[1]=Slope2
EPSP2[2]=tau2
EPSP2[3]=EPSP2derivative
EPSP2[4]=FVamp2
EPSP2[5]=FVminloc2
EPSP2[6]=FVmaxloc2
EPSP2[7]=PeakEPSPloc2
EPSP2[8]=Artifact2
EPSP2[9]=EPSPamp2
EPSP3[0]=PeakEPSP3
EPSP3[1]=Slope3
EPSP3[2]=tau3
EPSP3[3]=EPSP3derivative
EPSP3[4]=FVamp3
EPSP3[5]=FVminloc3
EPSP3[6]=FVmaxloc3
EPSP3[7]=PeakEPSPloc3
EPSP3[8]=Artifact3
EPSP3[9]=EPSPamp3
EPSP4[0]=PeakEPSP4
EPSP4[1]=Slope4
EPSP4[2]=tau4
EPSP4[3]=EPSP4derivative
EPSP4[4]=FVamp4
EPSP4[5]=FVminloc4
EPSP4[6]=FVmaxloc4
EPSP4[7]=PeakEPSPloc4
EPSP4[8]=Artifact4
EPSP4[9]=EPSPamp4
EPSP5[0]=PeakEPSP5
EPSP5[1]=Slope5
EPSP5[2]=tau2
EPSP5[3]=EPSP5derivative

```
EPSP5[4]=FVamp5
EPSP5[5]=FVminloc5
EPSP5[6]=FVmaxloc5
EPSP5[7]=PeakEPSPloc5
EPSP5[8]=Artifact5
EPSP5[9]=EPSPamp5
EPSP6[0]=PeakEPSP6
EPSP6[1]=Slope6
EPSP6[2]=tau6
EPSP6[3]=EPSP6derivative
EPSP6[4]=FVamp6
EPSP6[5]=FVminloc6
EPSP6[6]=FVmaxloc6
EPSP6[7]=PeakEPSPloc6
EPSP6[8]=Artifact6
EPSP6[9]=EPSPamp6
EPSP7[0]=PeakEPSP7
EPSP7[1]=Slope7
EPSP7[2]=tau7
EPSP7[3]=EPSP7derivative
EPSP7[4]=FVamp7
EPSP7[5]=FVminloc7
EPSP7[6]=FVmaxloc7
EPSP7[7]=PeakEPSPloc7
EPSP7[8]=Artifact7
EPSP7[9]=EPSPamp7
Edit/W=(430.5,320,765,516.5)
EPSPlabels,EPSP1,EPSP2,EPSP3,EPSP4,EPSP5,EPSP6,EPSP7
dowindow/k EPSPtable
dowindow/c EPSPtable
If(FVmaxloc1<FVminloc1)
        print "Increase the Start window time for EPSP1"
        TextBox/C/N=text10/F=0/A=MC "ERROR: Increase start time
window\\Z14"
endif
if (FVmaxloc2<FVminloc2)
        print "Increase the Start window time for EPSP2"
        TextBox/C/N=text11/F=0/A=MC "ERROR: Increase start time
window\\Z14"
        endif
if (FVmaxloc3<FVminloc3)
        print "Increase the Start window time for EPSP3"
        TextBox/C/N=text11/F=0/A=MC "ERROR: Increase start time
window\\Z14"
        endif
```

```
if (FVmaxloc4<FVminloc4)
	print "Increase the Start window time for EPSP4"
	TextBox/C/N=text11/F=0/A=MC "ERROR: Increase start time
window\\Z14"
	endif
if (FVmaxloc5<FVminloc5)
	print "Increase the Start window time for EPSP5"
	TextBox/C/N=text11/F=0/A=MC "ERROR: Increase start time
window\\Z14"
	endif
if (FVmaxloc6<FVminloc6)
	print "Increase the Start window time for EPSP6"
	TextBox/C/N=text11/F=0/A=MC "ERROR: Increase start time
window\\Z14"
	endif
if (FVmaxloc7<FVminloc7)
	print "Increase the Start window time for EPSP7"
	TextBox/C/N=text11/F=0/A=MC "ERROR: Increase start time
window\\Z14"
	endif
end
```

Averaging EPSC waves

```
Macro averageEPSCs()
//assumes that waves are saved in the following way
//a is followed by the io curve stimulus intensity order and then by the sweep
number
//so a32 means it came from the 3rd stimulus intensity in the IO curve and it is
the 2nd sweep
//this number is given to a curve when the text file is loaded into IGOR
duplicate/o ad0_37 AMPA
duplicate/o ad0_76 NMDA
AMPA= (ad0_34+ad0_36+ad0_37)/3
NMDA= (ad0_76+ad0_77+ad0_78+ad0_79+ad0_80)/5
smooth 5, NMDA, AMPA
Display/w=(5.25,42.5,762,262.25) AMPA, NMDA
End
```

14 Hz low frequency fEPSP analysis

```
macro lowfreqanalysis(firstwave)
string firstwave
variable i, minimumy, a, b
String/g firstwave1
```

```
i=0
display wave3
Do
	a=105+(1429*i)
	b=1450+(1429*i)
	wavestats/q/r=(a,b) $firstwave
		minimumy=V_min
	print minimumy
	i+=1
	while(i<=60)
end
```

BIBLIOGRAPHY

1. Lynch, M. A. Long-term potentiation and memory. *Physiol Rev* **84**, 87-136 (2004).

2. Sweatt, J. D. Mechanisms of Memory (Elsevier, San Diego, 2003).

3. Angelo, M., Plattner, F. & Giese, K. P. Cyclin-dependent kinase 5 in synaptic plasticity, learning and memory. *J Neurochem* **99**, 353-70 (2006).

4. Angelo, M., Plattner, F., Irvine, E. E. & Giese, K. P. Improved reversal learning and altered fear conditioning in transgenic mice with regionally restricted p25 expression. *Eur J Neurosci* **18**, 423-31 (2003).

5. Fischer, A., Sananbenesi, F., Pang, P. T., Lu, B. & Tsai, L. H. Opposing roles of transient and prolonged expression of p25 in synaptic plasticity and hippocampus-dependent memory. *Neuron* **48**, 825-38 (2005).

6. Fischer, A., Sananbenesi, F., Schrick, C., Spiess, J. & Radulovic, J. Cyclin-dependent kinase 5 is required for associative learning. *J Neurosci* **22**, 3700-7 (2002).

7. Fischer, A., Sananbenesi, F., Schrick, C., Spiess, J. & Radulovic, J. Regulation of contextual fear conditioning by baseline and inducible septo-hippocampal cyclin-dependent kinase 5. *Neuropharmacology* **44**, 1089-99 (2003).

8. Ohshima, T. et al. Impairment of hippocampal long-term depression and defective spatial learning and memory in p35 mice. *J Neurochem* **94**, 917-25 (2005).

9. Hawasli, A. H. et al. Cyclin-dependent kinase 5 governs learning and synaptic plasticity via regulation of NMDA receptor degradation. *Nature Neuroscience* **Advanced Online Publication: 27 May 2007** (2007).

10. Tarricone, C. et al. Structure and regulation of the CDK5-p25(nck5a) complex. *Mol Cell* **8**, 657-69 (2001).

11. Mapelli, M. & Musacchio, A. The structural perspective on CDK5. *Neurosignals* **12**, 164-72 (2003).

12. Zheng, M., Leung, C. L. & Liem, R. K. Region-specific expression of cyclin-dependent kinase 5 (cdk5) and its activators, p35 and p39, in the

developing and adult rat central nervous system. *J Neurobiol* **35**, 141-59 (1998).

13. Lee, M. S. et al. Neurotoxicity induces cleavage of p35 to p25 by calpain. *Nature* **405**, 360-4 (2000).

14. Li, B. S. et al. Regulation of NMDA receptors by cyclin-dependent kinase-5. *Proc Natl Acad Sci U S A* **98**, 12742-7 (2001).

15. Ayala, R., Shu, T. & Tsai, L. H. Trekking across the brain: the journey of neuronal migration. *Cell* **128**, 29-43 (2007).

16. Gilmore, E. C., Ohshima, T., Goffinet, A. M., Kulkarni, A. B. & Herrup, K. Cyclin-dependent kinase 5-deficient mice demonstrate novel developmental arrest in cerebral cortex. *J Neurosci* **18**, 6370-7 (1998).

17. Ko, J. et al. p35 and p39 are essential for cyclin-dependent kinase 5 function during neurodevelopment. *J Neurosci* **21**, 6758-71 (2001).

18. Ohshima, T. et al. Targeted disruption of the cyclin-dependent kinase 5 gene results in abnormal corticogenesis, neuronal pathology and perinatal death. *Proc Natl Acad Sci U S A* **93**, 11173-8 (1996).

19. Chae, T. et al. Mice lacking p35, a neuronal specific activator of Cdk5, display cortical lamination defects, seizures, and adult lethality. *Neuron* **18**, 29-42 (1997).

20. Kwon, Y. T. & Tsai, L. H. A novel disruption of cortical development in p35(-/-) mice distinct from reeler. *J Comp Neurol* **395**, 510-22 (1998).

21. Gupta, A. & Tsai, L. H. Cyclin-dependent kinase 5 and neuronal migration in the neocortex. *Neurosignals* **12**, 173-9 (2003).

22. Fletcher, A. I. et al. Regulation of exocytosis by cyclin-dependent kinase 5 via phosphorylation of Munc18. *J Biol Chem* **274**, 4027-35 (1999).

23. Shuang, R. et al. Regulation of Munc-18/syntaxin 1A interaction by cyclin-dependent kinase 5 in nerve endings. *J Biol Chem* **273**, 4957-66 (1998).

24. Tomizawa, K. et al. Cdk5/p35 regulates neurotransmitter release through phosphorylation and downregulation of P/Q-type voltage-dependent calcium channel activity. *J Neurosci* **22**, 2590-7 (2002).

25. Cheng, K. & Ip, N. Y. Cdk5: a new player at synapses. *Neurosignals* **12**, 180-90 (2003).

26. Evans, G. J. & Cousin, M. A. Activity-dependent control of slow synaptic vesicle endocytosis by cyclin-dependent kinase 5. *J Neurosci* **27**, 401-11 (2007).

27. Graham, M. E. et al. The in vivo phosphorylation sites of rat brain dynamin I. *J Biol Chem* **282**, 14695-707 (2007).

28. Benavides, D. R. & Bibb, J. A. Role of Cdk5 in drug abuse and plasticity. *Ann N Y Acad Sci* **1025**, 335-44 (2004).

29. Bibb, J. A. Role of Cdk5 in neuronal signaling, plasticity, and drug abuse. *Neurosignals* **12**, 191-9 (2003).

30. Cruz, J. C. & Tsai, L. H. Cdk5 deregulation in the pathogenesis of Alzheimer's disease. *Trends Mol Med* **10**, 452-8 (2004).

31. Wang, Q., Walsh, D. M., Rowan, M. J., Selkoe, D. J. & Anwyl, R. Block of long-term potentiation by naturally secreted and synthetic amyloid beta-peptide in hippocampal slices is mediated via activation of the kinases c-Jun N-terminal kinase, cyclin-dependent kinase 5, and p38 mitogen-activated protein kinase as well as metabotropic glutamate receptor type 5. *J Neurosci* **24**, 3370-8 (2004).

32. Cho, S. & Meriney, S. D. The effects of presynaptic calcium channel modulation by roscovitine on transmitter release at the adult frog neuromuscular junction. *Eur J Neurosci* **23**, 3200-8 (2006).

33. Yan, Z., Chi, P., Bibb, J. A., Ryan, T. A. & Greengard, P. Roscovitine: a novel regulator of P/Q-type calcium channels and transmitter release in central neurons. *J Physiol* **540**, 761-70 (2002).

34. Buraei, Z., Schofield, G. & Elmslie, K. S. Roscovitine differentially affects CaV2 and Kv channels by binding to the open state. *Neuropharmacology* **52**, 883-94 (2007).

35. Wei, F. Y. et al. Control of cyclin-dependent kinase 5 (Cdk5) activity by glutamatergic regulation of p35 stability. *J Neurochem* **93**, 502-12 (2005).

36. Patel, L. S., Wenzel, H. J. & Schwartzkroin, P. A. Physiological and morphological characterization of dentate granule cells in the p35 knock-

out mouse hippocampus: evidence for an epileptic circuit. *J Neurosci* **24**, 9005-14 (2004).

37. Wenzel, H. J., Robbins, C. A., Tsai, L. H. & Schwartzkroin, P. A. Abnormal morphological and functional organization of the hippocampus in a p35 mutant model of cortical dysplasia associated with spontaneous seizures. *J Neurosci* **21**, 983-98 (2001).

38. Patrick, G. N. et al. Conversion of p35 to p25 deregulates Cdk5 activity and promotes neurodegeneration. *Nature* **402**, 615-22 (1999).

39. Lau, L. F. & Ahlijanian, M. K. Role of cdk5 in the pathogenesis of Alzheimer's disease. *Neurosignals* **12**, 209-14 (2003).

40. Fischer, A., Sananbenesi, F., Wang, X., Dobbin, M. & Tsai, L. H. Recovery of learning and memory is associated with chromatin remodelling. *Nature* (2007).

41. Ris, L. et al. Sexual dimorphisms in the effect of low-level p25 expression on synaptic plasticity and memory. *Eur J Neurosci* **21**, 3023-33 (2005).

42. Mizuno, K., Plattner, F. & Peter Giese, K. Expression of p25 impairs contextual learning but not latent inhibition in mice. *Neuroreport* **17**, 1903-5 (2006).

43. Morabito, M. A., Sheng, M. & Tsai, L. H. Cyclin-dependent kinase 5 phosphorylates the N-terminal domain of the postsynaptic density protein PSD-95 in neurons. *J Neurosci* **24**, 865-76 (2004).

44. Masliah, E., Crews, L. & Hansen, L. Synaptic remodeling during aging and in Alzheimer's disease. *J Alzheimers Dis* **9**, 91-9 (2006).

45. Whitlock, J. R., Heynen, A. J., Shuler, M. G. & Bear, M. F. Learning induces long-term potentiation in the hippocampus. *Science* **313**, 1093-7 (2006).

46. Bibb, J. A. et al. Effects of chronic exposure to cocaine are regulated by the neuronal protein Cdk5. *Nature* **410**, 376-380 (2001).

47. Bibb, J. A. et al. Phosphorylation of DARPP-32 by Cdk5 modulates dopamine signalling in neurons. *Nature* **402**, 669-71 (1999).

48. Cheung, Z. H., Fu, A. K. Y. & Ip, N. Y. Synaptic Roles of Cdk5: Implications in Higher Cognitive Functions and Neurodegenerative Diseases. *Neuron* **50**, 13-18 (2006).

49. Saito, T. et al. Developmental regulation of the proteolysis of the p35 cyclin-dependent kinase 5 activator by phosphorylation. *J. Neurosci.* **23**, 1189-97 (2003).

50. Wattler, S., Kelly, M. & Nehls, M. Construction of gene targeting vectors from lambda KOS genomic libraries. *Biotechniques* **26**, 1150-6, 1158, 1160 (1999).

51. Weber, P., Metzger, D. & Chambon, P. Temporally controlled targeted somatic mutagenesis in the mouse brain. *Eur J Neurosci* **14**, 1777-83 (2001).

52. Berton, O. et al. Essential Role of BDNF in the Mesolimbic Dopamine Pathway in Social Defeat Stress. *Science* **311**, 864-868 (2006).

53. Gold, S. J., Ni, Y. G., Dohlman, H. G. & Nestler, E. J. Regulators of G-Protein Signaling (RGS) Proteins: Region-Specific Expression of Nine Subtypes in Rat Brain. *J. Neurosci.* **17**, 8024-8037 (1997).

54. Chung, H. J., Huang, Y. H., Lau, L. F. & Huganir, R. L. Regulation of the NMDA receptor complex and trafficking by activity-dependent phosphorylation of the NR2B subunit PDZ ligand. *J Neurosci* **24**, 10248-59 (2004).

55. Guttmann, R. P. et al. Specific proteolysis of the NR2 subunit at multiple sites by calpain. *J Neurochem* **78**, 1083-93 (2001).

56. Nishi, A. et al. Regulation of DARPP-32 dephosphorylation at PKA- and Cdk5-sites by NMDA and AMPA receptors: distinct roles of calcineurin and protein phosphatase-2A. *J Neurochem* **81**, 832-41 (2002).

57. Powell, C. M. et al. The presynaptic active zone protein RIM1alpha is critical for normal learning and memory. *Neuron* **42**, 143-53 (2004).

58. Cooper, D. C., Chung, S. & Spruston, N. Output-mode transitions are controlled by prolonged inactivation of sodium channels in pyramidal neurons of subiculum. *PLoS Biol* **3**, e175 (2005).

59. Itoh, K., Shimono, K. & Lemmon, V. Dephosphorylation and internalization of cell adhesion molecule L1 induced by theta burst stimulation in rat hippocampus. *Mol Cell Neurosci* **29**, 245-9 (2005).

60. Tang, Y. P. et al. Genetic enhancement of learning and memory in mice. *Nature* **401**, 63-9 (1999).

61. Tsien, J. Z., Huerta, P. T. & Tonegawa, S. The essential role of hippocampal CA1 NMDA receptor-dependent synaptic plasticity in spatial memory. *Cell* **87**, 1327-38 (1996).

62. Bernasconi-Guastalla, S., Wolfer, D. P. & Lipp, H. P. Hippocampal mossy fibers and swimming navigation in mice: correlations with size and left-right asymmetries. *Hippocampus* **4**, 53-63 (1994).

63. Nakazawa, K. et al. Hippocampal CA3 NMDA receptors are crucial for memory acquisition of one-time experience. *Neuron* **38**, 305-15 (2003).

64. Monyer, H., Burnashev, N., Laurie, D. J., Sakmann, B. & Seeburg, P. H. Developmental and regional expression in the rat brain and functional properties of four NMDA receptors. *Neuron* **12**, 529-40 (1994).

65. Chenard, B. L. & Menniti, F. S. Antagonists selective for NMDA receptors containing the NR2B subunit. *Curr Pharm Des* **5**, 381-404 (1999).

66. Picconi, B. et al. NR2B subunit exerts a critical role in postischemic synaptic plasticity. *Stroke* **37**, 1895-901 (2006).

67. Paul, S. et al. The striatal-enriched protein tyrosine phosphatase gates long-term potentiation and fear memory in the lateral amygdala. *Biol Psychiatry* **61**, 1049-61 (2007).

68. Pelkey, K. A. et al. Tyrosine phosphatase STEP is a tonic brake on induction of long-term potentiation. *Neuron* **34**, 127-38 (2002).

69. Liu, L. et al. Role of NMDA receptor subtypes in governing the direction of hippocampal synaptic plasticity. *Science* **304**, 1021-4 (2004).

70. Guttmann, R. P. et al. Proteolysis of the N-methyl-d-aspartate receptor by calpain in situ. *J Pharmacol Exp Ther* **302**, 1023-30 (2002).

71. Simpkins, K. L. et al. Selective activation induced cleavage of the NR2B subunit by calpain. *J Neurosci* **23**, 11322-31 (2003).

72. Zhao, M. G. et al. Roles of NMDA NR2B subtype receptor in prefrontal long-term potentiation and contextual fear memory. *Neuron* **47**, 859-72 (2005).

73. Kutsuwada, T. et al. Impairment of suckling response, trigeminal neuronal pattern formation, and hippocampal LTD in NMDA receptor epsilon 2 subunit mutant mice. *Neuron* **16**, 333-44 (1996).

74. Husi, H., Ward, M. A., Choudhary, J. S., Blackstock, W. P. & Grant, S. G. Proteomic analysis of NMDA receptor-adhesion protein signaling complexes. *Nat Neurosci* **3**, 661-9 (2000).

75. Liu, M. C. et al. Comparing calpain- and caspase-3-mediated degradation patterns in traumatic brain injury by differential proteome analysis. *Biochem J* **394**, 715-25 (2006).

76. Dong, Y. N., Waxman, E. A. & Lynch, D. R. Interactions of postsynaptic density-95 and the NMDA receptor 2 subunit control calpain-mediated cleavage of the NMDA receptor. *J Neurosci* **24**, 11035-45 (2004).

77. Costa-Mattioli, M. et al. Translational control of hippocampal synaptic plasticity and memory by the eIF2alpha kinase GCN2. *Nature* **436**, 1166-73 (2005).

78. Kiyama, Y. et al. Increased thresholds for long-term potentiation and contextual learning in mice lacking the NMDA-type glutamate receptor epsilon1 subunit. *J Neurosci* **18**, 6704-12 (1998).

79. Suzuki, K. & Sorimachi, H. A novel aspect of calpain activation. *FEBS Lett* **433**, 1-4 (1998).

80. Bayer, K. U. et al. Transition from reversible to persistent binding of CaMKII to postsynaptic sites and NR2B. *J Neurosci* **26**, 1164-74 (2006).

81. Gardoni, F., Bellone, C., Cattabeni, F. & Di Luca, M. Protein kinase C activation modulates alpha-calmodulin kinase II binding to NR2A subunit of N-methyl-D-aspartate receptor complex. *J Biol Chem* **276**, 7609-13 (2001).

82. Hoelz, A., Nairn, A. C. & Kuriyan, J. Crystal structure of a tetradecameric assembly of the association domain of Ca2+/calmodulin-dependent kinase II. *Mol Cell* **11**, 1241-51 (2003).

83. Lynch, G., Rex, C. S. & Gall, C. M. LTP consolidation: substrates, explanatory power, and functional significance. *Neuropharmacology* **52**, 12-23 (2007).

84. Siman, R., Baudry, M. & Lynch, G. Regulation of glutamate receptor binding by the cytoskeletal protein fodrin. *Nature* **313**, 225-8 (1985).

85. Hu, R. J. & Bennett, V. In vitro proteolysis of brain spectrin by calpain I inhibits association of spectrin with ankyrin-independent membrane binding site(s). *J Biol Chem* **266**, 18200-5 (1991).

86. Rajgopal, Y. & Vemuri, M. C. Calpain activation and alpha-spectrin cleavage in rat brain by ethanol. *Neurosci Lett* **321**, 187-91 (2002).

87. Dunaevsky, A. Connecting the dots: from actin polymerization to synapse formation. *Neuron* **44**, 216-8 (2004).

88. Nimchinsky, E. A., Sabatini, B. L. & Svoboda, K. Structure and function of dendritic spines. *Annu Rev Physiol* **64**, 313-53 (2002).

89. Matus, A. Actin-based plasticity in dendritic spines. *Science* **290**, 754-8 (2000).

90. Fu, W. Y. et al. Cdk5 regulates EphA4-mediated dendritic spine retraction through an ephexin1-dependent mechanism. *Nat Neurosci* **10**, 67-76 (2007).

91. Kim, Y. et al. Phosphorylation of WAVE1 regulates actin polymerization and dendritic spine morphology. *Nature* **442**, 814-7 (2006).

92. Teranishi, F. et al. Calpain is involved in the HIV replication from the latently infected OM10.1 cells. *Biochem Biophys Res Commun* **303**, 940-6 (2003).

93. Diwan, P., Lacasse, J. J. & Schang, L. M. Roscovitine inhibits activation of promoters in herpes simplex virus type 1 genomes independently of promoter-specific factors. *J Virol* **78**, 9352-65 (2004).

94. Schang, L. M. Cyclin-dependent kinases as cellular targets for antiviral drugs. *J Antimicrob Chemother* **50**, 779-92 (2002).

95. Schang, L. M. Effects of pharmacological cyclin-dependent kinase inhibitors on viral transcription and replication. *Biochim Biophys Acta* **1697**, 197-209 (2004).

96. Schang, L. M. et al. Pharmacological cyclin-dependent kinase inhibitors inhibit replication of wild-type and drug-resistant strains of herpes simplex virus and human immunodeficiency virus type 1 by targeting cellular, not viral, proteins. *J Virol* **76**, 7874-82 (2002).

97. Cruz, J. C., Tseng, H. C., Goldman, J. A., Shih, H. & Tsai, L. H. Aberrant Cdk5 activation by p25 triggers pathological events leading to neurodegeneration and neurofibrillary tangles. *Neuron* **40**, 471-83 (2003).

98. Wang, J., Liu, S., Fu, Y., Wang, J. H. & Lu, Y. Cdk5 activation induces hippocampal CA1 cell death by directly phosphorylating NMDA receptors. *Nat Neurosci* **6**, 1039-47 (2003).

99. Arroyo, S. et al. Is refractory epilepsy preventable? *Epilepsia* **43**, 437-444 (2002).

100. Brodie, M. J. & Dichter, M. A. Antiepileptic drugs. *N Engl J Med* **334**, 168-75 (1996).

101. McNamara, J. O., Huang, Y. Z. & Leonard, A. S. Molecular signaling mechanisms underlying epileptogenesis. *Sci STKE* **2006**, re12 (2006).

102. Liang, S. et al. Major Cdk5-dependent phosphorylation sites of amphiphysin 1 are implicated in the regulation of the membrane binding and endocytosis. *J Neurochem* (2007).

103. Hawasli, A. H. & Bibb, J. A. Alternative roles for Cdk5 in learning and synaptic plasticity. *Biotechnol J* (2007).

104. Sananbenesi, F. et al. A hippocampal Cdk5 pathway regulates extinction of contextual fear. *Nature Neuroscience* **in press** (2007).

105. Sisodiya, S. M. et al. Abnormal expression of cdk5 in focal cortical dysplasia in humans. *Neurosci Lett* **328**, 217-20 (2002).

106. Sen, A. et al. Pathological Tau Tangles Localize to Focal Cortical Dysplasia in Older Patients. *Epilepsia* (2007).

107. Sen, A. et al. Deregulation of cdk5 in Hippocampal sclerosis. *J Neuropathol Exp Neurol* **65**, 55-66 (2006).

108. Sen, A. et al. Increased immunoreactivity of cdk5 activators in hippocampal sclerosis. *Neuroreport* **18**, 511-6 (2007).

109. Pitkanen, A., Schwartzhroin, P. A. & Moshe, S. L. Models of Seizures and Epilepsy (Elsevier, Oxford, 2006).

110. Gold, S. J., Heifets, B. D., Pudiak, C. M., Potts, B. W. & Nestler, E. J. Regulation of regulators of G protein signaling mRNA expression in rat brain by acute and chronic electroconvulsive seizures. *J Neurochem* **82**, 828-38 (2002).

111. Racine, R. J. Modification of seizure activity by electrical stimulation. I. After-discharge threshold. *Electroencephalogr Clin Neurophysiol* **32**, 269-79 (1972).

112. Shah, M. M., Anderson, A. E., Leung, V., Lin, X. & Johnston, D. Seizure-induced plasticity of h channels in entorhinal cortical layer III pyramidal neurons. *Neuron* **44**, 495-508 (2004).

113. Geyer, M. A. & Dulawa, S. C. (ed. Jacqueline Crawley, C. G., Michael Rogawski, David Sibley, Phil Skolnick, Susan Wray, Ron McKay, Gwen Taylor) (John Wiley & Sons, Inc., 2003).

114. Chemelli, R. M. et al. Narcolepsy in orexin knockout mice: molecular genetics of sleep regulation. *Cell* **98**, 437-51 (1999).

115. Fochtmann, L. J. Animal studies of electroconvulsive therapy: foundations for future research. *Psychopharmacol Bull* **30**, 321-444 (1994).

116. Swinyard, E. A. *Electrically induced convulsions*. In *Experimental Models of Epilepsy* (eds. Purpura, D. P., Penry, D., Tower, D. W., D.M. & Walter, R.) (Raven Press, New York, 1972).

117. Duman, R. S. & Vaidya, V. A. Molecular and cellular actions of chronic electroconvulsive seizures. *J Ect* **14**, 181-93 (1998).

118. Cohen, I., Navarro, V., Clemenceau, S., Baulac, M. & Miles, R. On the origin of interictal activity in human temporal lobe epilepsy in vitro. *Science* **298**, 1418-21 (2002).

119. Fisher, R. S. & Coyle, J. T. Neurotransmitters and epilepsy (Wiley-Liss, New York, 1991).

120. Ketelaars, S. O., Gorter, J. A., van Vliet, E. A., Lopes da Silva, F. H. & Wadman, W. J. Sodium currents in isolated rat CA1 pyramidal and dentate granule neurones in the post-status epilepticus model of epilepsy. *Neuroscience* **105**, 109-20 (2001).

121. Baulac, S. et al. A second locus for familial generalized epilepsy with febrile seizures plus maps to chromosome 2q21-q33. *Am J Hum Genet* **65**, 1078-85 (1999).

122. Escayg, A. et al. A novel SCN1A mutation associated with generalized epilepsy with febrile seizures plus--and prevalence of variants in patients with epilepsy. *Am J Hum Genet* **68**, 866-73 (2001).

123. Escayg, A. et al. Mutations of SCN1A, encoding a neuronal sodium channel, in two families with GEFS+2. *Nat Genet* **24**, 343-5 (2000).

124. Wallace, R. H. et al. Febrile seizures and generalized epilepsy associated with a mutation in the Na+-channel beta1 subunit gene SCN1B. *Nat Genet* **19**, 366-70 (1998).

125. Mulley, J. C., Scheffer, I. E., Petrou, S. & Berkovic, S. F. Channelopathies as a genetic cause of epilepsy. *Curr Opin Neurol* **16**, 171-6 (2003).

126. Muller, M. Morphological and functional consequences of chronic epilepsy in rat hippocampal slice cultures. *Pflugers Arch* **422**, 418-23 (1993).

127. Muller, M., Gahwiler, B. H., Rietschin, L. & Thompson, S. M. Reversible loss of dendritic spines and altered excitability after chronic epilepsy in hippocampal slice cultures. *Proc Natl Acad Sci U S A* **90**, 257-61 (1993).

128. Thompson, S. M. Consequence of epileptic activity in vitro. *Brain Pathol* **3**, 413-9 (1993).

129. Farrell, M. & Vinters, H. in Epilepsy: a comprehensive book (eds. Engel JJ & TA, P.) 157-75 (Lippincott-Raven, Philadelphia, 1997).

130. Pillai, J. & Sperling, M. R. Interictal EEG and the diagnosis of epilepsy. *Epilepsia* **47 Suppl 1**, 14-22 (2006).

131. Mikuni, N. et al. NMDA-receptors 1 and 2A/B coassembly increased in human epileptic focal cortical dysplasia. *Epilepsia* **40**, 1683-7 (1999).

132. Moddel, G. et al. The NMDA receptor NR2B subunit contributes to epileptogenesis in human cortical dysplasia. *Brain Res* **1046**, 10-23 (2005).

133. Najm, I. M. et al. Epileptogenicity correlated with increased N-methyl-D-aspartate receptor subunit NR2A/B in human focal cortical dysplasia. *Epilepsia* **41**, 971-6 (2000).

134. Ying, Z., Bingaman, W. & Najm, I. M. Increased numbers of coassembled PSD-95 to NMDA-receptor subunits NR2B and NR1 in human epileptic cortical dysplasia. *Epilepsia* **45**, 314-21 (2004).

135. Geyer, J. D., Bilir, E., Faught, R. E., Kuzniecky, R. & Gilliam, F. Significance of interictal temporal lobe delta activity for localization of the primary epileptogenic region. *Neurology* **52**, 202-5 (1999).

136. Normand, M. M., Wszolek, Z. K. & Klass, D. W. Temporal intermittent rhythmic delta activity in electroencephalograms. *J Clin Neurophysiol* **12**, 280-4 (1995).

137. Reiher, J., Beaudry, M. & Leduc, C. P. Temporal intermittent rhythmic delta activity (TIRDA) in the diagnosis of complex partial epilepsy: sensitivity, specificity and predictive value. *Can J Neurol Sci* **16**, 398-401 (1989).

138. Sridhar, J., Akula, N. & Pattabiraman, N. Selectivity and potency of cyclin-dependent kinase inhibitors. *Aaps J* **8**, E204-21 (2006).

139. Tsai, L. H., Delalle, I., Caviness, V. S., Jr., Chae, T. & Harlow, E. p35 is a neural-specific regulatory subunit of cyclin-dependent kinase 5. *Nature* **371**, 419-23 (1994).

140. Bibb, J. A. et al. Phosphorylation of protein phosphatase inhibitor-1 by Cdk5. *J Biol Chem* **276**, 14490-7 (2001).

141. Kerokoski, P., Suuronen, T., Salminen, A., Soininen, H. & Pirttila, T. Both N-methyl-D-aspartate (NMDA) and non-NMDA receptors mediate

glutamate-induced cleavage of the cyclin-dependent kinase 5 (cdk5) activator p35 in cultured rat hippocampal neurons. *Neurosci Lett* **368**, 181-5 (2004).

142. Kusakawa, G. et al. Calpain-dependent proteolytic cleavage of the p35 cyclin-dependent kinase 5 activator to p25. *J Biol Chem* **275**, 17166-72 (2000).

143. Nath, R. et al. Processing of cdk5 activator p35 to its truncated form (p25) by calpain in acutely injured neuronal cells. *Biochem Biophys Res Commun* **274**, 16-21 (2000).

144. Nguyen, M. D., Lariviere, R. C. & Julien, J. P. Deregulation of Cdk5 in a mouse model of ALS: toxicity alleviated by perikaryal neurofilament inclusions. *Neuron* **30**, 135-47 (2001).

145. Hisanaga, S. & Saito, T. The regulation of cyclin-dependent kinase 5 activity through the metabolism of p35 or p39 Cdk5 activator. *Neurosignals* **12**, 221-9 (2003).

146. Castillo, P. E., Schoch, S., Schmitz, F., Sudhof, T. C. & Malenka, R. C. RIM1alpha is required for presynaptic long-term potentiation. *Nature* **415**, 327-30 (2002).

147. Schoch, S. et al. RIM1alpha forms a protein scaffold for regulating neurotransmitter release at the active zone. *Nature* **415**, 321-6 (2002).

148. Verhage, M., Ghijsen, W. E. & Lopes da Silva, F. H. Presynaptic plasticity: the regulation of Ca(2+)-dependent transmitter release. *Prog Neurobiol* **42**, 539-74 (1994).

149. Kramar, E. A. et al. A novel mechanism for the facilitation of theta-induced long-term potentiation by brain-derived neurotrophic factor. *J Neurosci* **24**, 5151-61 (2004).

150. Ouyang, W., Wang, G. & Hemmings, H. C., Jr. Isoflurane and propofol inhibit voltage-gated sodium channels in isolated rat neurohypophysial nerve terminals. *Mol Pharmacol* **64**, 373-81 (2003).

151. Hommel, J. D., Sears, R. M., Georgescu, D., Simmons, D. L. & DiLeone, R. J. Local gene knockdown in the brain using viral-mediated RNA interference. *Nat Med* **9**, 1539-44 (2003).

152. Liu, Y. L. et al. Optimized production of high-titer recombinant adeno-associated virus in roller bottles. *Biotechniques* **34**, 184-9 (2003).

153. Zolotukhin, S. et al. Recombinant adeno-associated virus purification using novel methods improves infectious titer and yield. *Gene Ther* **6**, 973-85 (1999).

154. Freshney, R. I. Culture of Animal Cells: A Manual of Basic Technique (Wiley-Liss, Hoboken, 2000).

155. Tsien, J. Z. et al. Subregion- and cell type-restricted gene knockout in mouse brain. *Cell* **87**, 1317-26 (1996).

156. Benavides, D. R. et al. Cyclin-Dependent Protein Kinase 5 Controls Cocaine Responses, Motivation for Reward, and Striatal Neuron Excitability. *Manuscript in preparation* (2007).

157. Luikart, B. W. et al. TrkB has a cell-autonomous role in the establishment of hippocampal Schaffer collateral synapses. *J Neurosci* **25**, 3774-86 (2005).